

# A Flexible and Robust Non-Parametric Test of Exchangeability

ALAN J. AW<sup>\*1,2</sup>, JEFFREY P. SPENCE<sup>3</sup>, AND YUN S. SONG<sup>1,2,4,5</sup>

**ABSTRACT.** Many statistical analyses assume that the data points within a sample are exchangeable and their features have some known dependency structure. Given a feature dependency structure, one can ask if the observations are exchangeable, in which case we say that they are homogeneous. Homogeneity may be the end goal of a clustering algorithm or a justification for not clustering. Apart from random matrix theory approaches, few general approaches provide statistical guarantees of exchangeability or homogeneity without labeled examples from distinct clusters. We propose a fast and flexible non-parametric hypothesis testing approach that takes as input a multivariate individual-by-feature dataset and user-specified feature dependency constraints, without labeled examples, and reports whether the individuals are exchangeable at a user-specified significance level. Our approach controls Type I error across realistic scenarios and handles data of arbitrary dimension. We perform an extensive simulation study to evaluate the efficacy of domain-agnostic tests of stratification, and find that our approach compares favorably in various scenarios of interest. Finally, we apply our approach to post-clustering single-cell chromatin accessibility data and World Values Survey data, and show how it helps to identify drivers of heterogeneity and generate clusters of exchangeable individuals.

Keywords: exchangeability; non-parametric test; single-cell ATAC-seq; World Values Survey

## 1 Introduction

In modern statistics, data are generated at a faster rate than scientific hypotheses may be formulated. Having the data at hand even before the hypothesis is formulated, more and more scientists are developing methods and models to detect signals and to generate new, empirically testable theories. In the absence of dependent or response variables, it is typical to perform clustering to group observations into communities that are not only well separated but also homogeneous within each community.

Sample clustering is challenging for two reasons. First, samples are *realistically* randomly drawn without replacement from a finite population, implying that they are exchangeable. In numerous cluster homogeneity detection algorithms, samples are *assumed* randomly drawn with replacement from one infinite population, implying that they are assumed independent. Second, and perhaps more important, the features of the dataset are usually statistically dependent. Accounting for feature-feature dependencies is important for ensuring the efficacy of any clustering method, i.e., its ability to recover meaningful communities. Many successful clustering methods rely on domain-specific knowledge to account for feature-feature dependencies, for instance through grouping of features or feature engineering or statistical modeling. In practice, however, domain knowledge may be scarce, with the scarcity masking information needed for completely revealing the architecture of dependencies between features.

Insufficient domain knowledge reduces the efficacy of a clustering method and masks information from its output clusters. In particular, clustering may no longer guarantee the absence of meaningful subclusters in an output cluster. Reduced efficacy, if not addressed, could lead to undetected overfitting of the algorithm to a training set, resulting in out-of-sample classification errors or poor generalizability of the algorithm to

<sup>1</sup>DEPARTMENT OF STATISTICS, UNIVERSITY OF CALIFORNIA, BERKELEY, BERKELEY, CA

<sup>2</sup>CENTER FOR COMPUTATIONAL BIOLOGY, UNIVERSITY OF CALIFORNIA, BERKELEY, BERKELEY, CA

<sup>3</sup>DEPARTMENT OF GENETICS, SCHOOL OF MEDICINE, STANFORD UNIVERSITY, STANFORD, CA

<sup>4</sup>COMPUTER SCIENCE DIVISION, UNIVERSITY OF CALIFORNIA, BERKELEY, BERKELEY, CA

<sup>5</sup>CHAN ZUCKERBERG BIOHUB, SAN FRANCISCO, CA

*E-mail addresses:* alanaw1@berkeley.edu, jspence@stanford.edu, yss@eecs.berkeley.edu.

Manuscript under submission (October 1, 2021).

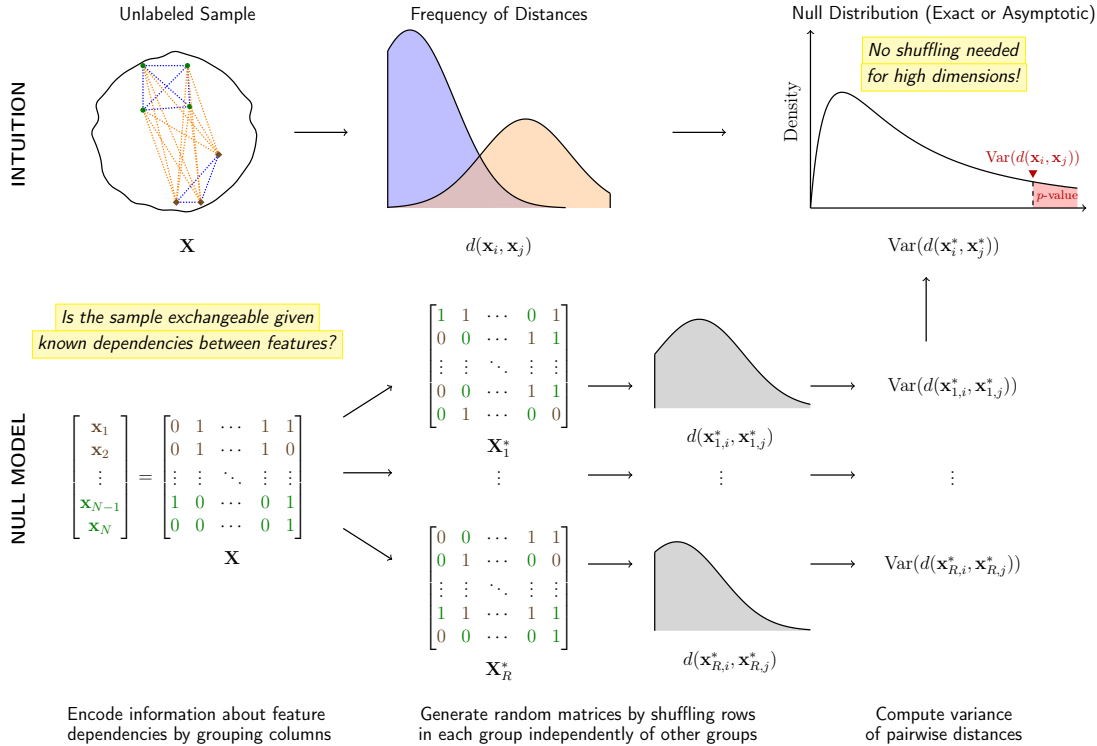


FIGURE 1. Overview of our method for detecting non-exchangeability or heterogeneity.

other datasets. Information masking, on the other hand, could result in only partially discovered information in post-clustering outputs.

One way to simultaneously enhance information discovery and increase clustering efficacy is to decide, with supervision from domain knowledge, whether the clusters or communities output by a clustering method resemble homogeneous groups. As our present work will demonstrate, this decision can be made transparently, and is based on the straightforward idea that a homogeneous cluster should have small spread of pairwise distances for a distance metric typically chosen judiciously by the user (see Figure 1). To help the reader follow our abstract exposition thus far, let us consider two real-life examples drawn from single cell biology and cultural studies.

Figure 2 (left) shows a two-dimensional projection of  $N = 7060$  single cell assays for transposase-accessible chromatin (scATAC-seq), where the dataset consists of  $P = 87,561$  peak count features per single cell sample.<sup>1</sup> The clustering in the figure was obtained by applying the unsupervised clustering algorithm UMAP (McInnes et al., 2018) to the samples after transforming the features of the latter samples using latent semantic indexing (LSI) (Deerwester et al., 1990). This approach is known to recover clusters comprising largely unique cell types, but there is no complete explanation of how the statistical dependencies between features accounted for by the method match biologically meaningful dependencies. Yet, if the samples themselves truly originated from distinct, separable communities (for instance, different cell types or different stages of the cell cycle), and the clustering method were efficacious as claimed, then we would expect the randomness within each cluster to be attributed entirely to noise. How could we leverage prior knowledge about peak counts to verify the hypothesis that within-cluster randomness is nothing more than noise?

In Figure 2 (right), we plot a heat map summarizing the correlation of responses by  $N = 1715$  Singaporean participants to a subset of  $P = 47$  questions from 440 World Values Survey (WVS) questions (Inglehart et al., 2014), where the sampling design ensures the dataset is representative of the population. Albeit

<sup>1</sup>The single cell ATAC-seq dataset — “10k Peripheral blood mononuclear cells (PBMCs) from a healthy donor” by Cell Ranger 3.1.0, 10x Genomics — is available through 10x Genomics upon filling in an online registration form.

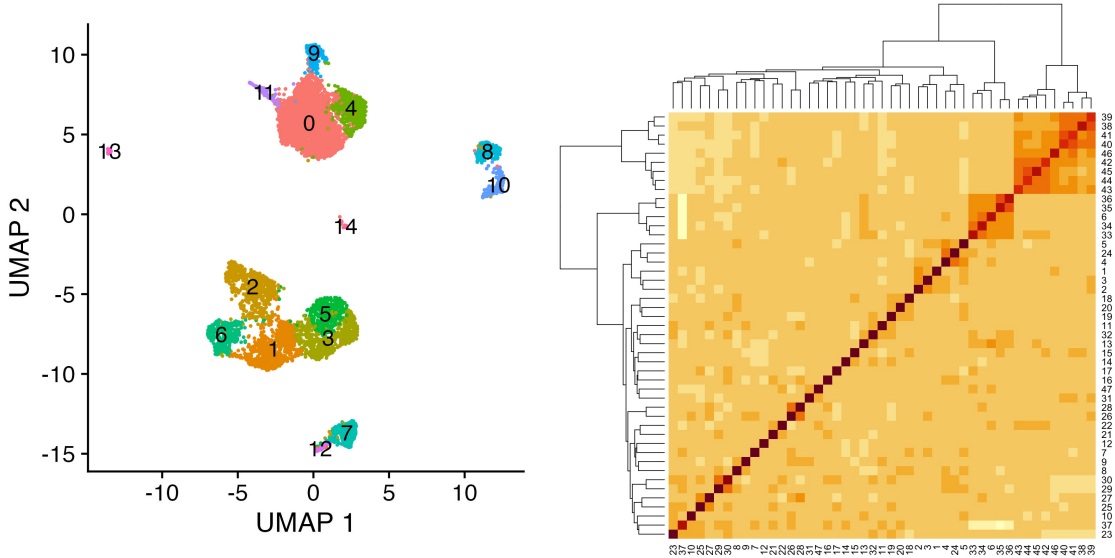


FIGURE 2. **Left.** Two-dimensional projections of clustered single cell ATAC-seq data. Each number (0 to 14) corresponds to a cluster label, with cluster labels approximately matching unique peripheral blood mononuclear cell types. See Figure 8 for cell type composition of each cluster. **Right.** A correlation heat map of categorical responses by Singaporean participants to World Values Survey questions. The dendrogram, constructed from hierarchical clustering with Ward linkage, depicts grouping of the questions.

representative of the population, the sample itself is not a priori homogeneous, meaning that there might be distinct communities among the individuals that explain the patterns observed about feature-feature correlations. Suppose we wish to detect such communities and find discerning questions between them; we do so by performing clustering and downstream differential analysis. Without a demonstrably efficacious method, naïve clustering could lead to double dipping (Kriegeskorte et al., 2009), in other words, committing a Type I error by performing clustering and reporting differential features on the dataset when it is in fact homogeneous. (An example using simulated data is illustrated in Section 6.) A more sensible approach is to account for dependencies between the features of the dataset before or while searching for communities. Having accounted for dependencies between features, perhaps with guidance from prior expectations about correlated responses to the survey questions, we can query the presence of communities without committing the Type I error described above.

The two challenges and two examples described above essentially raise the question: Given an  $N \times P$  individual-by-feature dataset, where the  $N$  individuals are drawn without replacement from some finite population, how can we decide, *without any external sample labels*, that its  $N$  individuals are “similar enough,” assuming some knowledge about the  $P$  features? We can state our question more formally. Let  $\mathbf{X} = (x_{np}) \in \mathbb{R}^{N \times P}$  be a individual-by-feature dataset,

$$\mathbf{X} = \begin{pmatrix} - & \mathbf{x}_1^T & - \\ - & \vdots & - \\ - & \mathbf{x}_N^T & - \end{pmatrix} = \begin{pmatrix} | & \cdots & | \\ \mathbf{x}^{(1)} & \cdots & \mathbf{x}^{(P)} \\ | & \cdots & | \end{pmatrix},$$

with  $\{\mathbf{x}_1, \dots, \mathbf{x}_N\}$  denoting the exchangeable sample and  $\mathbf{x}^{(1)}, \dots, \mathbf{x}^{(P)}$  denoting the features. Assuming that we have some information about the dependencies between  $\mathbf{x}^{(1)}, \dots, \mathbf{x}^{(P)}$ , how do we decide whether  $\mathbf{x}_1, \dots, \mathbf{x}_N$  are homogeneous or heterogeneous (i.e., originating from two or more distinct populations)?

## 1.1 Related Work

Whereas numerous unsupervised learning approaches detect heterogeneity by performing and reporting a clustering, hypothesis testing methods for unsupervised detection of non-exchangeability or heterogeneity are less widespread in applications. One approach exploits results from the spectral theory of random matrices

(also known as random matrix theory) (Bai and Silverstein, 2010), where for example it is known that the largest eigenvalue of the covariance matrix of  $N$  independently and identically distributed  $P$ -variate sub-Gaussian points have a distribution that is asymptotically Tracy-Widom as  $P$  and  $N$  tend to infinity with  $N/P \rightarrow c \in (0, \infty)$  (Soshnikov, 2002). This asymptotic law provides an approximate null distribution for the eigenvalues of a sample covariance matrix, forming the basis of an asymptotic test of homogeneity or absence of stratification for multivariate samples. This approach is proposed by Patterson et al. (2006) to analyze genetic data, and has seen subsequent refinements through residualization and block permutation resampling strategies (Zhou et al., 2018). A second approach, also appearing in genetic studies (Pinheiro et al., 2012), relies on the asymptotic theory of U-statistics, where a particular U-statistic with degree 2 kernel is known to be asymptotically equal in distribution to a linear combination of chi-square random variables under non-parametric settings, thus providing an approximate null distribution for the U-statistic.

Unsupervised tests of homogeneity have also been directly incorporated into clustering or community detection algorithms to detect the true number of underlying communities. In this setting, a network measuring between-individual distances is either pre-constructed from the multivariate sample or assumed available. Many of these tests assume an underlying generative model for the network in proposing a test statistic and its null distribution. Examples of generative models include the stochastic block models (Bickel and Sarkar, 2016) and the degree corrected mixed membership model (Jin et al., 2019); examples of test statistics include various subgraph and spectral statistics (Gao and Lafferty, 2017; Zhao et al., 2011).

Another perspective on unsupervised tests of homogeneity can be found in the work of Efron (2009). To test for sample independence, which is a special case of sample exchangeability, Efron proposes a method that is sensitive to the ordering of the  $N$  individuals, namely, permuting the entries of the first eigenvector of a double standardized version of the dataset. However, he also explains that the efficacy of spectral methods for testing independence is hindered by the column and row covariance matrices sharing the same eigenspectrum, such that a significant spectral statistic can be attributed to either feature dependencies (columns) or sample non-exchangeability (rows), or both. This complication raises an important fundamental point, which is that any unsupervised learning method performed on a multivariate sample (cluster reporting or testing) is efficacious conditioned on accounting for the structure shared between the features. This issue is well-recognized in both the statistical and scientific communities, and many recent developments can be viewed through the lens of addressing this fundamental problem. In domain-agnostic settings, methods like cyclic shifts (Zhou, 2019), models like matrix-variate distributions (Allen and Tibshirani, 2012) and statistical frameworks like parallel analysis (Dobriban et al., 2020), all provide approaches to preserve feature-feature correlations or reasonable models to separate noise from signal in the features. In domain-specific settings, notably in the biological sciences, the Marchenko-Pastur law of the empirical spectral distribution is used to account for signals in protein residue-residue column interactions to detect phylogenetic relationships between protein residue row sequences (Qin and Colwell, 2018), while eigenvector statistics for sparse random matrices are used to separate signal from noise components in single cell RNA-sequencing data (Aparicio et al., 2020). A recent method falling under the hypothesis testing framework has been proposed by Zhang et al. (2019) in the context of single cell RNA-sequencing, which uses truncated normal distributions to perform post-clustering differential analysis to correct for double dipping. (See also Chapter 7 of Huntley, 2016, which discusses how various well-known practical usages of PCA in scientific data analysis — e.g., statistical coupling analysis in the protein multiple sequence alignment studies — can be viewed through the lens of random matrix theory.) Even though the works above do not all fall under the framework of statistical testing, they nevertheless broadly address the problem of “signal retrieval” to pursue homogeneity, and moreover use mathematical ideas that either already underlie some unsupervised test of homogeneity (e.g., random matrix theory, residualization, resampling) or could potentially be applied to the testing framework.

## 1.2 Exchangeability and Homogeneity

Our present work addresses sample exchangeability and domain knowledge insufficiency, the two challenges facing sample clustering that we described earlier. Some care for conceptual underpinnings must be taken before we proceed. While we have used the term homogeneous as a non-technical desideratum of communities output by clustering, to disentangle statistical definitions from broader scientific colloquialisms, we elaborate on “statistical homogeneity” and “exchangeability.” In particular, we clarify that our proposed method does not generally detect statistical homogeneity, and should be interpreted first and foremost as a test of

exchangeability. This point underscores the importance of interpreting our test in practice, such as when it is incorporated as a stopping rule for clustering or run on a single dataset.

*Statistical homogeneity* between observations of a dataset colloquially refers to the statistical properties of any one part of the dataset being the same as any other part. This degree of colloquialism is not shared with sample exchangeability. An *exchangeable sample* is a sample the ordering of which does not matter. That is, for observations  $\mathbf{x}_1, \dots, \mathbf{x}_N$  drawn from a population, the distribution of the random vector  $(\mathbf{x}_{\pi(1)}, \dots, \mathbf{x}_{\pi(N)})$  is invariant to any permutation  $\pi$  of the indices (Aldous, 1985). As noted earlier, when drawing uniformly at random without replacement from a finite population, the resulting sample is exchangeable.

As described earlier, however, note that exchangeable samples need not be homogeneous. For example, drawing  $N$  points uniformly at random without replacement from a multimodal mixture of two or more finite distributions (viewed as a distribution itself) produces an exchangeable sample that is certainly not statistically homogeneous. As we will see in Section 2, our approach is to compute a test statistic that measures statistical homogeneity and to evaluate its significance under a distribution obtained by assuming sample exchangeability.

Despite the difference between exchangeability and statistical homogeneity, we recognize that many scientists use the term “heterogeneity” to refer to the presence of multiple subpopulations, or presence of stratification, which is synonymous with how we interpret exchangeability. Thus, we will use the phrase “test of homogeneity” colloquially in our applications to real data, whenever it is clear we are interested in exchangeability. We invite readers to explore this issue concretely at our online vignette [Exchangeability and Homogeneity](#)<sup>2</sup>.

### 1.3 Our Contributions

We propose a permutation resampling approach to test for exchangeability of a multivariate dataset  $\mathbf{X}$ . We assume that the multivariate features are binary or binarizable to facilitate exposition, but Section 4.2 discusses how our approach can be immediately extended to all types of multivariate features, including those lying in abstract metric spaces. Unlike random matrix theory or spectral approaches underlying many previous works, which principally rely on sample covariances, we use between-individual distances to construct our test statistic. Unlike previous works that do not address computational limitations of permutation resampling, we use asymptotic theory to obtain large-dimensionality and large-sample approximations of our permutation null distribution, which allow our testing procedure to scale to high-dimensional datasets. Our approach also adapts to feature-feature dependencies in an interpretable fashion: similar to the block permutation approach of Zhou et al. (2018), dependent features can be grouped in blocks before performing permutations, with the user choosing the block groupings. The user chooses groupings guided by available domain knowledge, making the test transparent and contingent on interpretable domain-relevant assumptions. Moreover, unlike Zhou et al. (2018), we prove that our large-dimensionality approximation works even under this dependent feature setting, allowing our resampling approach to surmount computational difficulties faced by block permutation tests. Finally, unlike previous domain-agnostic works that avoid substantial assessment of applicability to real datasets, we perform an extensive simulation study for evaluating the efficacy of domain-agnostic tests to realistic datasets with characteristics commonly encountered in practical scenarios. Through evaluating both our approach and a random matrix theory approach using this framework, we find that our approach is robust to sampling artifacts and designs reflective of real datasets. Moreover, we also identify practical scenarios where using one approach might be better than the other.

The remainder of the paper is organized as follows. In Section 2, we state our test and formulate our algorithm in the ideal scenario where the features are assumed independent. We also state our large-dimensionality approximation results that allow our framework to scale to high-dimensional datasets. Section 3 reports Type I error control of our test (Section 3.1) as well as the simulation study we perform to evaluate the power (Section 3.2) and efficacy (Section 3.3) of our test on realistic datasets. In Section 4, we state how our approach can be adapted to scenarios where features are dependent, showing that it still scales to high-dimensional datasets and remains exact. Furthermore, we describe how our test generalizes to arbitrary non-binary datasets. Section 5, largely technical, reports the accuracy of the approximations stated in Section 2. Finally, in Section 6, we apply our approach to analyze datasets in population genetics, single cell biology,

---

<sup>2</sup>[https://alanaw1.github.io/flintyR/articles/ex\\_vs\\_hom.html](https://alanaw1.github.io/flintyR/articles/ex_vs_hom.html)

and the social sciences. We conclude with a discussion of our approach, including limitations that motivate potential avenues for future research.

To guide users interested in applying our methods to their work, we provide open-source software and accessible vignettes for our analyses of scATAC-seq and WVS data. Our software is named *flinty* (*flexible and interpretable non-parametric tests of exchangeability*), and is available in both R (*flintyR*) and Python (*flintyPy*).

## 2 Permutation Test of Exchangeability

Let  $\mathbf{X} = (x_{np})$  be our  $N \times P$  dataset. We assume the features  $\mathbf{x}^{(1)}, \dots, \mathbf{x}^{(P)}$  are binary, or at least binarizable, so that each entry  $x_{np}$  of  $\mathbf{X}$  is either 0 or 1. Section 4.2 describes a generalization of our treatment to arbitrary-valued features. Intuitively, if the sample  $\mathbf{x}_1, \dots, \mathbf{x}_N$  were homogeneous, then by comparing every subsample of size  $M < N$ , we should expect small differences between them. We can measure the overall difference between  $M$ -subsets by comparing how a summary statistic of an  $M$ -subset of  $\{\mathbf{x}_1, \dots, \mathbf{x}_N\}$  differs from the average value of the summary statistic computed across all  $M$ -subsets of  $\mathbf{X}$ .

### 2.1 Test Statistic

To formalize the intuition above, we define the test statistic

$$(2.1) \quad V_f(\mathbf{X}) = \frac{1}{P \binom{N}{M}} \sum_{S \in \binom{[N]}{M}} [f(\mathbf{X}|_S) - \mu_f]^2,$$

where  $f(\cdot)$ , which takes on scalar values, is a summary statistic chosen by the user and  $\mu_f = \frac{1}{\binom{N}{M}} \sum_{S \in \binom{[N]}{M}} f(\mathbf{X}|_S)$  denotes the average of  $f$  computed across all  $M$ -subsamples  $S$  of  $\mathbf{X}$ . Here,  $\binom{[N]}{M}$  denotes the family of all  $M$ -subsets of  $[N] = \{1, 2, \dots, N\}$  and  $\mathbf{X}|_S$  denotes the  $M \times P$  array obtained by including only observations belonging to the  $M$ -subset  $S$ .

For our present work, we set  $M = 2$  and let  $f$  to be the Hamming distance function  $d_H(\cdot, \cdot)$ , which counts the number of differences between a pair of individuals considered. That is,

$$f(\mathbf{X}|_S) = d_H(\mathbf{x}_i, \mathbf{x}_j) = \sum_{p=1}^P \mathbb{1}(x_{ip} \neq x_{jp}),$$

where  $S = \{i, j\}$  is an arbitrary 2-subset of  $\{1, \dots, N\}$ . Dropping the subscript  $f$  in  $V_f$ , this gives

$$(2.2) \quad V(\mathbf{X}) = \frac{1}{P \binom{N}{2}} \sum_{i < j} [d_H(\mathbf{x}_i, \mathbf{x}_j) - \mu]^2,$$

$$(2.3) \quad \mu = \frac{1}{\binom{N}{2}} \sum_{i < j} d_H(\mathbf{x}_i, \mathbf{x}_j).$$

Given the test statistic in (2.2), we now describe its null distribution. Recall from Section 1.2 that whenever vector-valued observations  $\{\mathbf{x}_1, \dots, \mathbf{x}_N\}$  are drawn uniformly at random without replacement from a single population, the resulting sequence  $(\mathbf{x}_1, \dots, \mathbf{x}_N)$  is exchangeable:  $(\mathbf{x}_1, \dots, \mathbf{x}_N) \stackrel{d}{=} (\mathbf{x}_{\pi(1)}, \dots, \mathbf{x}_{\pi(N)})$  for any permutation  $\pi$ . If we further assume that the  $P$  features are statistically independent, then the distribution of sequences satisfies a stronger permutation invariance property:  $(\mathbf{x}_1 = (x_{11}, \dots, x_{1P}), \dots, \mathbf{x}_N = (x_{N1}, \dots, x_{NP})) \stackrel{d}{=} (\mathbf{x}_1^\pi = (x_{\pi_1(1)1}, \dots, x_{\pi_P(1)P}), \dots, \mathbf{x}_N^\pi = (x_{\pi_1(N)1}, \dots, x_{\pi_P(N)P}))$ , where  $\pi_1, \dots, \pi_P$  are  $P$  independent permutations, and we denote by  $\mathbf{x}_i^\pi$  the result of applying the  $P$  independent permutations to each respective component of observation  $\mathbf{x}_i$ .

To formalize the intuition above, denote the column sums of  $\mathbf{X}$  by  $\mathbf{c}(\mathbf{X}) = (c_1, \dots, c_P)$ , so that  $c_p$  counts the number of ones appearing in  $\mathbf{x}^{(p)}$ . Conditioning on the column sums  $\mathbf{c} = \mathbf{c}(\mathbf{X})$  being fixed, the permutation resampling distribution of  $V$ , denoted  $F_{\text{perm}}$ , is the distribution induced on  $V$  by uniformly sampling from all permissible arrays  $\mathbf{X}^*$  obtained by permuting the positions of 1s and 0s along each independent feature  $\mathbf{x}^{(p)}$ .

**Algorithm 1** Computation of  $p$ -value from data array

- 
- 1: **Input:** Individual-by-feature array  $\mathbf{X}_{N \times P}$ , resampling number  $R$
  - 2: Record  $\mathbf{c} = \mathbf{c}(\mathbf{X})$ ,  $\mu$  and  $V_{\text{obs}} = V(\mathbf{X})$  (see (2.2) and (2.3))
  - 3: Set  $r = 0$ ,  $\mathcal{V}^* = \emptyset$
  - 4: **while**  $r < R$  **do**
  - 5: Generate resampled array  $\mathbf{X}^*$  from permutation null
  - 6: Compute  $V^* = V(\mathbf{X}^*)$
  - 7:  $\mathcal{V}^* \leftarrow \mathcal{V}^* \cup \{V^*\}$
  - 8:  $r \leftarrow r + 1$
  - 9: **end while**
  - 10: **Output:**  $p = \frac{1}{R} \cdot \#[V^* \geq V_{\text{obs}}]$
- 

Let  $\mathcal{Y}_{\mathbf{c}}$  be the set of all permutation resampled arrays  $\mathbf{X}^*$  conditioned on fixing the column sums, i.e.,

$$\mathcal{Y}_{\mathbf{c}} = \left\{ (\mathbf{x}_1, \dots, \mathbf{x}_N) \in \{0, 1\}^{N \times P} : \sum_{i=1}^N \mathbf{x}_i = \mathbf{c} \right\}.$$

A counting argument shows that the cardinality of  $\mathcal{Y}_{\mathbf{c}}$  is given by the quantity

$$|\mathcal{Y}_{\mathbf{c}}| = \prod_{p=1}^P \binom{N}{c_p},$$

which could grow exponentially in  $N$  and render resampling intractable. Hence, in implementing our test, we allow the user to specify a resampling number  $R$ , which sets the number of permuted arrays resampled to approximate the distribution. This Monte Carlo strategy effectively makes our test an *approximate* permutation test, as is typical of many permutation tests. (In our implementations, we typically set  $R = 5000$ .)

We describe our implementation of the test in Algorithm 1. Note that our permutation test is a test of exchangeability, even though the choice of test statistic,  $V$ , measures homogeneity.

## 2.2 Asymptotic Null Distributions

Running Algorithm 1 requires performing  $R$  independent resampling routines, with each routine performing independent permutations across  $P$  features and then computing  $O(N^2)$  pairwise Hamming distances to calculate the test statistic. These amount to  $R \times (NP + O(N^2P)) = O(N^2PR)$  operations, which can be slow when  $P$  or  $N$  is large. To speed things up, we propose three approximations to the null distribution that correspond to three limiting regimes: (1)  $P$  is large; (2) both  $N$  and  $P$  are large; and (3)  $N$  is large. Approximations (1) and (2) provide exact analytical expressions for the null distribution of our test statistic, which enable the use of much faster numerical integration methods to compute  $p$ -values. Approximation (3) is based on the bootstrap. We evaluate the accuracy and speed of our approximations using theory and simulations. To facilitate the exposition of our main results, we defer this evaluation to Section 5. We defer all proofs to Appendix C.

Let  $N$  binary vectors with  $P$  features be collected, and define the test statistic

$$V^{(N,P)}(\mathbf{X}) := \frac{1}{P \binom{N}{2}} \sum_{i < j} (d_H(\mathbf{x}_i, \mathbf{x}_j) - \mu)^2.$$

**Approximation 1 (Large  $P$ ):** The following theorem provides an approximation to the null distribution of the permutation-induced random variable  $V^{(N,P)*}$  associated with the test statistic when  $P$  is large. It says that  $V^{(N,P)*}$  is approximately distributed as a weighted sum of two chi-square random variables, with weights determined by the column sums of the dataset.

**Theorem 1** (Large- $P$  Limit). *Let  $V^{(N,P)*}$  be the random variable with the permutation null distribution of  $V^{(N,P)}$ . Define the quantities*

$$\begin{aligned}\alpha^{N,P} &= \frac{1}{P} \sum_{p=1}^P \frac{c_p(N-c_p)}{\binom{N}{2}} \left[ 1 - \frac{c_p(N-c_p)}{\binom{N}{2}} \right], \\ \beta^{N,P} &= \frac{1}{P} \sum_{p=1}^P \frac{c_p(N-c_p)}{\binom{N}{2}} \left[ \frac{1}{2} - \frac{c_p(N-c_p)}{\binom{N}{2}} \right], \\ \gamma^{N,P} &= \frac{1}{P} \sum_{p=1}^P \frac{c_p(N-c_p)}{\binom{N}{2}} \left[ \frac{(c_p-1)(N-c_p-1)}{\binom{N-2}{2}} - \frac{c_p(N-c_p)}{\binom{N}{2}} \right],\end{aligned}$$

and let

$$\begin{aligned}a_1^{N,P} &= \alpha^{N,P} + (N-4)\beta^{N,P} - (N-3)\gamma^{N,P}, \\ a_2^{N,P} &= \alpha^{N,P} - 2\beta^{N,P} + \gamma^{N,P}.\end{aligned}$$

Letting  $\lim_{P \rightarrow \infty} a_i^{N,P} = a_i^N$  for  $i = 1, 2$ , define the random variable

$$V^{(N,\infty)} = \frac{a_1^N \chi_{N-1}^2 + a_2^N \chi_{\binom{N-1}{2}-1}^2}{\binom{N}{2}},$$

where  $\chi_{N-1}^2$  and  $\chi_{\binom{N-1}{2}-1}^2$  denote independent chi-square random variables with  $N-1$  and  $\binom{N-1}{2}-1$  degrees of freedom, respectively. Then,  $V^{(N,P)*} \xrightarrow{d} V^{(N,\infty)}$  as  $P \rightarrow \infty$ .

Theorem 1 implies that, for  $P$  large,  $V^{(N,P)*}$  is approximately equal in distribution to  $V^{(N,\infty)}$ .

**Approximation 2 (Large  $P$  and large  $N$ ):** Next theorem tells us how to approximate the null distribution of  $V^{(N,P)*}$  when both  $N$  and  $P$  are large. It says that  $V^{(N,P)*}$  is roughly normally distributed, with mean and variance determined by the column sums of the dataset.

**Theorem 2** (Large- $P$ , large- $N$  Limit). *With the random variable  $V^{(N,P)*}$  and the quantities  $\alpha^{N,P}, \beta^{N,P}, \gamma^{N,P}, a_1^{N,P}, a_2^{N,P}$  defined as in Theorem 1, let  $\lim_{N,P \rightarrow \infty} \alpha^{N,P} = \alpha$  and define*

$$\begin{aligned}\tau_N &= \lim_{P \rightarrow \infty} \frac{2(N-1)(a_1^{N,P})^2 + 2 \left[ \binom{N-1}{2} - 1 \right] (a_2^{N,P})^2}{\binom{N}{2}^2} \\ &= \frac{2(N-1)(a_1^N)^2 + 2 \left[ \binom{N-1}{2} - 1 \right] (a_2^N)^2}{\binom{N}{2}^2}.\end{aligned}$$

Then  $\tau_N^{-1/2} (V^{(N,P)*} - \alpha) \xrightarrow{d} \mathcal{N}(0, 1)$  as  $P \rightarrow \infty$  and  $N \rightarrow \infty$ .

Consequently, for  $N$  and  $P$  large,  $V^{(N,P)*}$  is approximately distributed as  $\mathcal{N}(\alpha, \tau_N)$ .

**Approximation 3 (Large  $N$ ):** We show in Appendix A that the exact distribution of  $V$  is a quadratic mapping of an exponential family distribution conditioned on a sufficient statistic, where the  $P$ -parameter exponential family distribution is given by (A.1). Differentiating the log-partition function reveals that the MLE of the parameter  $\boldsymbol{\theta}$  is  $\hat{\boldsymbol{\theta}} = \mathbf{c}/N$ , which is the column frequency vector of the dataset. Owing to the consistency of the MLE, for large  $N$  we may use the MLE  $\hat{\boldsymbol{\theta}}$  (obtained from the dataset) to obtain maximum likelihood estimates of the probability mass function of each  $P$ -dimensional binary vector  $\mathbf{x}$ , and plug these latter estimates into (A.1) to obtain the parametric bootstrap distribution. Another way to view this distribution is that we resample datasets  $\mathbf{X}^*$  by drawing each sample as a realization of a product of Bernoulli distributions, where the parameters of these Bernoulli distributions are estimated as  $\hat{\boldsymbol{\theta}} = \mathbf{c}/N$  from the dataset.

As discussed in Section 5, in practice Approximation 1 works well even for surprisingly small  $P$  ( $\sim 50$ ). Because both Approximation 1 and Approximation 2 rely on highly efficient numerical integration routines,

we find no substantial difference in our results when applying Approximation 1 over Approximation 2, even in situations where Approximation 2 is appropriate. On the other hand, we find that Approximation 3 offers only modest speed gain over the permutation test and can even be slower than the latter. In our simulations and analyses of real datasets we rely on Approximation 1 whenever applicable. We provide details for choosing an appropriate approximation in Section 5.

### 3 Statistical Calibration, Power and Robustness

We evaluate our test (V-test) by considering its control of false positive rate (FPR) and its statistical power on simulated data. We consider a variety of simulation scenarios when evaluating statistical power, effectively providing a systematic framework for measuring the robustness of *any* unsupervised test of exchangeability. We study the robustness of our test using this framework, and report the area under the receiver-operating curve (AUROC) obtained by pairing a null model with a non-exchangeable alternative model. To allow for comparison, we also evaluate the performance of a ‘‘Tracy-Widom’’ (TW) approach based on the largest eigenvalue of the centered Gram matrix of  $\mathbf{X}$ , which we now describe.

Assume that  $\mathbf{X} \in \mathbb{R}^{N \times P}$  consists of  $N$  i.i.d. sub-Gaussian vectors in  $\mathbb{R}^P$ , where for each vector the  $P$  components are independent and each is distributed with zero mean and unit variance. A celebrated result in random matrix theory says that under the assumptions (i)  $N \rightarrow \infty, P \rightarrow \infty$ , and (ii) the ratio  $P/N$  stays uniformly bounded by a constant lying in  $(0, \infty)$ , the normalized maximum singular value  $s = \sigma_{\max}(\mathbf{X})$  satisfies

$$\frac{s^2 - (\sqrt{N-1} + \sqrt{P})^2}{(\sqrt{N-1} + \sqrt{P}) \left( \frac{1}{\sqrt{N-1}} + \frac{1}{\sqrt{P}} \right)^{1/3}} \xrightarrow{d} F_1(s),$$

where  $F_1$  is the Tracy-Widom distribution with ensemble index 1 (Tracy and Widom, 2002), i.e.,

$$(3.1) \quad F_1(x) = \exp \left( - \int_x^\infty [u(s) + (s-x)u^2(s)] ds \right) \quad \text{for } x \in \mathbb{R},$$

with  $u(s)$  defined as the solution to the nonlinear ordinary differential equation  $u'' = 2u^3 + su$  with asymptotic condition  $u(s) \sim \frac{1}{2\sqrt{\pi}s^{1/4}} \exp(-\frac{2}{3}s^{3/2})$  as  $s \rightarrow \infty$ . (The ODE is called the Painlevé II equation and its solution the Hastings-McLeod solution.)

Because the square of the maximum singular value  $\sigma_{\max}(\mathbf{X})$  is just the eigenvalue of the Gram matrix  $\mathbf{X}\mathbf{X}^T$ , an asymptotic test can be devised immediately. Let  $\mathbf{M} := \mathbf{X}_\circ \mathbf{X}_\circ^T$ , where  $\mathbf{X}_\circ$  denotes the column-centered and column-scaled version of  $\mathbf{X}$ . This test, a variant of which was proposed by Patterson et al. (2006) in population-genetic studies, works as follows. Given an individual-by-feature array  $\mathbf{X}$ , for each column  $j \in \{1, \dots, P\}$ , subtract column means  $c_j/N$  from each entry and divide each entry by the normalizing factor,  $\sqrt{\frac{c_j}{N} (1 - \frac{c_j}{N})}$ . Then, an approximate (two-sided)  $p$ -value, under the assumption that  $N$  observations are independently generated, is given by

$$(3.2) \quad p = 2 \times \min \left\{ F_1^{-1} \left( \frac{\lambda(\mathbf{M}) - (\sqrt{N-1} + \sqrt{P})^2}{(\sqrt{N-1} + \sqrt{P}) \left( \frac{1}{\sqrt{N-1}} + \frac{1}{\sqrt{P}} \right)^{1/3}} \right), 1 - F_1^{-1} \left( \frac{\lambda(\mathbf{M}) - (\sqrt{N-1} + \sqrt{P})^2}{(\sqrt{N-1} + \sqrt{P}) \left( \frac{1}{\sqrt{N-1}} + \frac{1}{\sqrt{P}} \right)^{1/3}} \right) \right\},$$

where  $\lambda(\mathbf{M})$  is the largest eigenvalue of  $\mathbf{M}$  and  $F_1$  is the cumulative distribution function in (3.1).

We refer to (3.1) as the TW null distribution, and call  $p$ -values computed using (3.2) the TW test. Anticipating readers who might suspect a ‘‘straw man’’ in the midst of our comparison, we note that some of the approaches mentioned in Section 1.1 have proposed modifications to the TW test to deal with idiosyncrasies like feature dependencies and finite-sample bias. These include using method of moments estimates, pruning or performing regression on features, and fitting reasonably flexible parametric models before performing the test. Here, we are interested in comparing two equally straightforward approaches requiring as few modifications to the original dataset as possible. We also want to provide an honest and helpful evaluation of ‘‘folk wisdom’’ that the TW approximation, per se, is ‘‘surprisingly good,’’ which we believe benefits the broader scientific community.

For the rest of this Section, we describe our choice of null and non-null simulation models and report the AUROCs computed from a null and non-null pair. Results for statistical power and false positive rate analyses are included in Appendix D.

### 3.1 Null Models to Estimate Type I Error

We simulate binary datasets under three simple generative models corresponding to three scenarios: (i) markers have uniformly low population frequencies, (ii) markers have varying population frequencies, and (iii) markers have uniformly high population frequencies. Concretely, each sampled row we draw to form the array is a realization of a product of Bernoulli's,  $\text{Bern}(\theta_1) \times \dots \times \text{Bern}(\theta_P)$ , where the vector of parameters  $\vec{\theta} = (\theta_j : j = 1, \dots, P)$  is fixed and determined by the scenario as follows.

- (i) Low frequencies: Each  $\theta_j \in [0.1, 0.2]$ .
- (ii) Varying frequencies: Each  $\theta_j \in [0.2, 0.55]$ .
- (iii) High frequencies: Each  $\theta_j \in [0.8, 0.9]$ .

To demonstrate the performance of our approach on a range of possible numbers of features present in datasets, we also vary  $P$  by allowing  $P \in \{10, 100, 1000\}$ . Note scenario (i) produces sparse arrays, by which we mean that the number of non-zero entries in  $\mathbf{X}$  is very small compared to the size  $N \times P$  of  $\mathbf{X}$ . In contrast, scenario (iii) produces dense arrays.

### 3.2 Non-Exchangeable Models to Estimate Power

We simulate datasets under a simple hierarchical generative model. We incorporate various sampling designs, parameter choices, and data processing or collection artifacts that reflect realistic datasets, with there being at least 2 distinct populations from which observations are drawn to make up the dataset. Our general model assumes that there are  $K \geq 2$  distinct populations from which  $N_k$  observations are drawn from Population  $k$  ( $1 \leq k \leq K$ ) to make up a sample of size  $N$ . These populations are distinct owing to the frequency of each binary feature being distinct at the population level. To produce these distinct population frequencies in turn, we generate them as realizations of uniform distributions. The entire generative process can be described concretely as follows (see Figure 3 for a plate diagram).

- (1) Fix  $\varepsilon$ , a hyperparameter that controls the range of marker frequencies for the population, and also determines overall how discerning the  $P$  markers are between distinct populations.
- (2) For a population  $k$  ( $1 \leq k \leq K$ ), independently draw  $P$  realizations from a uniform distribution parametrized by  $\varepsilon$  and dependent on  $k$ . For example,

$$\theta_j^{(k)} \stackrel{\text{iid}}{\sim} \text{Uniform}[0.5 + 0.075 \cdot (-1)^k - \varepsilon, 0.5 + 0.075 \cdot (-1)^k + \varepsilon].$$

This produces marker frequencies for Population  $k$ . (Details on dependency of the uniform distribution on  $k$  are described in the Appendix D.2.)

- (3) To draw a sample of size  $N_k$  from Population  $k$ , independently draw  $P$  realizations of Bernoulli distributions, where each Bernoulli distribution  $j$  is parametrized by  $\theta_j^{(k)}$ . In other words, for  $i = 1, \dots, N_k$ ,

$$\mathbf{x}_i \stackrel{\text{iid}}{\sim} \text{Bern}(\theta_1^{(k)}) \times \dots \times \text{Bern}(\theta_P^{(k)}).$$

Our sampling designs, parameter choices, and data processing artifacts fall under seven scenarios, as listed in Table 1. To compare statistical power, we generate our datasets by pairing Scenarios 3-7 with Scenarios 1 and 2 in Table 1, illustrating the impact of the sample size  $N$  and the closeness of subpopulation features on the particular former scenario. Moreover, to investigate the performance of our approach on a range of possible numbers of features present in datasets, we also vary  $P$  by allowing  $P \in \{10, 100, 1000\}$ . We estimate power by averaging the true positive rate. Because Section 5.1 shows that the large- $P$  approximation is good for  $P \geq 50$ , we apply the large- $P$  approximate test whenever  $P \in \{100, 1000\}$ . Altogether, we perform  $[5 \times 4 \times (6 + 9 + 9)] \times 3 \times 2 = 2880$  sets of simulations and power estimations, across the two test types (TW versus V).

### 3.3 ROC Analysis Reveals Robustness of Non-parametric Test

As we report in Appendices D.1 and D.2, results from running simulations described above reveal complex performances of our test and of the TW test. To provide a holistic comparison of our approach against TW,

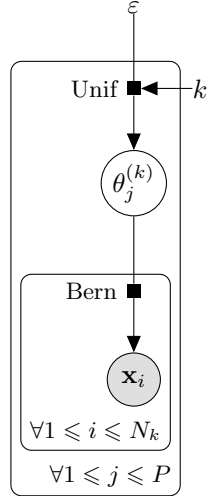


FIGURE 3. Plate diagram for our generative process. Specifically, the generative mechanism for observations drawn from an arbitrary population  $k$  ( $1 \leq k \leq K$ ) is shown. Note that the endpoints of the uniform distribution depend on  $k$ .

TABLE 1. Seven scenarios we consider when generating non-exchangeable samples.

Scenario	Relevance or Meaning
1. Number of observations	The sample size $N$ of the dataset on which the test is to be performed.
2. Closeness of subpopulation features or parameters	How close the true marker frequencies are between the populations whose representatives make up the sample.
3. Number of subpopulations	The number of distinct true populations, $K$ , from which observations were drawn to make up the sample.
4. Sparsity of discriminative features	The number of features among all $P$ features that truly discriminate between the populations whose representatives make up the sample.
5. Evenness of sampling	How evenly represented the various distinct populations are in the sample.
6. Different sources of heterogeneity	How differences in population marker frequencies affect row sums.
7. Column flipping	For binary or binarizable markers, where the binarization provides an interpretation of ‘1’ and ‘0’ for the resulting binary array, the existence or absence of erroneous binarization.

we consider our test as a binary decision procedure, whereby a dataset is assumed to be drawn uniformly at random from exactly one of a specified pair of generative models, and classified as exchangeable or heterogeneous based on a user-specified significance level  $\alpha$ . We pair our null models from Section 3.1 against the non-null generative models considered in Section 3.2, and generate receiver-operating characteristic (ROC) curves by sliding the user-specified significance level  $\alpha$  from 0 to 1. We evaluate classification accuracy by computing the area under the ROC curve (AUROC). A total of  $3 \times (4 + 9 + 9) \times (3 \times 3) \times 4 \times 2 = 4752$  AUROCs are computed across all pairings (null with non-null), subpopulation closeness parameters (four choices of  $\varepsilon$ ) and test types (TW versus V). See Appendix D.3 for details.

We find that our test achieves AUROC at least 0.5, across all sample sizes  $N$ , numbers of features  $P$ , and pairings considered; see Figure 4A. This shows that our test performs at least as well as a random classifier,

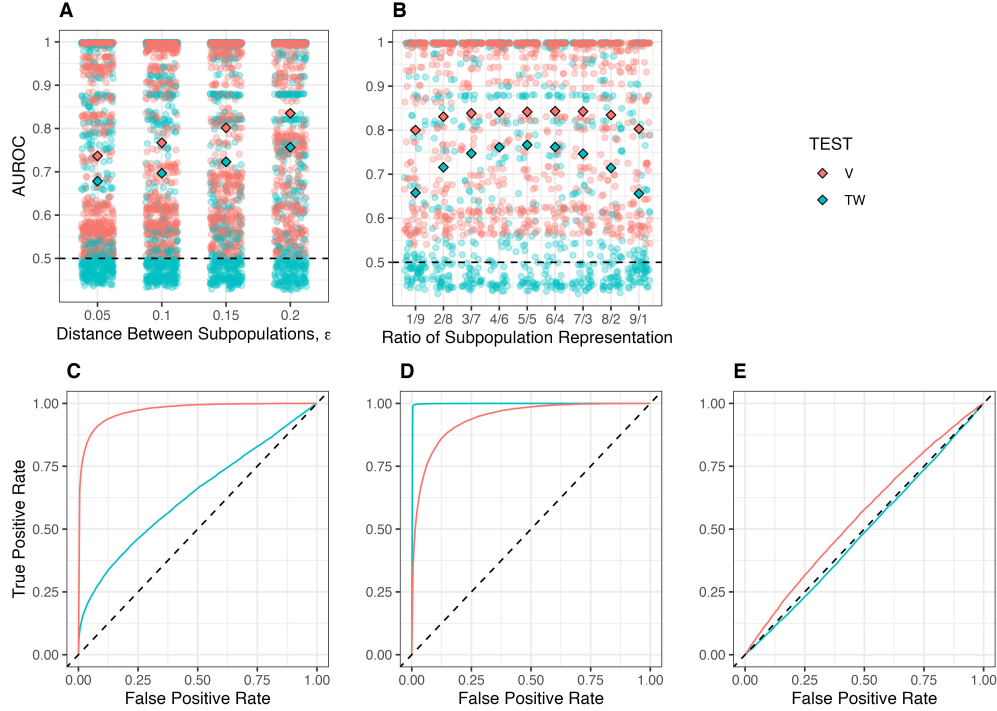


FIGURE 4. **Top Row** shows AUROCs of the V-test and of the TW test for pairings of a null model and a non-exchangeable model, with solid diamond points reporting the mean AUROCs for the particular test. **Bottom Row** shows ROCs generated from pairing a null model and a non-exchangeable model, both of which generate samples containing  $N = 50$  observations and  $P$  features. **A.** AUROC points are split into different distances between subpopulations (Scenario 2, Table 1). **B.** AUROC points are split into different choices of sampling unevenness (Scenario 5, Table 1). **C.**  $P = 100$  features generated. For the non-exchangeable model, individuals are drawn from  $K = 2$  populations such that 5 individuals are drawn from Population 1 and the remaining 45 are drawn from Population 2; population closeness set to  $\epsilon = 0.2$ . **D.** 25 individuals are drawn each from  $K = 2$  populations, with  $P = 1000$  features only 20% of which truly discriminate between the two source populations; population closeness set to  $\epsilon = 0.2$ . **E.** 25 individuals are drawn each from  $K = 2$  populations, with  $P = 100$  features only 20% of all features truly discriminate between the two source populations; population closeness set to  $\epsilon = 0.2$ .

*regardless of* the choice of non-exchangeable model — which is one indication of robustness. The same is not true for the TW test. That many AUROCs for the TW test lie below 0.5 leads to our test being a better classifier on the whole. (See Figures S12-S14 for AUROCs plotted against the various non-exchangeable models considered.) More precisely, we also find that our test is particularly robust to sampling unevenness. Figure 4B shows that V on average has a higher AUROC and less variability than TW when varying the degree of evenness while holding all other scenario variables constant. In fact, as Figure 4C shows, in case the representation of subpopulations in the sample is very uneven, our test still has reasonably high AUROC, but the TW test has a markedly smaller AUROC.

Finally, we find that our test is a relatively weak classifier in cases where the number of discerning features is small; see Figure 4D, for example. (Figure S13 reports all AUROCs against this scenario.) In such cases, the TW test achieves higher classification accuracy overall, even though for small to moderate number  $P$  of features, our test is still more efficacious, owing to the TW test having AUROC less than 0.5; see Figure 4E for example.

## 4 Adapting to Feature Dependencies

Statistical independence between features does not hold in many realistic settings. There are many ways in which the  $P$  features of  $\mathbf{X}$  can depend on each other, for instance, as observations of an undirected graphical model, or as draws from a stochastic process, or as blocks satisfying between-block independence and within-block dependence. In our present work we consider the setting where the  $P$  features are *partitionable*. That is, our  $P$  features can be partitioned into  $B$  sets or blocks  $\{1, \dots, P_1\}, \dots, \{P_{B-1} + 1, \dots, P_B\}$  with block delimiters  $1 \leq P_1 < \dots < P_B = P$ , so that features within the same block are not statistically independent, but features belonging to different blocks are. We modify our permutation null hypothesis to accommodate such dependencies as follows: instead of permuting the  $P$  features independently, we permute the  $B$  sets or blocks independently, keeping the configuration within each block of observations fixed. We call this resulting distribution on resampled arrays the block permutation null distribution. This procedure is formalized as Algorithm 2 in Appendix B.

### 4.1 Asymptotic Null Distribution

Our asymptotic theory carries over to this setting when  $B \rightarrow \infty$  as  $P \rightarrow \infty$ : as in the independent features case (cf. Theorem 1), we may approximate the block permutation null distribution with a convolution of two scaled chi-square distributions. This enables our approach to scale to wide datasets ( $P \gg N$ ) even when the features of the dataset are dependent, as long as the number of independent blocks  $B$  is large enough. This theoretical result is described in the following theorem below.

**Theorem 3** (Large- $P$  and Large- $B$  Approximation of Block Permutation Null). *Let  $V^{(N,B,P)*}$  be the random variable with the block permutation null distribution of  $V^{(N,P)}$ , where the blocks have delimiters  $1 \leq P_1 < \dots < P_B = P$ . For each block  $b = 1, \dots, B$ , let  $d^{(b)}(\mathbf{x}, \mathbf{x}')$  denote the partial Hamming distance of binary vectors  $\mathbf{x}$  and  $\mathbf{x}'$ , that is, the Hamming distance computed along that block only. (Note that under this definition the Hamming distance  $d_H(\mathbf{x}, \mathbf{x}') = \sum_{b=1}^B d^{(b)}(\mathbf{x}, \mathbf{x}')$ .) Define the quantities*

$$\begin{aligned} \alpha^{N,B,P} &= \frac{1}{P} \sum_{b=1}^B \left( \overline{d^{(b)}(\mathbf{x}_{i_1}, \mathbf{x}_{i_2})^2} - \left[ \overline{d^{(b)}(\mathbf{x}_{i_1}, \mathbf{x}_{i_2})} \right]^2 \right), \\ \beta^{N,B,P} &= \frac{1}{P} \sum_{b=1}^B \left( \overline{d^{(b)}(\mathbf{x}_{i_1}, \mathbf{x}_{i_2}) d^{(b)}(\mathbf{x}_{i_1}, \mathbf{x}_{i_3})} - \left[ \overline{d^{(b)}(\mathbf{x}_{i_1}, \mathbf{x}_{i_2})} \right]^2 \right), \\ \gamma^{N,B,P} &= \frac{1}{P} \sum_{b=1}^B \left( \overline{d^{(b)}(\mathbf{x}_{i_1}, \mathbf{x}_{i_2}) d^{(b)}(\mathbf{x}_{i_3}, \mathbf{x}_{i_4})} - \left[ \overline{d^{(b)}(\mathbf{x}_{i_1}, \mathbf{x}_{i_2})} \right]^2 \right), \end{aligned}$$

where the indices  $i_1, i_2, i_3$  and  $i_4$  are distinct and the overline notation denotes taking the average over all pairs, triples, or quadruples of observations. Further, define the quantities

$$\begin{aligned} b_1^{N,B,P} &= \alpha^{N,B,P} + (N-4)\beta^{N,B,P} - (N-3)\gamma^{N,B,P}, \\ b_2^{N,B,P} &= \alpha^{N,B,P} - 2\beta^{N,B,P} + \gamma^{N,B,P}. \end{aligned}$$

Letting  $\lim_{B,P \rightarrow \infty} b_i^{N,B,P} = b_i^N$  for  $i = 1, 2$  and assuming the limits exist, define the random variable

$$V^{(N,\infty,\infty)} = \frac{b_1^N \chi_{N-1}^2 + b_2^N \chi_{\binom{N-1}{2}}^2}{\binom{N}{2}}.$$

Then,  $V^{(N,B,P)*} \xrightarrow{d} V^{(N,\infty,\infty)}$  as  $B, P \rightarrow \infty$ . In other words, for  $B$  and  $P$  large,  $V^{(N,B,P)*} \stackrel{d}{=} V^{(N,\infty,\infty)}$  approximately.

To evaluate the approximation accuracy of Theorem 3 in practice, we empirically evaluate its control of FPR. We simulate data under two different generative models that produce samples with partitionable features: (1) concatenation of a binarized autoregressive time series; and (2) concatenation of a coalescent model commonly used as a generative model for population-genetic datasets. Whereas Model (1) produces blocks of the same size, Model (2) does not. In both cases we fix  $B = 50$  and consider varying sample sizes  $N \in \{10, 50, 100, 500, 1000\}$ , and perform Monte Carlo estimation of the FPR at significance threshold  $\alpha = 0.05$  by simulating 200,000 replications for each model and running the approximate test. As shown

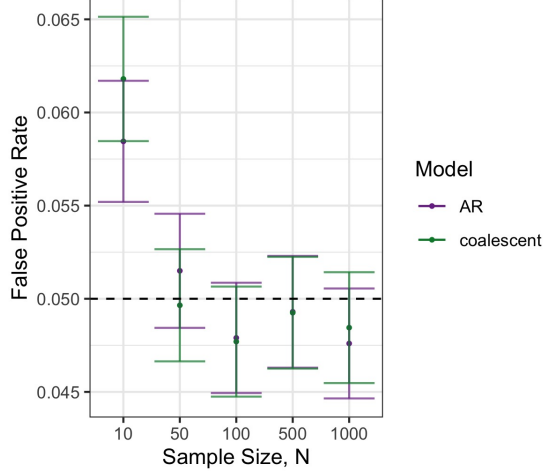


FIGURE 5. Monte Carlo estimates of FPR of the approximation to the block permutation null distribution on datasets simulated under an autoregressive model (AR) and a population-genetic coalescent model. Error bars denote 95% confidence intervals.

in Figure 5, we find our block permutation null largely controls FPR, with the approximation rejecting the null more frequently than  $\alpha$  only when  $N = 10$ . This provides evidence that our approximation is good for reasonably large sample sizes. (One can run the permutation test on datasets with few observations, which is not time-consuming.)

## 4.2 A General Non-parametric Test of Exchangeability

The statement of Theorem 3 reveals an even more general version of our test of exchangeability, one that requires only pairwise distance data across a set of independent blocks of features of a multivariate dataset. Suppose that we are given a  $N \times P$  dataset  $\mathbf{X}$  containing  $P$  partitionable features, with the features grouped into  $B$  blocks. Each feature can be real- or complex-valued, or even be objects lying in a metric space ( $B = P$  corresponds to the scenario where the  $P$  univariate features are independent, and so each block consists of a single feature.) For each pair of observations  $\mathbf{x}, \mathbf{x}'$ , let  $\{d^{(b)}(\mathbf{x}, \mathbf{x}') : b = 1, \dots, B\}$  be the collection of  $B$  distances where each distance is computed on one of the blocks of features. In case the  $B$  blocks of features come from  $B$  underlying metric spaces  $\{(\Omega_b, d^{(b)}) : b = 1, \dots, B\}$ , then all that is needed are the distances computed on the observed data objects. Note  $d^{(b)}(\cdot, \cdot)$  and  $d^{(b')}(\cdot, \cdot)$  need not be the same distance function for distinct blocks  $b$  and  $b'$ . In practice, these distance functions are chosen based on the user application, especially when different groups of features come from distinct data modalities. For concreteness we list two examples with two blocks ( $b = 1, b' = 2$ ).

- We could have  $d^{(b)}(\mathbf{x}, \mathbf{x}') = \frac{1}{2} \|\mathbf{x}_{1:P_1} - \mathbf{x}'_{1:P_1}\|_1$  and  $d^{(b')}(\mathbf{x}, \mathbf{x}') = \max(\mathbf{x}_{(P_1+1):P_2} - \mathbf{x}'_{(P_1+1):P_2})$ , where  $\mathbf{x}_{k:\ell}$  denotes the subvector of  $\mathbf{x}$  obtained by keeping components  $k$  up to  $\ell$  of the original.
- Suppose each sample  $\mathbf{x} = (\omega_b, \omega_{b'})$  lies in the product of metric spaces  $(\Omega_b, d^{(b)}) \otimes (\Omega_{b'}, d^{(b')})$ . Here the space  $(\Omega_b, d^{(b)})$  could be a space of phylogenetic trees equipped with some tree metric (e.g., Billera-Holmes-Vogtmann treespace with the BHV metric (Billera et al., 2001)), while  $(\Omega_{b'}, d^{(b')})$  could be a space of compactly supported probability distributions equipped with the Wasserstein metric.

Instead of  $V$  defined by (2.2), we now let  $d_g(\mathbf{x}, \mathbf{x}') = \sum_{b=1}^B d^{(b)}(\mathbf{x}, \mathbf{x}')$ , and define

$$(4.1) \quad V_g(\mathbf{X}) = \frac{1}{P \binom{N}{2}} \sum_{i < j} [d_g(\mathbf{x}_i, \mathbf{x}_j) - \mu_g]^2,$$

with

$$(4.2) \quad \mu_g = \frac{1}{\binom{N}{2}} \sum_{i < j} d_g(\mathbf{x}_i, \mathbf{x}_j).$$

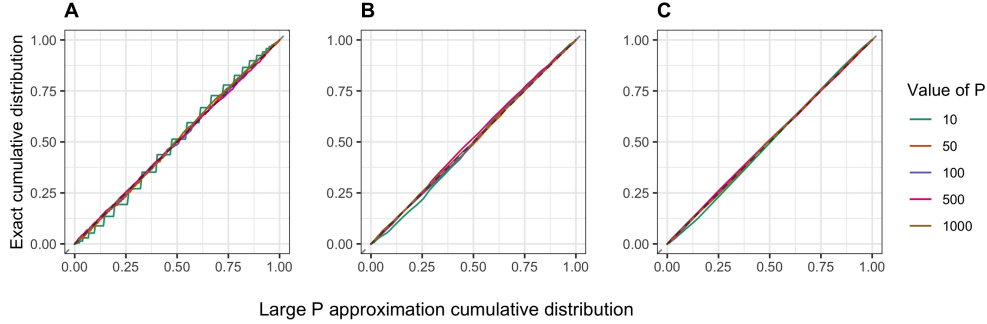


FIGURE 6. Probability-probability plots of the permutation-based distribution,  $F_{\text{perm}}$ , against the large  $P$  approximation. **A.**  $N = 10$ . **B.**  $N = 100$ . **C.**  $N = 1000$ .

With these quantities, the general test is then permuting the blocks independently across the observations and computing the proportion of resampled  $V_g$  values larger than or equal to the observed value. This procedure is formalized as Algorithm 3 in Appendix B.

Similar to Theorem 3, a “large  $B$  and large  $P$ ” chi-square approximation to the block permutation null distribution can be obtained for the statistic  $V_g^*$ .

To our knowledge, this general version of our test is the first test of exchangeability requiring only pairwise distance data. Moreover, in practical applications it can be exploited to reduce the memory burden of performing the permutation test on ultra-high dimensional data sets with only a small number of independent blocks, where large  $P$  asymptotics are invalid and thus inappropriate. We provide examples in our online vignette [Extras](#)<sup>3</sup>.

## 5 Speed and Accuracy of Asymptotic Approximations

We justify the use of our approximate null distributions in practice, by investigating both the accuracy of these approximations via theory and simulations, as well as the speed gains by implementing these approximations over permutation resampling.

### 5.1 Theory and Simulations Verify Accuracy of Approximations

We find that the total variation distance between the permutation null distribution  $F_{\text{perm}}$  as described in Section 2, and the large  $P$  distribution as described in Theorem 1, goes to zero at a rate proportional to the square root of the number of independent features,  $P$ .

**Theorem 4** (Large  $P$  Approximation Convergence Rate). *For any fixed sample size  $N$ , the rate of convergence of the permutation null distribution to its large  $P$  approximate distribution, measured by a bound in the total variation distance, is of order at most  $O(P^{-1/2})$ . Specifically, for a fixed sample size  $N$ , let  $V^{(N,P)*}$  and  $V^{(N,\infty)}$  be defined as in Theorem 1. Then, there exists a positive constant  $C$ , which depends only on  $N, a_1^N$  and  $a_2^N$ , such that for all  $t \geq 0$ ,*

$$\left| \mathbb{P}(V^{(N,P)*} \leq t) - \mathbb{P}(V^{(N,\infty)} \leq t) \right| \leq \frac{C}{\sqrt{P}}.$$

In practice, we find that for  $P = 50$  independent features — regardless of the magnitude of the sample size  $N$  (Figure 6) — the approximation is accurate. This is consistent with the “rule of thumb” for the Central Limit Theorem to kick in.

We observe similar fast convergence in practice for the large  $P$  and large  $N$  approximation as described in Theorem 2 (Figure S16), but we also find that the parametric bootstrap described in Section 2.2 converges slower to the null (Figure S15). Based on our simulations we recommend using the chi-square approximation as long as  $P \geq 50$ , and recommend using the parametric bootstrap approximation only when  $P < 50$  and  $N \geq 500$ . When  $N \geq 50$  and  $P \geq 50$  the normal approximation is also fine. Note these recommendations

<sup>3</sup><https://alanaw1.github.io/flintyR/articles/extras.html#test-of-exchangeability-using-pairwise-distances-1>

TABLE 2. Average runtime (in seconds) for each algorithm to compute a single  $p$ -value from arrays with varying dimensionalities. **Boldfaced times** indicate that the algorithm is statistically appropriate for the problem’s dimensionalities as evidenced by the analysis in Section 5.1.

Dimensionality	Permutation-Based	Chi-square	Bootstrap	Normal
$N = 50, P = 50$	<b>4.52</b>	$3.99 \times 10^{-3}$	3.20	$9.40 \times 10^{-4}$
$N = 50, P = 500$	<b>27.81</b>	$1.07 \times 10^{-2}$	8.30	$7.87 \times 10^{-3}$
$N = 500, P = 50$	<b>37.36</b>	$1.33 \times 10^{-2}$	<b>97.81</b>	$1.11 \times 10^{-2}$
$N = 500, P = 500$	<b>96.01</b>	$4.10 \times 10^{-2}$	<b>81.68</b>	$3.78 \times 10^{-2}$

are based solely on the approximation accuracy; as we will see in Section 5.2 accounting for efficiency will narrow down our recommendations even further.

A similar analysis can be performed on the large  $B$  and large  $P$  approximation to the block permutation null distribution described in Section 4. Specifically, owing to similar boundedness assumptions holding in the block permutation null setting, a convergence rate of  $O(B^{-1/2})$ , where  $B$  is the number of independent blocks, can also be obtained for the approximation in Theorem 3. Like the independent features case, we have observed empirically faster rates of convergence, making our large  $B$  and large  $P$  approximation suitable in settings where the number of independent blocks  $B$  is as small as 50 — with block sizes possibly varying across blocks — as long as  $N \geq 50$ .

## 5.2 Speed Gains for Wide and High-Dimensional Arrays

To compare the speed gains from running our approximations, we run our permutation test and its approximations on 100 simulated datasets with varying dimensionalities  $(N, P) \in \{(50, 500), (50, 50), (500, 50), (500, 500)\}$ , calculating the time it takes for each algorithm to compute 100  $p$ -values from 100 generated arrays of varying dimensions. For both the exact and the parametric bootstrap resampling algorithms, we set the resampling number  $R = 5000$ . We run all algorithms on a Macbook Pro CPU with 4 cores, a 2.3GHz processor and 16GB memory.

Table 2 summarizes our runtime experiment, where we report the average runtime across all 100  $p$ -value computations. We find that the chi-square test is on average at least 2000 times faster than the permutation test. We also find that the parametric bootstrap can surprisingly be slower than the permutation test for problem dimensionalities where it is applicable. This is likely to do with our optimized implementation of the permutation test, where we (1) compute Hamming distances with C or C++ bitwise operations, and (2) cache pairwise Hamming distances with their corresponding sample indices, to avoid costly Hamming distance computations required per permutation.

Considering both the accuracy and the speed gains of our approximations, we find that the chi-square approximation is the most reliable in practice and we recommend its use as long as  $P \geq 50$ . (In all other cases, use the permutation test.) The normal approximation is also reliable, but considering the practically insignificant differences in runtimes we do not strongly recommend it.

## 6 Application to Data

We demonstrate our approach on one simulated and two real datasets, showing how careful use of our exchangeability test provides statistically sound and interpretable information about the data. We keep our exposition self-contained at the cost of technical details, but interested users should explore our accompanying vignettes, which elaborate on the domain-specific technicalities and summarize key steps about repurposing our methods for other similar datasets.

### 6.1 How to avoid risking double dipping: illustration using simulated genomes

Double dipping, which was described in the Introduction, arises when insufficient care is taken in data analysis that involves multiple stages of computational work. While there are at least three well-documented instances of the phenomenon (Kriegeskorte et al., 2009), here we focus on a two-stage pipeline involving clustering and differential analysis, where the result of clustering can bias differential analysis due to the clustering method inherently searching for discriminative features to determine clusters.

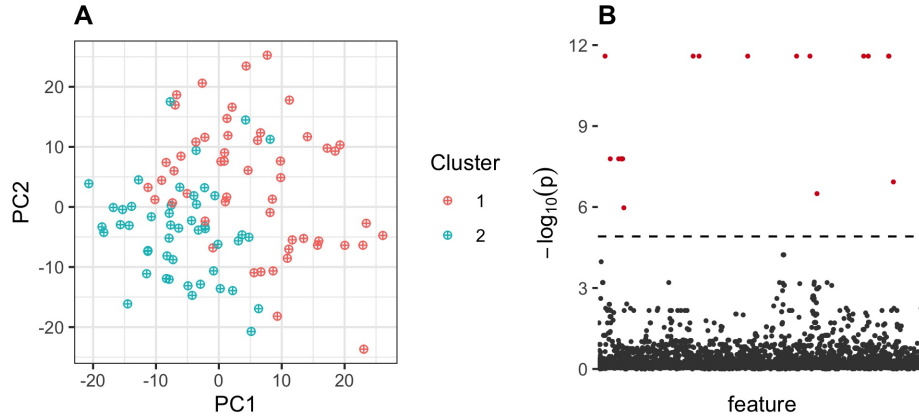


FIGURE 7. **A.** Projection of the  $N = 100$  individuals onto their first two principal components. **B.** Plot of transformed  $p$ -values, with significance threshold set at  $0.05/P$  ( $P$  denoting the number of features) to control for FWER at 0.05.

As mentioned in Section 1.1, one way to avoid double dipping is to ensure that the post-clustering differential analysis accounts for inherent “biases” in the clustering algorithm. This is the approach taken by Zhang et al. (2019) and by Gao et al. (2021). We show that our approach can be used to avoid risking double dipping, by *deciding beforehand* whether clustering is necessary.

To illustrate our approach, we simulate exchangeable genomes that share a population history using the coalescent simulator `msprime` (Kelleher et al., 2016). We choose to simulate genomes because it underscores the importance of accounting for feature dependencies, which we view as critical to the efficacy of our approach in practice. A simpler “domain-agnostic” simulation study involving Gaussian samples comprised of independent entries is provided in our online vignette [Introduction](#)<sup>4</sup>.

In haploid organisms, the genome can be viewed as a binary vector  $\mathbf{x} \in \{0, 1\}^P$ , where each component is a genetic variant (either of ancestral or mutant type). The cellular process of recombination breaks down dependencies between variants situated far apart within the same chromosome, with intrachromosomal variants in high linkage disequilibrium appearing correlated. In our simulation, we sample  $N = 100$  genomes from a large randomly mating population, where genetic variants (also known as single nucleotide polymorphisms, SNPs) are drawn from  $B = 10$  chromosomes to make up the  $N \times P$  dataset. Because of the way mutations are generated, the number of SNPs  $P_b$  contributed by each chromosome  $b$  differs. (Overall, for our particular simulation we observe  $P = \sum_{b=1}^B P_b = 4067$  SNPs across all 10 chromosomes.) In this setup, our  $B = 10$  blocks are independent but block sizes are not the same, and moreover the 100 genomes  $\{\mathbf{x}_1, \dots, \mathbf{x}_N\}$  are putatively exchangeable.

If we were handed  $\mathbf{X}$  without knowing its generative mechanism completely, we might want to perform clustering as part of exploratory data analysis. We compute Prevosti’s distance (Prevosti et al., 1975) between each pair of individuals, and perform hierarchical clustering with Ward linkage and the resulting matrix of Prevosti distances. We consider a clustering of the individuals into  $k = 2$  clusters by cutting the hierarchical clustering tree where there are two clusters, obtaining a cluster assignment for each sample. We can visualize the clustering using PCA, as shown in Figure 7A. Next, we perform Wald-Wolfowitz runs tests (Wald and Wolfowitz, 1943) between the two clusters for each binary SNP feature, applying Bonferroni correction to control the family-wise error rate (FWER) at  $\alpha = 0.05$ . We find many features — shown in the Manhattan plot of Figure 7B — that are statistically significant, which the user might erroneously report as discriminative features. Put in a population-genetic context, such significant features would be candidate SNPs for ancestrally informative markers, which we know to be false given that the observations were really drawn from a single, panmictic population.

We can avoid the Type I error described above by running our test on  $\mathbf{X}$ . However, owing to linkage disequilibrium, correlations between SNPs lying in the same chromosome exist. These feature correlations

<sup>4</sup><https://alanaw1.github.io/flintyR/articles/intro.html>

induce spurious correlations between observations, which could falsely suggest the presence of subpopulations. Without accounting for these feature dependencies (i.e., if the independent features version of our test were applied), we would falsely find evidence of heterogeneity ( $p$ -value = 0).

Instead, a correct application of our test of homogeneity must account for feature-feature dependencies. By running the independent blocks version of our test, where the 10 blocks correspond to the 10 chromosomes, we obtain a  $p$ -value of 0.1476, which shows that there is insufficient evidence (even at  $\alpha = 0.1$  significance) that  $\mathbf{X}$  is heterogeneous. We therefore correctly conclude that  $\mathbf{X}$  is homogeneous, or unstratified.

To ensure our particular simulated sample and conclusion above are not purely coincidental, we repeat the simulation experiment 200 times. Additionally, we compare with EIGENSOFT (v7.2.1) (Patterson et al., 2006), a method based on the Tracy-Widom theory described in Subsection 3.2, albeit with some modifications. When implementing EIGENSOFT, instead of grouping SNPs into blocks to account for feature correlations, we consider both LD pruning and regression of markers to remove linkage-induced correlations between neighbouring SNPs, as recommended by the authors (see pp. 2077-2078 of Patterson et al., 2006). For both approaches, as well as our V test, we compute the false positive proportion at  $\alpha = 0.05$ . We find that V has a false positive proportion of 0.02, whereas both implementations of EIGENSOFT yielded inflated false positive proportions (LD pruning FPP = 0.585, marker regression FPP = 0.905). We report this study in greater detail in our online vignette [Population Stratification](#)<sup>5</sup>.

This example also reveals the tension between feature dependencies and sample exchangeability, a fundamental dilemma in the unsupervised analysis of multivariate data. The interested reader can find a deeper exploration of this tension in our online vignette [Exchangeability and Homogeneity](#)<sup>6</sup>.

## 6.2 Are single cell clusters homogeneous?

In cellular biology, the study of single cells allows biologists to discover mechanisms not detectable by studying only bulk populations of cells. In recent years, advances in sequencing technologies have enabled the quantification of a variety of features (e.g., transcriptome, proteome, metabolome, 3D contact maps), and such datasets have in turn provided new statistical challenges and spurred the development of new probabilistic models (Lähnemann et al., 2020). Key to discovering mechanisms from single cell data are analyses of heterogeneity between single cell populations and the modeling of features of homogeneous cell populations. Heterogeneous patterns across multiple biological features reveal biological differences between groups of cells that differ by physical location, temporal factors, or some other biological function, and such differences can subsequently help generate hypotheses relating features to function.

To demonstrate our method, we analyze human peripheral blood mononuclear cell (PBMC) scATAC-seq data provided by 10X Genomics<sup>7</sup>. First, using Seurat (Stuart et al., 2019) and its extension, Signac (v1.3.0) (Stuart et al., 2020), we perform all steps of data processing up to non-linear dimension reduction and clustering. Briefly, these steps comprise (1) filtering individual cells according to quality control metrics; (2) feature engineering as a pre-clustering step to remove technical noise; and (3) clustering. We obtain  $N = 7060$  cells separated into 15 clusters, whose visualization is shown in Figure 2 in the Introduction. To interpret the clusters, we perform an additional step of cell type annotation using accompanying single cell RNA-sequencing measurements of the same individual cells. Assuming that these annotations are the ground truth labels, we find that the clusters are mostly homogeneous with respect to cell types, with a clearly dominant cell type making up each cluster (see Figure 8).

To detect if any sources of heterogeneity remain in the clusters, we ran the independent features version of our test with  $\ell_2$  metric (Euclidean distance) on each cluster and each cell type subcluster. We obtained  $p$ -values of  $10^{-16}$  using the asymptotic test, which shows that the null hypothesis of cluster exchangeability and independence of features is false. This implies that either the clusters and subclusters are heterogeneous, or that the peaks are not independent, or both.

The features of our dataset are normalized peak counts at physical regions along the genome. We expect statistical dependencies between these peaks, because chromatin, comprising DNA and all of the proteins that contribute to its 3D structure in the cell nucleus, modulates its accessibility during gene regulation,

<sup>5</sup>[https://alanaw1.github.io/flintyR/articles/pop\\_strat.html](https://alanaw1.github.io/flintyR/articles/pop_strat.html)

<sup>6</sup>[https://alanaw1.github.io/flintyR/articles/ex\\_vs\\_hom.html](https://alanaw1.github.io/flintyR/articles/ex_vs_hom.html)

<sup>7</sup>The single cell ATAC-seq dataset — “10k Peripheral blood mononuclear cells (PBMCs) from a healthy donor” by Cell Ranger 3.1.0, 10x Genomics — is available through 10x Genomics upon filling in an online registration form, <https://www.10xgenomics.com/resources/datasets>.

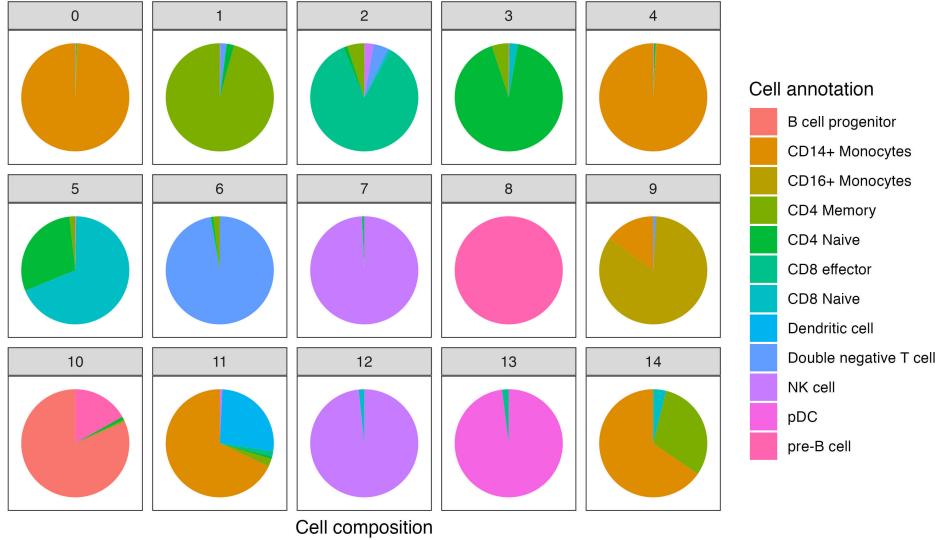


FIGURE 8. Pie chart of cell type composition of each cluster. See Table S1 in the Appendix for cell composition percentages.

so that genes that are co-regulated could potentially induce co-accessibility of the corresponding physical regions. Thus, to obtain blocks of potentially dependent features we group peaks by shared membership in topologically associating domains (TADs), which are regions in the 3D genome within which loci are in frequent contact. We obtain our TADs using publicly available Hi-C data and the TAD calling algorithm DomainCaller, and restrict to Chromosome 1 peaks to reduce the analysis runtime. This results in Chromosome 1 peaks grouped into contiguous blocks.

After running the independent blocks version of our test ( $B = 232$  blocks in total) at  $\alpha = 0.05$  significance, we still find that all clusters and cell type subclusters had  $p$ -values much smaller than  $\alpha$ , except for three subclusters (6 CD4 Memory cells and 5 CD4 Naive cells from Cluster 0, 7 CD4 Memory cells from Cluster 6). Thus, our test provides evidence of heterogeneity or stratification in most clusters and their cell type subclusters, if we assume that the grouping of features into TAD blocks to account for correlations induced on peaks is reasonable. Alternatively, if we assert that the clusters and subclusters are exchangeable, then grouping peaks by common TAD membership does not completely capture the complex dependencies between peaks.

To further explore the first interpretation, we consider Cluster 12 (60 cells) and focus on the subcluster consisting of 59 NK cells (one cell is CD8 Naive). We find that about 80% of this subcluster’s features have 90% of their normalized peaks equal to 0. This shows that the peak counts matrix is sparse. After removing features from each block that are too sparse and running our test once more, we find that the subcluster is homogeneous at  $\alpha = 0.05$  ( $p = 0.16$ ). Thus, for this subcluster we see that sparsity can explain the heterogeneity in the data. This explanation has a mathematical basis: given that sparsity manifests in the presence of non-zero values for a select few cells, having many sparse features renders these selected cells closer together relative to the other cells. In practice, we observe that many of the sparse features also have very small variances, which supports our explanation (Figure 9, top).

We next pursue the alternative interpretation, that is, under what dependency structure of peaks would clusters appear exchangeable? We focus on Cluster 8, which is made up of 244 pre-B cells. To group the peaks, we perform hierarchical clustering with Ward linkage and distance matrix constructed from peak-peak correlations. Using the Dindex metric, we find that the optimal number of groups is  $B = 46$ . When we ran the independent blocks version of our test at  $\alpha = 0.05$ , we find that the pre-B cell cluster is exchangeable ( $p = 0.31$ ). To interpret the grouping, we visualize how peaks within the same group are distributed. We find that the peaks do not group neatly by physical location, unlike what a TAD grouping would suggest (Figure 9, bottom). This finding suggests that “long-range” peak interactions must be accounted for to explain the homogeneity of the cluster. Such a finding has implications for mathematical and statistical

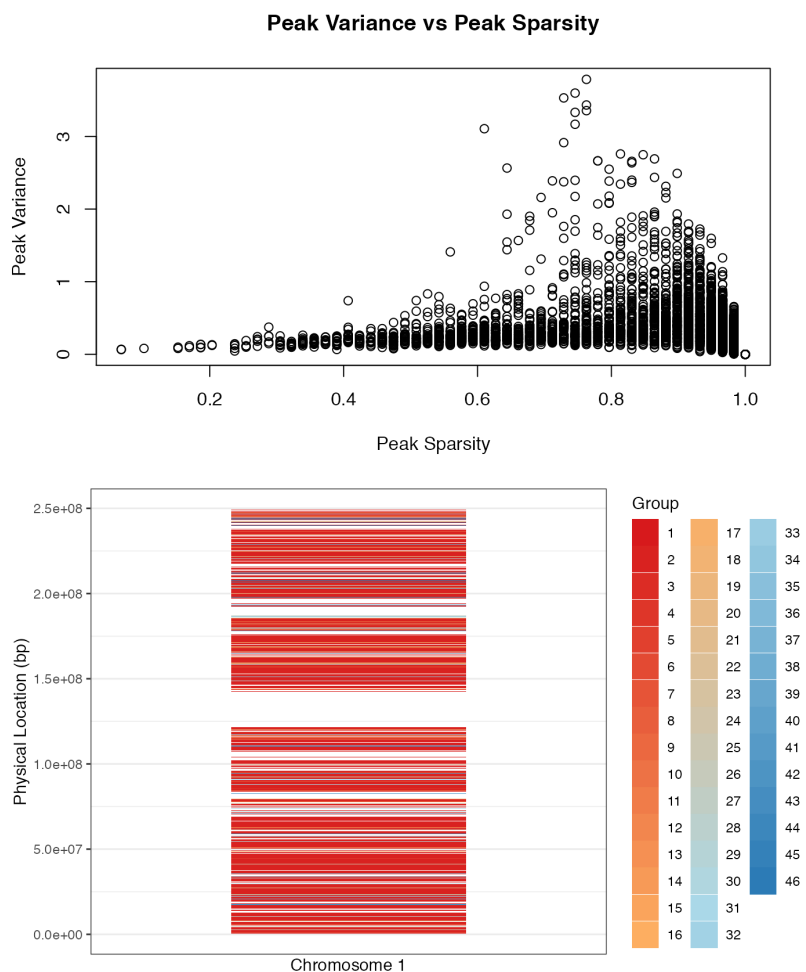


FIGURE 9. **Top.** Scatterplot of sparsity and variance of each normalized peak (column) of the NK cell subcluster of Cluster 12. Along the  $x$ -axis, peaks range from low sparsity (mostly non-zero normalized reads) to high sparsity (almost all zero normalized reads). **Bottom.** Group labels for each peak, with peaks stacked vertically according to their corresponding physical region along Chromosome 1. Labels are obtained from performing hierarchical clustering on normalized peaks of the 244 pre-B cells, as described in the main text. White spaces indicate absence of peaks.

modeling of peak data, namely, that any model relating 3D chromatin structure to chromatin accessibility should not assume that the relationship can be simply localized within contiguous, discrete clusters.

The interested reader can find more details of this application at our online vignette [Analysis of scATAC-seq Data](#)<sup>8</sup>.

### 6.3 Are there cultural differences among Singaporeans?

In cultural and psychological studies, the lack of replicability and generalizability of findings — in part a result of decades of analyses of data originating from primarily Western, Educated, Industrial, Rich and Democratic (WEIRD) societies — has motivated the development of metrics that quantify meaningful differences between societies (Muthukrishna et al., 2020). In contrast to between-society differences that reflect important cultural heterogeneities, differences within putatively singular societies could suggest the presence of distinct communities that reflect meaningful sociological or demographic characteristics. For example, it

<sup>8</sup><https://alanaw1.github.io/flintyR/articles/single-cell-atac-seq.html>

is known that genealogical communities exist within the United States, and the persistence of homogamous mating in such communities is manifested in genetic differences (Han et al., 2017).

We apply our method to analyze data from Wave 6 of the World Values Survey (WVS), a research program aimed at understanding how beliefs, values and norms change over time and across nations globally. Motivated by the question of within-society differences, we focus on interrogating the cultural homogeneity of Singaporeans based on a representative collection of responses to the WVS questionnaire. First, we restrict the features to a subset of WVS questions included by Muthukrishna et al. (2020) in their computation of cultural distances, reducing the number of features to  $P = 51$ . We next recode the categorical responses based on a scheme provided by Muthukrishna et al. (2020) and filter out constant features resulting from the recoding, leading to  $P = 47$  variable features. Finally, we one-hot encode the recoded features to obtain the binarized data on which to perform our statistical tests.

We run the block version of our test on the resulting dataset, with each block corresponding to a one-hot encoded feature, effectively treating question responses as statistically independent. We obtain a  $p$ -value that is less than 0.001. This is not surprising, given that we expect the assumption of statistical independence between responses to be false. For example, it is likely that responses to “Do you believe in God?” and “Do you believe in hell?” are statistically dependent, and indeed we observed a correlation of 0.69 between the responses to these two questions in our data. See Figure 2 (right) for evidence of correlation between questions. We next tried grouping these features into blocks by performing hierarchical clustering with Ward linkage and distance matrix constructed from sample-sample correlations, but we still find that no matter how many blocks  $B$  we select (amounting to cutting the clustering dendrogram to form  $B$  clusters), we still obtain  $p = 0$ . This suggests the correlation structure between the features is complex, and it is likely that there are clusters within the sample that have distinct cluster-specific correlation structures between their features. In a demographic context, we suspect that there are distinct communities of Singaporeans, wherein the responses to the WVS questions have correlation patterns unique to that community.

We cluster the sample using hierarchical clustering with Ward linkage and distance matrix constructed from Euclidean distances between the individuals, assuming that such a clustering is efficacious at recovering demographically meaningful communities.<sup>9</sup> (The “correct” number of clusters,  $K = 10$ , is chosen by 10-fold cross-validation using the Dindex metric.) After obtaining 10 sample clusters, we group the features independently for each sample cluster using the same hierarchical clustering approach described in the preceding paragraph. We then perform the block version of our test at multiple number of blocks  $B$  partitioning our features, where each configuration corresponds to cutting the clustering dendrogram to form  $B$  feature clusters. Note by varying  $B$ , we are exploring how the grouping of question responses affects whether the variation of responses in a sample cluster can be explained away by randomness or is instead indicative of heterogeneity.

After performing the steps above, we find that all but one cluster (Cluster 8 consisting of  $N = 241$  individuals) returned significant  $p$ -values that imply heterogeneity. However, for the only homogeneous cluster, we find that up to  $B = 10$  blocks, the sample appears homogeneous. This is no longer true when we treat all  $P = 47$  features as statistically independent. Thus, for this cluster, the variation in responses can be attributed to partitionable feature dependencies.

Interpreting our findings in a sociological context, Figure 10 shows a correlation heatmap of responses by individuals in Cluster 8 to the questions; compare with Figure 2 (right). When we run the same hierarchical clustering procedure to group features as we did for the entire sample, we find that for this exchangeable cluster of Singaporeans, responses to questions to do with religion and morality are grouped separately from those to do with obeying civil laws, with the latter group of questions agglomerated together with questions to do with corporate culture. This is in contrast to the agglomeration of the two groups of questions in the overall sample.

The interested reader can find more details of our findings at our online vignette [Analysis of World Values Survey Data](#)<sup>10</sup>.

---

<sup>9</sup>We are at risk of identifying meaningless clusters. However, as we have alluded to in the Introduction, if we treat our clustering as efficacious (i.e., retrieves what we perceive as the ground truth grouping), then the burden is no longer on our algorithm but on our understanding of the ground truth.

<sup>10</sup><https://alanaw1.github.io/flintyR/articles/wvs.html>

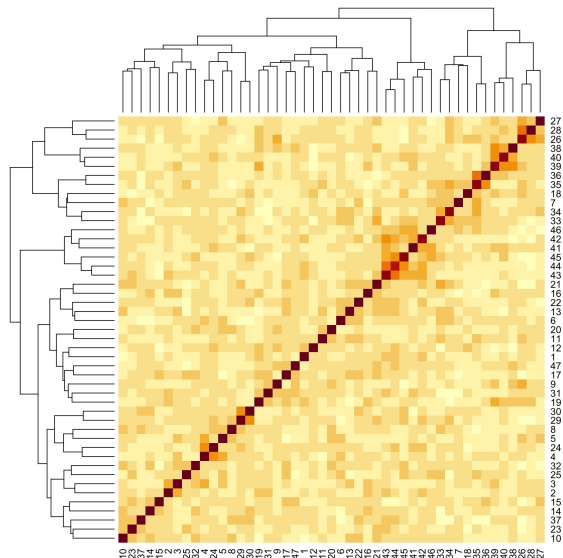


FIGURE 10. Heatmap of correlations between responses to 47 WVS questions by 241 individuals in Cluster 8.

## 7 Discussion

We have presented an exact, non-parametric and unsupervised approach to testing if a multivariate  $N$ -sample dataset is exchangeable. We have shown that our approach is flexible on multiple fronts, including scalability to high dimensionalities of the dataset and accounting for feature dependencies obeying a partitionable dependency structure. We have also demonstrated, through extensive simulations, when our approach is robust, especially so by making comparisons with eigenanalysis approaches that have gained popularity in recent works. Through applications to simulated and real datasets spanning multiple domains, we have provided multiple concrete ways in which our approach can be used by practitioners. These include avoiding risking double dipping, interpreting drivers of heterogeneity, and obtaining and characterizing homogeneous, or unstratified, communities.

Our present work is not without limitations. One obvious limitation of our approach is the need for feature dependencies to be partitionable. This is not true for many real datasets, where complex dependency structures underlie the observed feature-feature correlations. In such a setting, it is difficult to construct a permutation of observations that preserves the dependency structure. This is consistent with many methods in practice relying on parametric resampling, i.e., empirical Bayes, approach after fitting a graphical model on the features. From another perspective, however, given that it is oftentimes not clear how to choose a reasonable model to capture the dependency structure, our approach provides the clarity and interpretability desired of any preliminary approach for analyzing homogeneity while accounting for feature dependencies to some degree. Our analysis also shows that at least for the independent features case, parametric resampling controls FPR less well than the asymptotic approximation does. (This raises the question of when parametric resampling is well-calibrated for testing hypotheses, and, related to that, whether this calibration matters in practice.)

Another limitation is that we have diagnosed the efficacy of our test only under the setting where the  $P$  features are independent and binarizable. Although we surmise that the broad conclusions derived from our simulation study will likely port over to the non-independent version of our test (or even the most general version described in Section 4.2), we acknowledge that it will be more revealing to perform a thorough diagnosis of our approach against real and simulated datasets with multivariate partitionable dependent features.

Apart from the limitations described above, we believe our present work also warrants several natural extensions. First, we can modify the test statistic in several ways, including (1) exploring functionals other than the variance of the Hamming distance, and (2) introducing weights to the features when computing differences. We surmise that such modifications may identify even more powerful tests, but we also suspect

that obtaining asymptotic approximations will be challenging. Second, given the prominence of finite-sample tail bounds in the recent literature on high-dimensional statistics, it is possible that such tail bounds can be used to compute lower tails of our observed test statistic, providing an efficient simulation- and “CDF integration”-free means to obtain  $p$ -values. We pursued this direction and encountered difficulty in obtaining tight and achievable upper bounds on sub-Gaussian and sub-exponential parameters, which matter in practice. Third, in our simulation study verifying robustness, it would be interesting to include the scenario of missing data. Missing data arises a lot in practice, and there are multiple ways to deal with it depending on the user context, including imputation and observation or feature removal. In view of the multitude of ways in which data missingness occurs and also the multiplicity of methods that exist to handle data missingness, we believe that an extensive study exploring the robustness of *any* test of exchangeability across *all* such scenarios will be fruitful.

Finally, even though we have mainly applied our methods in a clustering setting, we also believe our work may be useful in other venues. We mention two such venues. In causal inference studies, the validity of an estimated treatment effect hinges on the exchangeability, across all potentially confounding features, of the sample comprising both untreated and treated individuals (Hernán and Robins, 2020). Exchangeability plays a historically important role in statistical inference (Lindley and Novick, 1981), and relates Bayesian modeling approaches to valid inferences (Saarela et al., 2020). We point the reader to Draper et al. (1993), which describes a somewhat similar approach to ours of detecting exchangeability, albeit without open-source software. (It was also written contemporaneously with the then-emerging field of “Tukey”-style data analysis.) Given the abundance of high-dimensional data sets today that potentially already contain relevant features for empirical study, our approach and our software may therefore be of interest to practitioners and researchers. On the other hand, in population-genetic studies, as we have seen in Section 6.1, alleles are binarized, resulting in datasets that are of the type we have analyzed extensively in our present work. In statistical models of evolution, biologically meaningful parameters like selection and recombination rates have, with few exceptions, effects localized to a chromosome. This implies that the genome can be grouped into mutually independent blocks of features. Remarkably, our conditioning on the column sums being fixed translates into conditioning on the sample frequency spectrum, a summary statistic used in demography inference (Kamm et al., 2020). Our test statistic,  $V$ , on the other hand is the empirical second moment of pairwise sequence diversity (the first moment is the nucleotide diversity index  $\pi$ , a historically important measure of polymorphism in a population, see paragraph containing eqs. (25) and (26) in Nei and Li, 1979). We plan to explore the application of our approach to population genetics more thoroughly in future work, potentially incorporating suggestions from the previous paragraph as well.

In summary, our contribution emphasizes methodological clarity and efficacy on realistic datasets, which can sometimes be conflicting objectives in the age of big data and black box models. Given that our analyses reveal multiple scenarios where our methods are efficacious, we believe our analyses will provide guidance for practitioners who hope to adopt our approach — or even the TW approach and its many extensions in the literature — to their specific domain. Ultimately, because of its interpretability and simplicity, we believe our approach has the potential to empower scientists across multiple domains to discover previously unknown but meaningful communities or patterns from multivariate datasets.

## Code and Data Availability

flintyR is available on CRAN (<https://cran.r-project.org/web/packages/flintyR/>) and flintyPy is available on PyPI (<https://pypi.org/project/flintypy/>). To enhance reproducibility and serve users of our methods, we provide detailed and pedagogical versions of all data analyses reported in our paper at <https://alanaw1.github.io/flintyR/articles/index.html>.

## Acknowledgements

We thank Dan Erdmann-Pham, Nick Patterson, and Sebastián Prillo for helpful discussions. We thank Rachel Spicer and Tim Stuart for feedback on our online vignettes about the application of our methods to the World Values Survey and to the single cell ATAC-seq data. This research is supported in part by an NIH grant R35-GM134922. Y.S.S. is a Chan Zuckerberg Biohub Investigator.

## Appendix

We provide details supplementing parts of the main text and present proofs of results reported in the main text.

### A Connection to Hypergeometric Distributions and Exponential Families

Our work is related to the theory of sampling from hypergeometric distributions that arise from exponential families conditioned on a sufficient statistic (Diaconis and Sturmfels, 1998). In this theory, we think of sampling as being performed on *counts* of each unique length  $P$  binary vector. This perspective will allow us to precisely characterize  $H_{\mathbf{c}}$ , the resampling distribution of  $\mathbf{X}$  introduced very recently above. Let  $\{0, 1\}^P$  denote the collection all length  $P$  binary vectors. For  $\mathbf{x} \in \{0, 1\}^P$ , let  $\kappa(\mathbf{x}) = \#\{\mathbf{x}_i = \mathbf{x}\}$  be the number of observations  $\mathbf{x}_i$  of  $\mathbf{X}$  equal to  $\mathbf{x}$ . Observe that because the ordering of the observations that make up the resampled dataset  $\mathbf{X}^*$  does not matter for our computation of  $V^* = V(\mathbf{X}^*)$ , therefore sampling from the permutation resampling distribution on  $\mathbf{X}$  (i.e., uniformly sampling from  $\mathcal{Y}_{\mathbf{c}}$ ) is equivalent to sampling from the following collection of *count statistic vectors*  $\kappa^* : \{0, 1\}^P \rightarrow \mathbb{Z}_0^+$ ,

$$\mathcal{F}_{\mathbf{c}} = \left\{ \kappa : \sum_{\mathbf{x} \in \{0, 1\}^P} \kappa(\mathbf{x}) \cdot \mathbf{x} = \mathbf{c}, \sum_{\mathbf{x} \in \{0, 1\}^P} \kappa(\mathbf{x}) = N \right\}.$$

Hence, we may characterize  $H_{\mathbf{c}}$  as a distribution on count statistic vectors, where each resampled array  $\mathbf{X}^*$  has a unique corresponding count statistic vector  $\kappa^*$  (but not the other way round).

To make the connection with exponential families, suppose  $N$  length  $P$  binary vectors,  $\mathbf{x}_1, \dots, \mathbf{x}_N$ , are sampled *with replacement* from  $\{0, 1\}^P$ , where the distribution over  $\{0, 1\}^P$  is parametrized by  $\boldsymbol{\theta} = (\theta_1, \dots, \theta_P) \in (0, 1)^P$ . For a binary vector  $\mathbf{x} = (x_1, \dots, x_P)^T$ , let the probability of picking  $\mathbf{x}$  be  $\pi_{\mathbf{x}} = \prod_{j=1}^P (\theta_j x_j + (1 - \theta_j)(1 - x_j))$ . Under such a sampling scheme, the corresponding count statistic distribution is a multinomial distribution,

$$G_{\boldsymbol{\theta}}(\kappa) = \binom{N}{(\kappa(\mathbf{x}) : \mathbf{x} \in \{0, 1\}^P)} \prod_{\mathbf{x} \in \{0, 1\}^P} \pi_{\mathbf{x}}^{\kappa(\mathbf{x})}.$$

The product term above is some combination  $\prod_{j=1}^P \theta_j^{\omega_j} (1 - \theta_j)^{\zeta_j}$ . After stacking  $\mathbf{x}_1^T, \dots, \mathbf{x}_N^T$  row-wise to obtain a  $N \times P$  array  $\mathbf{X}$ , notice the indices  $\omega_j$  and  $\zeta_j$  are simply

$$\begin{aligned} \omega_j &= \#\{\mathbf{x}_i \text{ contains } 1 \text{ in column } j\}, \\ \zeta_j &= \#\{\mathbf{x}_i \text{ contains } 0 \text{ in column } j\} = N - \omega_j. \end{aligned}$$

Let the random vector  $\mathbf{C} = \mathbf{C}(\mathbf{x}_1, \dots, \mathbf{x}_N) = \sum_{i=1}^N \mathbf{x}_i = \sum_{\mathbf{x} \in \{0, 1\}^P} \kappa(\mathbf{x}) \cdot \mathbf{x}$  summarize the number of 1's appearing in each column. By relating  $\mathbf{C}$  to the quantities  $\omega_j$  and  $\zeta_j$ , we may write

$$(A.1) \quad G_{\boldsymbol{\theta}}(\kappa) = \binom{N}{(\kappa(\mathbf{x}) : \mathbf{x} \in \{0, 1\}^P)} \exp \left[ \mathbf{C}^T \text{logit}(\boldsymbol{\theta}) + N \sum_{j=1}^P \log(1 - \theta_j) \right],$$

where  $\text{logit}(\mathbf{v})$  denotes the vector whose  $j$ th component is the one-to-one logit function  $t \mapsto \log[t/(1 - t)]$  applied to the  $j$ th component of  $\mathbf{v}$ . This is a  $P$ -parameter exponential family with sufficient statistic  $\mathbf{C}$ . More importantly, conditioned on  $\mathbf{C} = \mathbf{c}$ , where  $\mathbf{c}$  are the column sums of the observed dataset, we obtain the resampling distribution of  $\mathbf{X}$ . Thus,  $H_{\mathbf{c}}$  is the exponential family distribution  $G_{\boldsymbol{\theta}}(\kappa)$  conditioned on observing sufficient statistic  $\mathbf{C}$ . It moreover has a closed form probability mass function, given by the hypergeometric density

$$(A.2) \quad H_{\mathbf{c}}(\kappa) = \frac{N!}{|\mathcal{Y}_{\mathbf{c}}|} \left( \prod_{\mathbf{x} \in \{0, 1\}^P} \kappa(\mathbf{x})! \right)^{-1}.$$

While the mass function of  $H_{\mathbf{c}}$  is exact, the mass function and distribution  $F_{\text{perm}}$  of  $V^*$  are not. To see why, we simplify the expressions in eqs. (2.2) and (2.3). This simplification is summarized in Proposition 1 below.

**Proposition 1** (Simplification Equations). *Let  $\mathbf{c}$  denote the column sums of  $\mathbf{X}$ ,  $\kappa$  denote its associated count statistic vector, and  $\Delta_H = (d_H^2(\mathbf{x}, \mathbf{y}))_{\mathbf{x}, \mathbf{y} \in \{0,1\}^P}$  denote the  $2^P \times 2^P$  matrix of squared Hamming distances between each pair of length  $P$  binary vectors. Then, the expressions in (2.2) and (2.3) are equal to the following two expressions.*

$$(A.3) \quad V(\mathbf{X}) = \frac{1}{P} \cdot \frac{2N}{N-1} \left\langle \frac{\kappa}{N}, \Delta_H \frac{\kappa}{N} \right\rangle - \mu^2,$$

$$(A.4) \quad \mu = \frac{2N}{N-1} \sum_{p=1}^P \frac{c_p}{N} \left(1 - \frac{c_p}{N}\right).$$

*Proof of Proposition 1.* First, we verify (A.4). Observe

$$\begin{aligned} \mu &= \frac{1}{\binom{N}{2}} \sum_{i < j} \sum_{p=1}^P \mathbb{1}(x_{ip} \neq x_{jp}) \\ &= \frac{1}{\binom{N}{2}} \sum_{p=1}^P \sum_{i < j} \mathbb{1}(x_{ip} \neq x_{jp}) \\ &= \frac{1}{\binom{N}{2}} \sum_{p=1}^P c_p (N - c_p), \end{aligned}$$

where the last equality follows from counting the number of pairs  $\{i, j\}$  in the  $p$ th column for which  $\mathbb{1}(x_{ip} \neq x_{jp}) = 1$ .

Next, we verify (A.3). Observe

$$\begin{aligned} V(\mathbf{X}) &= \frac{1}{\binom{N}{2}} \sum_{i < j} d_H^2(\mathbf{x}_i, \mathbf{x}_j) - \left[ \frac{2N}{N-1} \sum_{p=1}^P \frac{c_p}{N} \left(1 - \frac{c_p}{N}\right) \right]^2 \\ &= \frac{1}{\binom{N}{2}} \sum_{\{\mathbf{x}, \mathbf{y}\}: \mathbf{x}, \mathbf{y} \in \{0,1\}^P} d_H^2(\mathbf{x}, \mathbf{y}) \kappa(\mathbf{x}) \kappa(\mathbf{y}) - \left[ \frac{2N}{N-1} \sum_{p=1}^P \frac{c_p}{N} \left(1 - \frac{c_p}{N}\right) \right]^2 \\ &= \frac{2N}{N-1} \left\langle \frac{\kappa}{N}, \Delta_H \frac{\kappa}{N} \right\rangle - \left[ \frac{2N}{N-1} \sum_{p=1}^P \frac{c_p}{N} \left(1 - \frac{c_p}{N}\right) \right]^2, \end{aligned}$$

where the last equality follows from the definition of  $\Delta_H$ .  $\square$

From Proposition 1, we see that  $\mu$  depends only on  $\mathbf{c}$  and is universally bounded in  $N$  for any fixed  $P$ . Thus,  $V$  is dominated by a quadratic form in  $\kappa$ , and so  $F_{\text{perm}}$  is the image of a hypergeometric distribution under a quadratic map. Because (A.3) does not admit a straightforward inverse map, direct computation of  $F_{\text{perm}}$  is not possible. We thus rely on Algorithm 1 in practice to estimate  $p$ -values.

## B Algorithms

---

### Algorithm 2 Computation of $p$ -value from data array (block version)

---

- 1: **Input:** Individual-by-feature array  $\mathbf{X}_{N \times P}$ , resampling number  $R$ , block delimiters  $P_1, \dots, P_B$
  - 2: Record  $\mathbf{c} = \mathbf{c}(\mathbf{X})$ ,  $\mu$  and  $V_{\text{obs}} = V(\mathbf{X})$
  - 3: Set  $r = 0$ ,  $\mathcal{V}^* = \emptyset$
  - 4: **while**  $r < R$  **do**
  - 5:   Generate resampled array  $\mathbf{X}^*$  from block permutation null
  - 6:   Compute  $V^* = V(\mathbf{X}^*)$
  - 7:    $\mathcal{V}^* \leftarrow \mathcal{V}^* \cup \{V^*\}$
  - 8:    $r \leftarrow r + 1$
  - 9: **end while**
  - 10: **Output:**  $p = \frac{1}{R} \cdot \#\{V^* \geq V_{\text{obs}}\}$
-

**Algorithm 3** Computation of  $p$ -value from data array (general version)

- 
- 1: **Input:** Individual-by-feature array  $\mathbf{X}_{N \times P}$ , resampling number  $R$
  - 2: Record  $\mu_g$  and  $V_{\text{obs}} = V_g(\mathbf{X})$  (see main text above)
  - 3: Set  $r = 0$ ,  $\mathcal{V}^* = \emptyset$
  - 4: **while**  $r < R$  **do**
  - 5:   Generate resampled array  $\mathbf{X}^*$  from block permutation null
  - 6:   Compute  $V_g^* = V_g(\mathbf{X}^*)$
  - 7:    $\mathcal{V}^* \leftarrow \mathcal{V}^* \cup \{V_g^*\}$
  - 8:    $r \leftarrow r + 1$
  - 9: **end while**
  - 10: **Output:**  $p = \frac{1}{R} \cdot \#[V_g^* \geq V_{\text{obs}}]$
- 

**C Proofs of Main Results and Propositions**

Throughout, we append a vector or a variable with an asterisk (e.g.,  $x$  becomes  $x^*$ ) to denote their random version induced by permuting the entries of each column of the original dataset  $\mathbf{X}$ . When articulating a mathematical statement requiring no reasoning about randomness (e.g., an equality between two algebraic expressions), we typically drop the asterisk to make the distinction.

*Proof of Theorem 1.* We describe our proof strategy before dotting the “i”s and crossing the “t”s.  
Steps Outlining Proof

- (1) Write  $V^{(N,P)*}$  as the squared  $\ell_2$  norm of a random vector,  $\vec{M}^*$ , with  $\vec{M}^*$  itself being a mean of independent zero-mean random vectors.
- (2) Apply the Central Limit Theorem to  $\vec{M}^*$ . Together with Step 1, this implies  $V^{(N,P)*}$  is approximately weighted chi-square distributed as  $P \rightarrow \infty$ .
- (3) Because the covariance matrix of  $\vec{M}^*$  is non-diagonal and singular (conditioning on the sufficient statistic decrements the degrees of freedom by one), apply an orthogonal transformation to  $\vec{M}^*$  to quantify the weights of the chi-square distribution.

Step 1: For  $1 \leq i < j \leq N$ , let  $M_{ij} = \frac{1}{P}(d_H(\mathbf{x}_i, \mathbf{x}_j) - \mu)$  be the centered normalized Hamming distance between observations  $\mathbf{x}_i$  and  $\mathbf{x}_j$ , where  $\mu$  is the average Hamming distance defined in (2.3). By permuting the entries of each column of the original dataset  $\mathbf{X}$ , we obtain random variables  $\mathbf{x}_i^*$ ,  $\mathbf{x}_j^*$  and  $M_{ij}^*$ . Note that  $\mu$  is permutation-invariant, being a deterministic function of the column sum vector  $\mathbf{c} = (c_1, \dots, c_P)$  (as verified in Proposition 1). Define

$$(C.1) \quad \vec{M}^* := \left( M_{ij}^* : \{i, j\} \in \binom{[N]}{2} \right),$$

a length  $\binom{N}{2}$  random vector whose entries are the random variables  $M_{ij}^*$ . Then  $V^{(N,P)*} = \frac{P}{\binom{N}{2}} \|\vec{M}^*\|_2^2$ , verifying the squared  $\ell_2$  norm assertion.

Next, we verify that  $\vec{M}^*$  in (C.1) is the mean of  $P$  independent zero-mean random vectors. For each feature  $p \in [P]$  let  $\mu_p = [c_p(N - c_p)] / \binom{N}{2}$ , so that  $\mu = \mu_1 + \dots + \mu_P$  (as verified in the proof of Proposition 1). Define

$$\mathbb{R}^{\binom{N}{2}} \ni \mathbf{v}_p = \begin{pmatrix} (x_{1p} - x_{2p})^2 \\ (x_{1p} - x_{3p})^2 \\ \vdots \\ (x_{1p} - x_{Np})^2 \\ \vdots \\ (x_{(N-1)p} - x_{Np})^2 \end{pmatrix} - \mu_p \cdot \vec{\mathbf{1}},$$

which is the centered vector whose entries are the distances between pairs of observations. Notice that for any pair of distinct features  $p$  and  $p'$ , the random vectors  $\mathbf{v}_p^*$  and  $\mathbf{v}_{p'}^*$  are independent. Moreover, for each feature  $p$  and pair of observations  $i$  and  $j$ , the random variable  $(x_{ip}^* - x_{jp}^*)^2$  is marginally distributed as Bernoulli with success probability  $\mu_p$ , so that  $\mathbb{E}[\mathbf{v}_p^*] = \mathbf{0}$ . Finally, the Hamming distance satisfying

$d_H(\mathbf{x}_i, \mathbf{x}_j) = \sum_{p=1}^P (x_{ip} - x_{jp})^2$ , it follows that  $\sum_{p=1}^P \mathbf{v}_p = P\vec{M}$ . This shows  $\vec{M}^*$  is the mean of  $P$  independent zero-mean random vectors.

Step 2: Let  $\Sigma_p = \mathbb{E}[\mathbf{v}_p^*(\mathbf{v}_p^*)^T]$  be the covariance matrix of  $\mathbf{v}_p^*$ , and define  $\Sigma = \frac{1}{P}(\Sigma_1 + \dots + \Sigma_P)$ . We claim that

$$(C.2) \quad \sqrt{P} \cdot \vec{M}^* \xrightarrow{d} \mathcal{N}(\mathbf{0}, \Sigma).$$

By the Cramér-Wold theorem, as long as we can verify that any non-zero linear combination of  $\vec{M}^*$  converges to the corresponding univariate normal distribution, then the convergence in (C.2) is true. Thus, let  $\vec{t} \in \mathbb{R}^{\binom{N}{2}} \setminus \{\mathbf{0}\}$ . We must show that

$$(C.3) \quad \langle \vec{t}, \vec{M} \rangle \xrightarrow{d} N\left(\mathbf{0}, \frac{1}{P} \langle \vec{t}, \Sigma \vec{t} \rangle\right).$$

The rest of this Step will be to verify (C.3).

First, we compute  $\Sigma$ . Recall that  $\Sigma = \frac{1}{P}(\Sigma_1 + \dots + \Sigma_P)$ . To compute a covariance matrix  $\Sigma_p$ , we must compute covariances  $\text{Cov}\left((x_{ip}^* - x_{jp}^*)^2, (x_{kp}^* - x_{lp}^*)^2\right)$  for pairs of 2-subsets  $\{i, j\}$  and  $\{k, \ell\}$ . Fortunately, these covariances can be computed by splitting into three cases, with each case requiring a combinatorial argument to arrive at the covariance quantity.

- (Case I:  $\{i, j\} = \{k, \ell\}$ ) Then,

$$\text{Cov}\left((x_{ip}^* - x_{jp}^*)^2, (x_{kp}^* - x_{lp}^*)^2\right) = \text{Var}\left((x_{ip}^* - x_{jp}^*)^2\right) = \frac{c_p(N - c_p)}{\binom{N}{2}} \left[1 - \frac{c_p(N - c_p)}{\binom{N}{2}}\right].$$

- (Case II:  $|\{i, j\} \cap \{k, \ell\}| = 1$ ) Then,

$$\text{Cov}\left((x_{ip}^* - x_{jp}^*)^2, (x_{kp}^* - x_{lp}^*)^2\right) = \frac{c_p(N - c_p)}{N(N - 1)} - \left[\frac{c_p(N - c_p)}{\binom{N}{2}}\right]^2.$$

- (Case III:  $|\{i, j\} \cap \{k, \ell\}| = 0$ ) Then,

$$\text{Cov}\left((x_{ip}^* - x_{jp}^*)^2, (x_{kp}^* - x_{lp}^*)^2\right) = \frac{4c_p(N - c_p)(c_p - 1)(N - c_p - 1)}{N(N - 1)(N - 2)(N - 3)} - \left[\frac{c_p(N - c_p)}{\binom{N}{2}}\right]^2.$$

Thus, (abusing notation  $ij = \{i, j\}$  and) letting  $ij$  and  $k\ell$  each run over all 2-subsets of  $[N]$ ,

$$[\Sigma_p]_{ij, k\ell} = \begin{cases} \frac{c_p(N - c_p)}{\binom{N}{2}} \left[1 - \frac{c_p(N - c_p)}{\binom{N}{2}}\right] & \text{if } ij = k\ell \\ \frac{c_p(N - c_p)}{N(N - 1)} - \left[\frac{c_p(N - c_p)}{\binom{N}{2}}\right]^2 & \text{if } |ij \cap k\ell| = 1 \\ \frac{4c_p(N - c_p)(c_p - 1)(N - c_p - 1)}{N(N - 1)(N - 2)(N - 3)} - \left[\frac{c_p(N - c_p)}{\binom{N}{2}}\right]^2 & \text{if } |ij \cap k\ell| = 0 \end{cases}$$

By summing the matrices  $\Sigma_p$ , the calculations above imply that the entries of  $\Sigma$  satisfy

$$[\Sigma]_{ij, k\ell} = \begin{cases} \frac{1}{P} \sum_{p=1}^P \left( \frac{c_p(N - c_p)}{\binom{N}{2}} \left[1 - \frac{c_p(N - c_p)}{\binom{N}{2}}\right] \right) = \alpha^{N, P} & \text{if } ij = k\ell \\ \frac{1}{P} \sum_{p=1}^P \left( \frac{c_p(N - c_p)}{N(N - 1)} - \left[\frac{c_p(N - c_p)}{\binom{N}{2}}\right]^2 \right) = \beta^{N, P} & \text{if } |ij \cap k\ell| = 1 \\ \frac{1}{P} \sum_{p=1}^P \left( \frac{4c_p(N - c_p)(c_p - 1)(N - c_p - 1)}{N(N - 1)(N - 2)(N - 3)} - \left[\frac{c_p(N - c_p)}{\binom{N}{2}}\right]^2 \right) = \gamma^{N, P} & \text{if } |ij \cap k\ell| = 0 \end{cases}$$

Now that  $\Sigma$  is computed, we verify (C.3) by checking that the Lyapunov condition holds. Here, we require two facts that will be proved in Step 3.

(A) The matrix  $\Sigma$  has eigenvalues

$$\begin{cases} 0, & \text{with multiplicity } 1 \\ \alpha^{N,P} + (N-4)\beta^{N,P} - (N-3)\gamma^{N,P}, & \text{with multiplicity } N-1 \\ \alpha^{N,P} - 2\beta^{N,P} + \gamma^{N,P}, & \text{with multiplicity } \binom{N-1}{2} - 1 \end{cases}$$

(B) The eigenspaces associated with each eigenvalue are as follows.

- For eigenvalue 0,  $\mathcal{S}_1 = \text{span}(\{\vec{\mathbf{1}}\})$ .
- For eigenvalue  $\alpha + (N-4)\beta - (N-3)\gamma$ ,  $\mathcal{S}_2 = \text{span}(\{\mathbf{x}^1, \dots, \mathbf{x}^N\})$ , where  $\mathbf{x}^n$  are defined in Theorem 1.
- For eigenvalue  $\alpha - 2\beta + \gamma$ ,  $\mathcal{S}_3 = \text{span}(\{\mathbf{w}^{12}, \dots, \mathbf{w}^{N-1,N}\})$ , where  $\mathbf{w}^{ij}$  are defined in Theorem 1.

When  $\vec{t} = \lambda \vec{\mathbf{1}}$  in (C.3), observe that  $\langle \vec{M}^*, \vec{\mathbf{1}} \rangle = 0$ , a consequence of each component of  $\vec{M}^*$  having mean zero. Together with Fact (B) ensuring that  $\langle \vec{t}, \Sigma \vec{t} \rangle = 0$  whenever  $\vec{t} \in \mathcal{S}_1$ , (C.3) holds trivially. Thus, we assume for the rest of our argument that  $\vec{t} \notin \mathcal{S}_1$ .

For  $\vec{t}$  picked, let its projection onto  $\mathcal{S}_1$  be  $\vec{t}_o$  and its projection onto the orthocomplement (i.e., the space  $\mathcal{S}_2 \oplus \mathcal{S}_3$ ) be  $\vec{t}_\perp$ . Note that  $\vec{t} = \vec{t}_o + \vec{t}_\perp$ . From Step 1, we have the identity

$$\langle \vec{t}, \vec{M} \rangle = \frac{1}{P} (\langle \vec{t}, \mathbf{v}_1 \rangle + \dots + \langle \vec{t}, \mathbf{v}_P \rangle).$$

To show the Lyapunov condition holds, we must verify that there exists  $\delta > 0$  such that

$$(C.4) \quad \lim_{P \rightarrow \infty} \frac{1}{s_P^{2+\delta}} \sum_{p=1}^P \mathbb{E} [|\langle \vec{t}, \mathbf{v}_p^* \rangle - \mathbb{E}[\langle \vec{t}, \mathbf{v}_p^* \rangle]|^{2+\delta}] = 0,$$

where

$$s_P := \sqrt{\sum_{p=1}^P \text{Var}(\langle \vec{t}, \mathbf{v}_p \rangle)}.$$

As it turns out, essentially the boundedness of the sum of entries of  $\mathbf{v}_p^*$  ( $= c_p$ , a constant in  $P$ ) guarantees that (C.4) holds for *any*  $\delta > 0$ .<sup>11</sup> We check this carefully below.

From earlier computations we know that  $s_P = \sqrt{P \cdot \langle \vec{t}, \Sigma \vec{t} \rangle}$ . For brevity, introduce shorthand notation for the two non-zero eigenvalues:

$$\begin{aligned} \lambda_1 &= \alpha^{N,P} + (N-4)\beta^{N,P} - (N-3)\gamma^{N,P} \\ \lambda_2 &= \alpha^{N,P} - 2\beta^{N,P} + \gamma^{N,P}. \end{aligned}$$

Further algebra and use of Fact (B) imply that  $s_P = \sqrt{P \cdot (\lambda_1 \|\vec{t}_{\perp,2}\|_2^2 + \lambda_2 \|\vec{t}_{\perp,3}\|_2^2)}$ , where  $\vec{t}_\perp = \vec{t}_{\perp,2} + \vec{t}_{\perp,3}$  is a further projection of  $\vec{t}_\perp$  on the remaining two subspaces  $\mathcal{S}_2$  and  $\mathcal{S}_3$ . Note at least one of the vectors  $\vec{t}_{\perp,2}$  and  $\vec{t}_{\perp,3}$  is non-zero, by assumption.

Now, let's bound each summand  $\mathbb{E} [|\langle \vec{t}, \mathbf{v}_p^* \rangle - \mathbb{E}[\langle \vec{t}, \mathbf{v}_p^* \rangle]|^{2+\delta}]$  of the numerator of (C.4). First, observe that the random vector  $\mathbf{v}_p^*$  always contains  $c_p(N - c_p)$  ones and  $\binom{N}{2} - c_p(N - c_p)$  zeros. Denoting by the random variable  $W_p^*$  the linear combination, that is  $W_p^* := \langle \vec{t}, \mathbf{v}_p^* \rangle = \sum_{\{i,j\} \in \binom{[N]}{2}} t_{ij} (\mathbf{v}_p^{ij})^*$ , then  $W_p^*$  is supported on the interval with endpoints

$$\begin{aligned} \tau_{\min}^p &:= \min \left\{ \sum_{\{i,j\} \in \mathcal{A}} t_{ij} : \mathcal{A} \text{ ranges over all subsets of } \binom{[N]}{2} \text{ of size } c_p(N - c_p) \right\} \\ \tau_{\max}^p &:= \max \left\{ \sum_{\{i,j\} \in \mathcal{A}} t_{ij} : \mathcal{A} \text{ ranges over all subsets of } \binom{[N]}{2} \text{ of size } c_p(N - c_p) \right\} \end{aligned}$$

and moreover  $\mathbb{E}[W_p^*] = 0$  since  $\mathbb{E}[\mathbf{v}_p^*] = \mathbf{0}$ .

<sup>11</sup>This boundedness also implies that the weaker Lindeberg condition holds, which is also sufficient for verifying (C.3).

Set  $\hat{\tau}_p = |\tau_{\max}^p| \vee |\tau_{\min}^p|$ . Then observe that  $\hat{\tau}_p \leq \|\vec{t}\|_1 \leq \sqrt{\binom{N}{2}} \|\vec{t}\|_2$ . Moreover,  $\frac{W_p^*}{\hat{\tau}_p}$  is bounded between  $-1$  and  $1$ . Recalling the definition of  $W_p^*$  and rearranging terms, we obtain the upper bound

$$\mathbb{E} [|\langle \vec{t}, \mathbf{v}_p^* \rangle - \mathbb{E}[\langle \vec{t}, \mathbf{v}_p^* \rangle]|^{2+\delta}] \leq (\hat{\tau}_p)^\delta \text{Var}(\langle \vec{t}, \mathbf{v}_p^* \rangle).$$

Now define  $\hat{\tau} = \max_{p \in [P]} \hat{\tau}_p$ . Observe that  $\hat{\tau} \leq \|\vec{t}\|_1 \leq \sqrt{\binom{N}{2}} \|\vec{t}\|_2$ , which is finite. Moreover, upon replacing  $\hat{\tau}_p$  with  $\hat{\tau}$  in the upper bound above and summing over  $p$ , we obtain the following upper bound on the numerator of (C.4):

$$\frac{1}{s_P^{2+\delta}} \sum_{p=1}^P \mathbb{E} [|\langle \vec{t}, \mathbf{v}_p^* \rangle - \mathbb{E}[\langle \vec{t}, \mathbf{v}_p^* \rangle]|^{2+\delta}] \leq \left( \frac{\hat{\tau}}{s_P} \right)^\delta.$$

To finish the verification of Lyapunov's condition, it suffices to show that the ratio  $s_P/\hat{\tau}$  increases in  $P$ . We compute this using earlier working:

$$\begin{aligned} \frac{s_P}{\hat{\tau}} &\geq \sqrt{\frac{P \cdot (\lambda_1 \|\vec{t}_{\perp,2}\|_2^2 + \lambda_2 \|\vec{t}_{\perp,3}\|_2^2)}{\binom{N}{2} \|\vec{t}\|_2^2}} \\ &= \sqrt{P} \cdot \frac{1}{\sqrt{\binom{N}{2}}} \cdot \sqrt{\frac{\lambda_1 \|\vec{t}_{\perp,2}\|_2^2 + \lambda_2 \|\vec{t}_{\perp,3}\|_2^2}{\|\vec{t}_{\circ}\|_2^2 + \|\vec{t}_{\perp,2}\|_2^2 + \|\vec{t}_{\perp,3}\|_2^2}}. \end{aligned}$$

From the final expression on RHS above it is clear that  $s_P/\hat{\tau}$  grows at least like  $\sqrt{P}$ , which completes the verification of (C.4).

Step 3: We have just shown that (C.2) holds. If  $\Sigma$  were diagonal, then the continuous mapping theorem applied to

$$(C.5) \quad f : \mathbb{R}^{\binom{N}{2}} \rightarrow \mathbb{R}, f(\mathbf{z}) = \frac{1}{\binom{N}{2}} \|\mathbf{z}\|_2^2$$

would imply that  $V^{(N,P)*} = f(\sqrt{P}\vec{M}^*)$  is approximately a weighted sum of chi-square random variables with one degree of freedom, where the weights are the diagonal entries of  $\Sigma$ . Because  $\Sigma$  is not actually diagonal, we have to diagonalize  $\Sigma$  by performing an extra eigendecomposition step.

To this end, we shall state and prove a general lemma concerning ‘‘combinatorial matrices,’’ by which we mean matrices whose dimensions are indexed by subsets and whose entries are determined by intersection properties of these subsets.<sup>12</sup>

**Lemma 2** (Eigendecomposition of combinatorial matrices). *Let  $\Sigma$  be a  $\binom{N}{2} \times \binom{N}{2}$  matrix, whose dimensions are indexed by the 2-subsets  $\{i, j\}$  of  $[N]$ . Let the entries of  $\Sigma$  be exactly one of three quantities —  $a, b$  and  $c$  — with the positions of  $a, b$  and  $c$  determined by the intersection of the 2-subset indices, as described by the equation below:*

$$[\Sigma]_{ij, k\ell} = \begin{cases} a & \text{if } ij = k\ell \\ b & \text{if } |ij \cap k\ell| = 1 \\ c & \text{if } |ij \cap k\ell| = 0 \end{cases}$$

Then,  $\Sigma$  has the the following eigenvalues,

$$\begin{aligned} a + (2N - 4)b + \binom{N-2}{2}c \\ a + (N - 4)b - (N - 3)c \\ a - 2b + c \end{aligned}$$

with multiplicities  $1$ ,  $(N-1)$  and  $\binom{N-1}{2} - 1$  respectively. The eigenspaces and eigenvectors can be summarized as follows:

- For eigenvalue  $a + (2N - 4)b + \binom{N-2}{2}c$ , the eigenspace is  $\text{span}(\{\mathbf{1}\})$ , which has dimension 1.

<sup>12</sup>Such matrices, and their higher-order tensor analogues, arise naturally in non-parametric statistics, under the guise of terms involved in computing the second and higher moments of a random vector having a uniform distribution over all permutations.

- For eigenvalue  $a + (N - 4)b - (N - 3)c$ , the eigenspace is  $\text{span}(\{\mathbf{x}^1, \dots, \mathbf{x}^N\})$ , where

$$\mathbf{x}_{ij}^n = \begin{cases} 1 & \text{if } n \in \{i, j\} \\ \frac{-2}{N-2} & \text{if } n \notin \{i, j\} \end{cases},$$

and moreover  $\mathbf{x}^1 + \dots + \mathbf{x}^N = \mathbf{0}$ .

- For eigenvalue  $a - 2b + c$ , the eigenspace is  $\text{span}\left(\left\{\mathbf{w}^{ij} : ij \in \binom{[N]}{2}\right\}\right)$ , where

$$\mathbf{w}_{kl}^{ij} = \begin{cases} 1 & \text{if } \{i, j\} = \{k, \ell\} \\ \frac{-1}{N-2} & \text{if } |\{i, j\} \cap \{k, \ell\}| = 1, \\ \frac{1}{\binom{N-2}{2}} & \text{if } |\{i, j\} \cap \{k, \ell\}| = 0 \end{cases},$$

and moreover, for any fixed  $i$ ,  $\sum_{j \neq i} \mathbf{w}^{ij} = \mathbf{0}$ .

Remark that the covariance matrix  $\Sigma$  in our problem is a special case of Lemma 2, with  $a = \alpha^{N,P}$ ,  $b = \beta^{N,P}$ ,  $c = \gamma^{N,P}$ . It is a healthy exercise in algebra to verify that  $a + (2N - 4)b + \binom{N-2}{2}c = 0$  for our problem, and to check that Facts (A) and (B) are special cases of this general lemma.

*Proof of Lemma 2.* We shall construct the eigenvectors explicitly. Like  $\Sigma$ , the components of these eigenvectors are indexed by 2-subsets, which will allow us to reason about them combinatorially.

First, consider the vector of all 1s,  $\mathbf{1}$ . For a row in  $\Sigma$  indexed by the 2-subset  $\{i, j\}$ , we can freely replace  $i$  with any  $k \in [N] \setminus \{j\}$  and vice-versa to obtain a 2-subset that overlaps  $\{i, j\}$  by one, so there are exactly  $2(N - 2)$  such subsets. We can obtain a subset that does not overlap  $\{i, j\}$  by choosing two indices from  $[N] \setminus \{i, j\}$  so there are  $\binom{N-2}{2}$  such subsets. Therefore, the row sum of  $\Sigma$  corresponding to pair  $\{i, j\}$  is  $a + (2N - 4)b + \binom{N-2}{2}c$ . Because  $\{i, j\}$  was arbitrary, this is the row sum for each row. Therefore

$$\Sigma \mathbf{1} = \left( a + (2N - 4)b + \binom{N-2}{2}c \right) \mathbf{1}.$$

We now consider a vector  $\mathbf{x}$  constructed as follows:

$$\mathbf{x}_{ij} := \begin{cases} 1 & \text{if } 1 \in \{i, j\} \\ \eta & \text{if } 1 \notin \{i, j\} \end{cases},$$

with

$$\eta := \frac{-2b - (N - 3)c}{(N - 2)b + \binom{N-2}{2}c} = \frac{-2}{N - 2}.$$

That is, for every index corresponding to a subset containing 1 the vector's entry is 1, and for all indices that do not contain 1 the entry is  $\eta$ . We now have two cases to consider. First, consider a row of  $\Sigma$  that corresponds to a pair that contains 1, and call this row  $\Sigma_{\text{inc}}$ .

$$\Sigma_{\text{inc}}^T \mathbf{x} = a + (N - 2)b + (N - 2)b\eta + \binom{N-2}{2}c\eta,$$

which follows because this entry contains 1 and so  $a$  has coefficient 1. Then, there are  $(N - 2)$  pairs that overlap this set that also contain 1, hence the term  $(N - 2)b$ . There are also  $(N - 2)$  pairs that overlap this set but do not contain 1 resulting in the term  $(N - 2)b\eta$ . Finally there are  $\binom{N-2}{2}$  pairs that do not contain 1 and also do not overlap this set, corresponding to the  $\binom{N-2}{2}c\eta$  term. Rearranging terms, we obtain

$$\begin{aligned} \Sigma_{\text{inc}}^T \mathbf{x} &= a + (N - 2)b + \left[ (N - 2)b + \binom{N-2}{2}c \right] \eta \\ &= a + (N - 2)b - 2b - (N - 3)c \\ &= a + (N - 4)b - (N - 3)c. \end{aligned}$$

Now, consider a row of  $\Sigma$  that corresponds to a pair that does not contain 1, and call this row  $\Sigma_{\text{exc}}$ .

$$\Sigma_{\text{exc}}^T \mathbf{x} = a\alpha + 2b + 2(N - 3)b\eta + (N - 3)c + \binom{N-3}{2}c\eta.$$

The first term is because the set under consideration does not contain 1. There are then exactly two sets that overlap the present set that also contain 1, resulting in  $2b$ . Meanwhile, there are  $2(N - 3)$  sets that

overlap the present set but do not contain 1 giving  $2(N-3)b\eta$ . The term  $(N-3)c$  comes from the  $N-3$  sets that contain 1 but do not overlap the present set. Finally, there are  $\binom{N-3}{2}$  sets that do not overlap the present set and also do not contain 1 resulting in  $\binom{N-3}{2}c\eta$ . We can now rearrange and use the definition of  $\eta$  to see

$$\begin{aligned}\Sigma_{\text{exc}}^T \mathbf{x} &= \left( a + 2(N-3)b + \binom{N-3}{2}c \right) \eta + 2b + (N-3)c \\ &= \left( a + 2(N-3)b + \binom{N-3}{2}c \right) \eta - \left( (N-2)b + \binom{N-2}{2}c \right) \eta \\ &= (a + (N-4)b - (N-3)c) \eta.\end{aligned}$$

Therefore  $\mathbf{x}$  is an eigenvector with eigenvalue  $a + (N-4)b - (N-3)c$ .

Because treating 1 as being “special” in the construction of  $\mathbf{x}$  was arbitrary we can repeat this process  $N$  times to obtain  $N$  eigenvectors,  $\mathbf{x}^1, \dots, \mathbf{x}^N$ . We now check that these  $N$  eigenvectors span a space of dimension  $N-1$ . Observe that

$$\mathbf{x}^1 + \dots + \mathbf{x}^N = \mathbf{0},$$

since each component  $ij$  of this sum of vectors is exactly  $2 + (N-2)\eta = 2 - 2 = 0$ . On the other hand, suppose that  $\lambda_1, \dots, \lambda_n$  are scalars such that  $\sum_{k=1}^N \lambda_k \mathbf{x}^k = \mathbf{0}$ . By considering each component of this sum, we obtain linear equations involving each 2-subset  $\{i, j\}$  of  $[N]$ :

$$\lambda_i + \lambda_j = \frac{2}{N-2} \sum_{k \in [N] \setminus \{i, j\}} \lambda_k.$$

By adding  $2/(N-2) \cdot (\lambda_i + \lambda_j)$  to each side of the equation and multiplying by  $(N-2)$ , we recover  $N(\lambda_i + \lambda_j) = N(\lambda_{i'} + \lambda_{j'})$ , from which it is easy to see that  $\lambda_1 = \dots = \lambda_N$ . This shows that  $\dim(\text{span}(\mathbf{x}^1, \dots, \mathbf{x}^N)) = N-1$ , as desired.

For the final eigenvalue, we now consider 2 “special” indices. Without loss of generality take these special indices to be 1 and 2. We will separately consider subsets that overlap zero times, once, or twice of  $\{1, 2\}$  and allow each to have independent values. Concretely, consider the vector  $\mathbf{w}$  whose components are given by

$$\mathbf{w}_{ij} := \begin{cases} 1 & \text{if } \{1, 2\} \cap \{i, j\} = 2 \\ \zeta & \text{if } \{1, 2\} \cap \{i, j\} = 1, \\ \vartheta & \text{if } \{1, 2\} \cap \{i, j\} = 0 \end{cases}$$

with

$$\begin{aligned}\zeta &:= \frac{-1}{N-2} \\ \vartheta &:= \frac{1}{\binom{N-2}{2}}.\end{aligned}$$

Now, as before, we consider the corresponding three types of rows of  $\Sigma$ . First, consider the row that corresponds to the focal pair  $\{1, 2\}$ , which we will call  $\Sigma_{\text{focal}}$ . We see

$$\Sigma_{\text{focal}}^T \mathbf{w} = a + (2N-4)b\zeta + \binom{N-2}{2}c\vartheta,$$

which follows easily because for the focal pair, the sets that overlap exactly, partially, or not at all are exactly those that we used to construct  $\mathbf{w}$ . Substituting the definitions of  $\zeta$  and  $\vartheta$  we get

$$\Sigma_{\text{focal}}^T \mathbf{w} = a - 2b + c.$$

Consider a row whose indexing subset partially overlaps  $\{1, 2\}$ , and call it  $\Sigma_{\text{partial}}$ .

$$\Sigma_{\text{partial}}^T \mathbf{w} = \zeta a + b + (N-2)\zeta b + (N-3)\vartheta b + (n-3)\zeta c + \binom{n-3}{2}\vartheta c.$$

By construction  $\{1, 2\}$  partially overlaps the present subset and vice-versa giving us  $\zeta a + b$ . There are  $N-2$  subsets that partially overlap  $\{1, 2\}$  and the present subset resulting in  $(N-2)\zeta b$ . The term  $(N-3)\vartheta b$  comes from the  $N-3$  pairs that do not overlap  $\{1, 2\}$  but do partially overlap the present subset. Conversely, there are  $(N-3)$  subsets that do not overlap the present subset but do overlap  $\{1, 2\}$  giving  $(N-3)\zeta c$ . Finally,

there are  $\binom{N-3}{2}$  subsets that do not overlap the present pair of  $\{1, 2\}$  resulting in  $\binom{N-3}{2}\vartheta c$ . We again collect terms and apply the definitions of  $\zeta$  and  $\vartheta$  to see

$$\begin{aligned}\Sigma_{\text{partial}}^T \mathbf{w} &= \left(a + (N-2)b + (N-3)c\right)\zeta + b + (N-3)\vartheta b + \binom{N-3}{2}\vartheta c \\ &= \left(a + (N-2)b + (N-3)c\right)\zeta - (N-2)b\zeta - \frac{(N-2)(N-3)}{\binom{N-2}{2}}b\zeta - \frac{(N-2)\binom{N-3}{2}}{\binom{N-2}{2}}c\zeta \\ &= (a - 2b + c)\zeta\end{aligned}$$

Lastly, consider a row whose indexing subset does not overlap  $\{1, 2\}$  and call it  $\Sigma_{\text{non}}$ .

$$\Sigma_{\text{non}}^T \mathbf{w} = \vartheta a + c + 4\zeta b + (2N-8)\vartheta b + (2N-8)\zeta c + \binom{N-4}{2}\vartheta c,$$

where we get  $\vartheta a$  and  $c$  because the present subset does not overlap  $\{1, 2\}$  and vice-versa. There are exactly 4 subsets that partially overlap  $\{1, 2\}$  and the present subset, giving  $4\zeta b$ . Meanwhile, there are  $(2N-8)$  sets that overlap the present subset but do not overlap  $\{1, 2\}$  and vice-versa giving  $(2N-8)\vartheta b$  and  $(2N-8)\zeta c$ . Lastly, there are  $\binom{N-4}{2}$  subsets that do not overlap the present subset or  $\{1, 2\}$  yielding  $\binom{N-4}{2}\vartheta c$ . Rearranging we see

$$\begin{aligned}\Sigma_{\text{non}}^T \mathbf{w} &= \left(a + (2N-8)b + \binom{N-4}{2}c\right)\vartheta + c + 4\zeta b + (2N-8)\zeta c \\ &= \left(a + (2N-8)b + \binom{N-4}{2}c\right)\vartheta + \binom{N-2}{2}c\vartheta - \frac{4\binom{N-2}{2}}{N-2}b\vartheta - \frac{(2N-8)\binom{N-2}{2}}{N-2}c\vartheta \\ &= (a - 2b + c)\vartheta.\end{aligned}$$

Therefore  $\mathbf{w}$  is an eigenvector with eigenvalue  $a - 2b + c$ .

We again can repeat this process choosing different ‘‘special’’ pairs of indices. This results in  $\binom{N}{2}$  eigenvectors,  $\mathbf{w}^{12}, \dots, \mathbf{w}^{N-1, N}$ . It is easy to see that there are  $N$  redundant eigenvectors (e.g., consider all pairs that contain 1 — the eigenvector corresponding to the last pair is a linear combination of the first  $N-2$ ). By mirroring the analysis in the case of the second eigenvalue above, we see that these  $\binom{N}{2}$  eigenvectors span a space of dimension  $\binom{N}{2} - N = \binom{N-1}{2} - 1$ .  $\square$

Lemma 2 implies the following eigendecomposition for our covariance matrix  $\Sigma$ . Let

$$(C.6) \quad \Sigma = U\Lambda U^T,$$

with

$$\Lambda = \text{diag} \left( \underbrace{\alpha^{N,P} + (N-4)\beta^{N,P} - (N-3)\gamma^{N,P}}_{(N-1) \text{ times}}, \underbrace{\alpha^{N,P} - 2\beta^{N,P} + \gamma^{N,P}}_{\binom{N-1}{2}-1 \text{ times}}, 0 \right),$$

and the orthogonal matrix  $U = \begin{bmatrix} | & \cdots & | \\ \mathbf{u}_1 & \cdots & \mathbf{u}_{\binom{N}{2}} \\ | & \cdots & | \end{bmatrix}$  satisfying

- $\mathbf{u}_1, \dots, \mathbf{u}_{N-1}$  obtained by performing Gram-Schmidt on the set  $\{\mathbf{x}^1, \dots, \mathbf{x}^N\}$  (should obtain  $N-1$  orthogonal vectors from  $\mathbf{x}^1, \dots, \mathbf{x}^{N-1}$ ).
- $\mathbf{u}_N, \dots, \mathbf{u}_{\binom{N}{2}-1}$  obtained by performing Gram-Schmidt on the set  $\{\mathbf{w}^{ij} : ij \in \binom{[N]}{2}\}$ .
- $\mathbf{u}_{\binom{N}{2}} = \frac{1}{\sqrt{\binom{N}{2}}}\mathbf{1}$ .

By (C.2),  $\vec{Y}^* = U^T \vec{M}^*$  satisfies

$$\sqrt{P} \cdot \vec{Y}^* \xrightarrow{d} \mathcal{N}(\mathbf{0}, \Lambda).$$

Because the map defined by (C.5) is invariant to orthogonal transformations ( $\|\vec{Y}\|_2^2 = \vec{M}^T U U^T \vec{M} = \|\vec{M}\|_2^2$ ), we obtain by the continuous mapping theorem

$$V^{(N,P)*} = f(\sqrt{P}\vec{M}^*) = f(\sqrt{P}\vec{Y}^*) \xrightarrow{d} V^{(N,\infty)},$$

which concludes the proof.  $\square$

*Proof of Theorem 2.* The proof of Theorem 1 showed that when  $P$  is large,  $V^{(N,P)*}$  is approximately a weighted sum of  $\binom{N}{2} - 1$  chi-square random variables. Concretely, let  $\lambda_1 = \dots = \lambda_{N-1} = \sigma_1^2$  and  $\lambda_N = \dots = \lambda_{\binom{N}{2}-1} = \sigma_2^2$ , where

$$\sigma_1^2 = a_1^N, \quad \sigma_2^2 = a_2^N$$

with the quantities  $a_1^N$  and  $a_2^N$  defined in Theorem 1. Then,

$$V^{(N,P)*} \stackrel{d}{=} \frac{1}{\binom{N}{2}} \left( Y_1^2 + \dots + Y_{\binom{N}{2}-1}^2 \right)$$

holds approximately as long as  $P$  is large, where  $Y_n \stackrel{\text{ind}}{\sim} N(0, \lambda_n)$ . Thus, we can immediately apply the Central Limit Theorem (in  $N$ ) to the sequence  $\{Y_n^2 : n = 1, \dots, \binom{N}{2}\}$  and obtain the conclusion. All that remains is to check that the mean and variance of  $V^{(N,\infty)}$  converge to the quantities stated in Theorem 2. For the variance, there is nothing to check. For the mean, notice that

$$\begin{aligned} \lim_{N \rightarrow \infty} \mathbb{E}[V^{(N,\infty)}] &= \lim_{N \rightarrow \infty} \left[ \frac{a_1^N(N-1) + a_2^N \left( \binom{N-1}{2} - 1 \right)}{\binom{N}{2}} \right] \\ &= \lim_{N \rightarrow \infty} \left[ \left( 1 - \frac{1}{\binom{N}{2}} \right) \alpha^N + \left( \frac{2}{\binom{N}{2}} - \frac{4}{N} \right) \beta^N - \left( 1 + \frac{1}{\binom{N}{2}} - \frac{4}{N} \right) \gamma^N \right] \\ &= \alpha, \end{aligned}$$

where the last equality follows from  $\lim_{N,P \rightarrow \infty} \gamma^{N,P} = 0$  (a healthy exercise) and the fact that  $\alpha^N, \beta^N$  and  $\gamma^N$  are uniformly bounded in  $N$ .

Finally, as a technical point, because  $a_1^{N,P}$  and  $a_2^{N,P}$  are uniformly bounded in both  $N$  and  $P$ , we have  $\lim_{N,P \rightarrow \infty} a_i^{N,P} = \lim_{N \rightarrow \infty} \lim_{P \rightarrow \infty} a_i^{N,P} = \lim_{N \rightarrow \infty} a_i^N$  for  $i = 1, 2$ , assuming these limits exist. Similar reasoning justifies  $\alpha = \lim_{N,P \rightarrow \infty} \alpha^{N,P} = \lim_{N \rightarrow \infty} (\lim_{P \rightarrow \infty} \alpha^{N,P}) = \lim_{N \rightarrow \infty} \alpha^N$  and  $0 = \lim_{N,P \rightarrow \infty} \gamma^{N,P} = \lim_{N \rightarrow \infty} (\lim_{P \rightarrow \infty} \gamma^{N,P}) = \lim_{N \rightarrow \infty} \gamma^N$ , which are equalities implicitly invoked in the previous paragraph.  $\square$

*Proof of Theorem 3.* Our proof strategy is identical to the proof of Theorem 1. However, unlike the latter, where there are  $P$  independent features, here we have  $B$  independent blocks. Concretely, define

$$\mathbb{R}^{\binom{N}{2}} \ni \mathbf{v}_b = \begin{pmatrix} d^{(b)}(\mathbf{x}_1, \mathbf{x}_2) \\ d^{(b)}(\mathbf{x}_1, \mathbf{x}_3) \\ \vdots \\ d^{(b)}(\mathbf{x}_1, \mathbf{x}_N) \\ \vdots \\ d^{(b)}(\mathbf{x}_{N-1}, \mathbf{x}_N) \end{pmatrix} - \overline{d^{(b)}(\mathbf{x}_{i_1}, \mathbf{x}_{i_2})} \cdot \vec{1},$$

which is the vector of partial Hamming distances associated with block  $b$ . Let  $\Sigma_b = \mathbb{E}[\mathbf{v}_b^* (\mathbf{v}_b^*)^T]$ . Then, by mirroring Step 2 in the proof of Theorem 1, it holds that

$$(C.7) \quad \sqrt{B} \left( \frac{1}{B} \sum_{b=1}^B \mathbf{v}_b^* \right) \xrightarrow{d} \mathcal{N}(\mathbf{0}, \Sigma),$$

where  $\Sigma := \frac{1}{B} (\Sigma_1 + \dots + \Sigma_B)$ .

Now, since  $\vec{M}$  defined in Step 1 of the proof of Theorem 1 satisfies  $\vec{M} = \frac{B}{P} \left( \frac{1}{B} \sum_{b=1}^B \mathbf{v}_b \right)$  and  $V^{(N,P)} = V^{(N,B,P)} = \frac{P}{\binom{N}{2}} \|\vec{M}\|_2^2$ ,

$$V^{(N,B,P)*} = \frac{P}{\binom{N}{2}} \left\| \frac{B}{P} \left( \frac{1}{B} \sum_{b=1}^B \mathbf{v}_b^* \right) \right\|_2^2 = \frac{1}{\binom{N}{2}} \left\| \sqrt{\frac{B}{P}} \cdot \sqrt{B} \left( \frac{1}{B} \sum_{b=1}^B \mathbf{v}_b^* \right) \right\|_2^2.$$

Applying (C.7) to the expression on the RHS above, we see that, similar to Step 3 in the proof of Theorem 1, if  $\Sigma' = \frac{B}{P} \cdot \Sigma$  were diagonal, then the continuous mapping theorem would imply that  $V^{(N,B,P)*}$  is approximately a weighted sum of chi-square random variables, where the weights are the diagonal entries of  $\Sigma'$ .

To finish the proof, we apply Lemma 2 to the matrix  $\Sigma'$ . It is a healthy exercise to reason that  $\alpha^{N,B,P}$ ,  $\beta^{N,B,P}$  and  $\gamma^{N,B,P}$  are the analogues of  $\alpha^{N,P}$ ,  $\beta^{N,P}$  and  $\gamma^{N,P}$  in Theorem 1, and that the argument of Step 3 there carries over mutatis mutandis to here.  $\square$

*Proof of Theorem 4.* We will rely on the following Berry-Esséen bound for sums of independent random vectors, due to Raič (2019). Suppose that  $\mathbf{v}_1, \dots, \mathbf{v}_P$  is a collection of independent but not necessarily identically distributed zero mean  $D$ -dimensional random vectors, and assume that  $\sum_{p=1}^P \text{Var}(\mathbf{v}_p) = I_D$ . Define the random vector  $\mathbf{w} = \sum_{p=1}^P \mathbf{v}_p$ , and denote the standard  $D$ -variate Gaussian law by  $\mathcal{N}(\mathbf{0}, I_D)\{\cdot\}$ , so that for any measurable set  $\mathcal{A} \subseteq \mathbb{R}^D$ ,  $\mathcal{N}(\mathbf{0}, I_D)\{\mathcal{A}\} = \int_{\mathcal{A}} (2\pi)^{-D/2} \exp(-\frac{1}{2}\|\mathbf{x}\|_2^2) d\mathbf{x}$ . Then, for any measurable convex set  $\mathcal{A} \subseteq \mathbb{R}^D$ ,

$$(C.8) \quad |\mathbb{P}(\mathbf{w} \in \mathcal{A}) - \mathcal{N}(\mathbf{0}, I_D)\{\mathcal{A}\}| \leq (42D^{1/4} + 16) \sum_{p=1}^P \mathbb{E}\|\mathbf{v}_p\|_2^3.$$

To apply the bound above, we let (a modification of) the random vectors  $\mathbf{v}_1^*, \dots, \mathbf{v}_P^*$ , as defined in the proof of Theorem 1, play the role of  $\mathbf{v}_1, \dots, \mathbf{v}_P$ . As in the proof of Theorem 1, we first describe our proof strategy before presenting the details.

#### Steps Outlining Proof

- (1) Denoting  $\text{Var}(\mathbf{v}_p^*) = \Sigma_p$  and  $\vec{M} = \frac{1}{P}(\mathbf{v}_1 + \dots + \mathbf{v}_P)$  just like we did in the proof of Theorem 1, we saw in that proof that the covariance matrix  $\Sigma = \frac{1}{P}(\Sigma_1 + \dots + \Sigma_P)$  of  $\sqrt{P} \cdot \vec{M}^*$  has eigenvalue 0 with multiplicity 1. We perform a truncation so that the resulting collection of independent random vectors has an invertible covariance matrix allowing the Berry-Esséen bound to be applied.
- (2) Using the identity  $V^{(N,P)*} = \frac{P}{\binom{N}{2}} \|\frac{1}{P} \sum_{p=1}^P \mathbf{v}_p^*\|_2^2$  (see Step 1 of proof of Theorem 1), we relate the multi-dimensional Berry-Esséen bound to the total variation bound for the random variable  $V^{(N,P)*}$ .

Step 1: Recall the orthogonal matrix  $U$  (see (C.6)) from the proof of Theorem 1, whose columns are the eigenvectors of  $\Sigma$  and moreover satisfies  $\Sigma = U\Lambda U^T$ . Define  $\vec{Y}_p^* = \frac{1}{\sqrt{P}} U^T \mathbf{v}_p^*$  for  $p = 1, \dots, P$ . (Note that  $U$  and  $\Lambda$  depend only on  $\mathbf{c}$ , which is fixed.)

By the invariance of the test statistic to orthogonal transformations of  $\vec{M}$ , we see that  $V^{(N,P)*} = \frac{1}{\binom{N}{2}} \|\vec{Y}^*\|_2^2$ , where  $\vec{Y}^* = \vec{Y}_1^* + \dots + \vec{Y}_P^*$  and satisfies  $\text{Cov}(\vec{Y}^*) = \Lambda$ . Moreover, because  $\mathbb{E}[\vec{Y}^*] = \sqrt{P} \cdot U^T \mathbb{E}[\vec{M}^*] = \mathbf{0}$ , the last component of  $\vec{Y}^*$  is 0.

Define  $\vec{W}_p = \vec{Y}_p^*[: -1]$ , which is  $\vec{Y}_p^*$  without its last component. Observe that  $\{\vec{W}_p^* : p = 1, \dots, P\}$  is a collection of independent random variables, and moreover  $V^{(N,P)*} = \frac{1}{\binom{N}{2}} \|\vec{W}_1^* + \dots + \vec{W}_P^*\|_2^2$ , because the last component of  $\vec{Y}^*$  is 0. Letting  $\vec{W} = \sum_{p=1}^P \vec{W}_p$ , we have  $\text{Cov}(\vec{W}^*) = \Lambda'$ , where  $\Lambda' = \text{diag}(\lambda_1, \dots, \lambda_1, \lambda_2, \dots, \lambda_2)$  is the invertible diagonal matrix obtained from excluding the last row and last column of  $\Lambda$ . (Note that  $\lambda_1$  and  $\lambda_2$  depend on  $\alpha^{N,P}$ ,  $\beta^{N,P}$  and  $\gamma^{N,P}$ , which in turn depend only on  $\mathbf{c}$ .)

Now, let  $D = \binom{N}{2} - 1$ . Then,  $\{(\Lambda')^{-1/2} \vec{W}_p^* : p = 1, \dots, P\}$  is a collection of  $\mathbb{R}^D$ -valued independent random vectors, each with mean  $\mathbf{0}$ . Letting  $\mathbf{w}$  denote their sum, we see that  $\text{Cov}(\mathbf{w}) = (\Lambda')^{-1/2} \Lambda' [(\Lambda')^{-1/2}]^T = I_D$ . Thus, (C.8) holds with  $(\Lambda')^{-1/2} \vec{W}_p^*$  in place of  $\mathbf{v}_p$  in the upper bound expression.

Step 2: Given the collection  $\{(\Lambda')^{-1/2} \vec{W}_p^* : p = 1, \dots, P\}$  satisfying the Berry-Esséen bound, we now verify that the multidimensional bound translates into the desired rate of convergence. To this end, we first establish a further upper bound on the multidimensional bound that depends only on the dimensionality of

the problem. Let us bound each term  $\mathbb{E}\|(\Lambda')^{-1/2}\vec{W}_p^*\|_2^3$  that appears on the RHS of (C.8). Observe

$$\begin{aligned} \|(\Lambda')^{-1/2}\vec{W}_p\|_2^3 &= (\vec{W}_p(\Lambda')^{-1}\vec{W}_p)^{3/2} \\ &\leq (\lambda_1 \wedge \lambda_2)^{-3/2}\|\vec{W}_p\|_2^3 \\ &\leq (\lambda_1 \wedge \lambda_2)^{-3/2}\|\vec{Y}_p\|_2^3 \\ &\leq P^{-3/2}(\lambda_1 \wedge \lambda_2)^{-3/2}\|\mathbf{v}_p\|_2^3. \end{aligned}$$

Let us bound the RHS expression above. By noticing that  $\mathbf{v}_p$  is a vector that contains  $c_p(N - c_p)$  copies of  $1 - \frac{c_p(N - c_p)}{\binom{N}{2}}$  and  $\binom{N}{2} - c_p(N - c_p)$  copies of  $\frac{-c_p(N - c_p)}{\binom{N}{2}}$ , it is a healthy exercise to show that  $\|\mathbf{v}_p\|_2^3 \leq \frac{1}{4}\binom{N}{2}^{3/2} = \frac{1}{4}(D + 1)^{3/2}$ . Combining these inequalities, we obtain  $\mathbb{E}\|(\Lambda')^{-1/2}\vec{W}_p^*\|_2^3 \leq \frac{1}{4}\left(\frac{D+1}{P \cdot \lambda_{\min}}\right)^{3/2}$ , where  $\lambda_{\min} = \lambda_1 \wedge \lambda_2$ . Therefore, we have

$$(C.9) \quad |\mathbb{P}(\mathbf{w} \in \mathcal{A}) - \mathcal{N}(\mathbf{0}, I_D)\{\mathcal{A}\}| \leq (42D^{1/4} + 16) \cdot P \cdot \frac{1}{4}\left(\frac{D+1}{P \cdot \lambda_{\min}}\right)^{3/2} \leq C \cdot P^{-1/2} \cdot D^{7/4},$$

where  $C$  is a constant depending only on  $\mathbf{c}$  and  $\mathcal{A}$  is any measurable convex set.

Given that we now have an upper bound in (C.9) that depends only on the dimensionality of the problem, we shall use it to derive our desired total variation bound. Observe that for any convex set  $\mathcal{A} \subseteq \mathbb{R}^D$ ,  $\mathbf{w} \in \mathcal{A}$  if and only if  $\vec{W}^* \in (\Lambda')^{1/2}\mathcal{A}$ , where  $(\Lambda')^{1/2}\mathcal{A} = \{(\Lambda')^{1/2}\mathbf{y} : \mathbf{y} \in \mathcal{A}\}$ , because the map  $\mathcal{A} \mapsto (\Lambda')^{-1/2}\mathcal{A}$  is invertible. This map also preserving measurability and convexity, we obtain  $|\mathbb{P}(\vec{W}^* \in \mathcal{A}) - \mathcal{N}(\mathbf{0}, \Lambda')\{\mathcal{A}\}| \leq C \cdot P^{-1/2} \cdot D^{7/4}$  for any convex and measurable  $\mathcal{A}$ . Now, recall that  $V^{(N,P)*} = \frac{1}{\binom{N}{2}}\|\vec{W}^*\|_2^2$ . Consider

the function  $f : \mathbb{R}^D \rightarrow \mathbb{R}_0^+$  given by  $f(\mathbf{z}) = \frac{1}{\binom{N}{2}}\|\mathbf{z}\|_2^2$ . Observe that  $V^{(N,\infty)} \stackrel{d}{=} f(\mathbf{z})$ , where  $\mathbf{z} \sim \mathcal{N}(\mathbf{0}, \Lambda')$ . Define, for any  $t \geq 0$ ,  $\mathcal{A}(t) = \{\mathbf{z} \in \mathbb{R}^D : f(\mathbf{z}) \leq t\}$ . Then  $\mathcal{A}(t)$  is convex (a healthy exercise). Moreover  $\mathbb{P}(\vec{W}^* \in \mathcal{A}(t)) = \mathbb{P}(V^{(N,P)*} \leq t)$  (the CDF of the permutation null) and  $\mathcal{N}(\mathbf{0}, \Lambda')\{\mathcal{A}(t)\} = \mathbb{P}(V^{(N,\infty)} \leq t)$  (the CDF of the large  $P$  distribution). These observations together imply that for any  $t \geq 0$ ,

$$|\mathbb{P}(V^{(N,P)*} \leq t) - \mathbb{P}(V^{(N,\infty)} \leq t)| \leq \frac{C \cdot D^{7/4}}{\sqrt{P}},$$

which is the desired total variation bound (after absorbing  $D^{7/4} = [\binom{N}{2} - 1]^{7/4}$  into the definition of the constant  $C$ ).  $\square$

## D Simulation Details

### D.1 Type I Error Control Study

In Subsection 3.1 we describe how we simulate data from null models to investigate FPR control. Here, we summarize the results of this simulation study.

Based on the setup described in Subsection 3.1, we perform Monte Carlo sampling to estimate the FPR of our test, and report approximate 95% confidence intervals using the point estimate of the FPR.

We find that our test is exact, meaning that it keeps the Type I error rate at the desired significance level, with occasional small fluctuations due to finite sampling. In the case of  $P = 100$  features per sampled row, as the middle row of Figure S1 shows, FPR estimates of our test, together with their 95% confidence intervals, include the nominal significance threshold, with slight deviations occurring mostly when the sample size  $N$  is small. (The slight deviations are an artifact of the asymptotic test used when  $P = 100$ .) On the other hand, the FPR of the TW test is markedly different from the nominal significance threshold, except when  $N$  is large. When we simulated datasets with  $P = 10$  and  $P = 1000$  features, corresponding to small and big datasets, we find that our test remains exact, whereas TW suffers from worse FPR control than seen in the  $P = 100$  case, with the FPR estimates and their 95% confidence intervals not including the nominal significance threshold a majority of the time. In particular, when  $P = 1000$  and  $N \leq 30$ , the Type I error rate is markedly *higher* than the nominal significance threshold (see the last row of Figure S1). This phenomenon reflects the impact of the scaling factor  $N/P$  and the sizes of  $P$  and  $N$  on the accuracy of the asymptotic TW distribution, an issue that does not surface for our finite-sample and non-parametric approach.

## D.2 Statistical Power Study

In Subsection 3.2 we describe a framework comprising seven scenarios and their pairings (Table 1), in order to investigate the statistical power of exchangeability tests such as ours. Here, we provide parametrization details for our seven scenarios and summarize the results of the simulation study.

First, the parametrization details.

- (1) *Number of observations.* We generally set  $N \in \{10, 50, 100, 500, 1000\}$  to cover a range of small, moderate and large sample sizes; see Scenario 3 for exceptions.
- (2) *Closeness of subpopulation features or parameters.* We control closeness by adjusting the hyperparameter  $\varepsilon$  of our hierarchical model ( $\varepsilon \in \{0.05, 0.1, 0.15, 0.2\}$ ).
- (3) *Multiple subpopulations.* We consider  $K \in \{2, 3, 4, 5\}$ . For  $K = 3$  and  $K = 4$ , to ensure both the number of observations drawn from each population is the same and the total number of observations is close to the  $K = 2$  default case, we set  $N \in \{12, 60, 120, 600, 1200\}$ .
- (4) *Sparsity of discriminative features.* We consider  $f \in \{0.1, \dots, 0.9\}$ , and let  $fP$  features be discriminative between our  $K$  populations while the remaining  $(1 - f)P$  features be non-discriminative features that are identically distributed across all  $K$  populations in reality but included when performing the statistical test.
- (5) *Uneven sampling.* Sample evenness depends on the sampling design when the dataset is not obtained from clustering. On the other hand, uneven representation of populations in a dataset is typical of clusters obtained from partitioning an originally larger dataset, as we expect good clustering algorithms to recover (approximately) homogeneous communities. We consider this scenario for  $K = 2$  distinct populations from which observations were drawn to make up the sample, and perform draws with ratios  $r \in \{9/1, 8/2, \dots, 2/8, 1/9\}$  to make up the sample. For example, to form a size  $N = 100$  sample with draw ratio 9 : 1, we draw 90 observations from Population 1 and 10 observations from Population 2.
- (6) *Different sources of heterogeneity.* For  $K = 2$  distinct populations, we consider two sources of heterogeneity, which impact the row sums of the overall sample: (i) overall differences in frequencies across all markers; (ii) differences in frequencies across all markers, despite the average marker frequencies for each population being roughly equal. Concretely, in category (i), we draw marker frequencies from the  $P$  features for Population 1 and Population 2 as described in Step 2 of the generative process reported in Subsection 3.2. In category (ii), we draw  $P/2$  marker frequencies for Population 1 and for Population 2 from the uniform distribution described in Step 2, and then append these marker frequency vectors to obtain two different length  $P$  marker frequency vectors for the two populations. For example, with  $P = 10$ , starting from  $(0.42, 0.435, 0.44, 0.422, 0.421)$  and  $(0.575, 0.58, 0.572, 0.6, 0.61)$ , we get  $(0.42, 0.435, 0.44, 0.422, 0.421, 0.575, 0.58, 0.572, 0.6, 0.61)$  and  $(0.575, 0.58, 0.572, 0.6, 0.61, 0.42, 0.435, 0.44, 0.422, 0.421)$  as the two final marker frequency vectors.

To visualize the difference between the two categories, consider the two datasets below, where the first two individuals belong to one population and the last two individuals to another distinct population. Both datasets have differences in frequencies across all markers, but the subsamples forming the right dataset have the same average marker frequencies  $((1 + 1 + 1 + 0 + 0 + 0)/6 = 0.5)$ .

$$\begin{pmatrix} 1 & 1 & 1 & 0 & 1 & 1 \\ 1 & 1 & 0 & 1 & 1 & 1 \\ 0 & 0 & 0 & 0 & 1 & 0 \\ 0 & 0 & 0 & 1 & 0 & 0 \end{pmatrix} ; \begin{pmatrix} 1 & 1 & 1 & 0 & 0 & 0 \\ 1 & 1 & 1 & 0 & 0 & 0 \\ 0 & 0 & 0 & 1 & 1 & 1 \\ 0 & 0 & 0 & 1 & 1 & 1 \end{pmatrix}$$

Category (i)      Category (ii)

Different sources of heterogeneity arise, for instance, often in biological datasets, where technical variation rather than true biological signal accounts for Category (i), which means data pre-processing is required to reduce overall differences before testing for differences that manifest in terms of Category (ii).

- (7) *Column flipping.* For binary or binarizable markers, where the binarization provides an interpretation of ‘1’ and ‘0’ for the resulting binary array, this refers to erroneous or opposite binarization, which could arise from errors executed earlier in the data processing pipeline. We perform randomized column flipping after simulating the dataset to further simulate erroneous binarization, and

do this alongside a simulation without erroneous binarization to analyze the impact of erroneous binarization on statistical power. We should expect no impact of this procedure on our test, given it is invariant to the “direction” of binarization.

We find that our test demonstrates robustness to uneven sampling (see Figures S4, S7 and S10). For example, for a small number of features  $P = 10$  (Figure S4), when subpopulations are sufficiently far apart, statistical power on an unevenly sampled dataset is no lower than 50% of the maximum power estimated for an evenly sampled dataset. Moreover, when the sample size is large enough, this ratio increases to 80%. In comparison, the TW test sees a drop in power from 1.00 to less than 0.4 for a large sample size  $N = 500$ .

We also find that the power of our test never falls below the nominal significance level  $\alpha$  at which statistical power  $\beta$  is estimated. This is true across all sample sizes  $N$ , numbers of features  $P$ , and non-null scenarios considered. In comparison, the power of the TW test falls below  $\alpha$ , typically when  $P$  or  $N$  is small, or when the dataset is unevenly sampled, or when the subpopulations from which observations are drawn are very close to each other. (See Figures S2-S10.)

Figure S11 illustrates our two main findings in the case of uneven sampling, where violin plots of statistical powers are compared between our test and the TW test across varying numbers of features  $P$  and degrees of evenness. Degree of evenness is measured by the binary Shannon entropy of the empirical frequencies of each sampled subpopulation included in the dataset (see Scenario 4 of Table 1); a higher quantity means more evenness. Figure S11 shows that the power of our test always lies to the right of the nominal significance level and also stochastically dominates the power of the TW test in extremely unevenly sampled datasets.

### D.3 Area under the receiver-operating curve (AUROC)

In Section 3.3 we report that 4752 AUROCs are computed. We show how we arrive at this number. First, we restrict pairs of sample sizes and feature dimensionality  $(N, P) \in \{10, 50, 100\} \times \{10, 100, 1000\}$ , since we may only find null and non-null models that generate datasets sharing such dimensionalities. Second, of any such pair, there are 4 non-null scenarios corresponding to Multiple Subpopulations (Scenario 3), Different Sources of Heterogeneity (Scenario 6), and Column Flipping versus Normal (Scenario 7); 9 non-null scenarios corresponding to Sparsity of Discriminative Features (Scenario 4); and another 9 non-null scenarios corresponding to Uneven Sampling (Scenario 5). Third, of any such pair, there are 3 null scenarios corresponding to low frequencies (“sparse”), varying frequencies (“regular”) and high frequencies (“dense”). Finally, there are 4 choices of hyperparameter  $\varepsilon$  controlling the Closeness of Subpopulation Features (Scenario 2), and 2 choices of tests to evaluate AUROCs for.

## Supplementary Figures and Tables

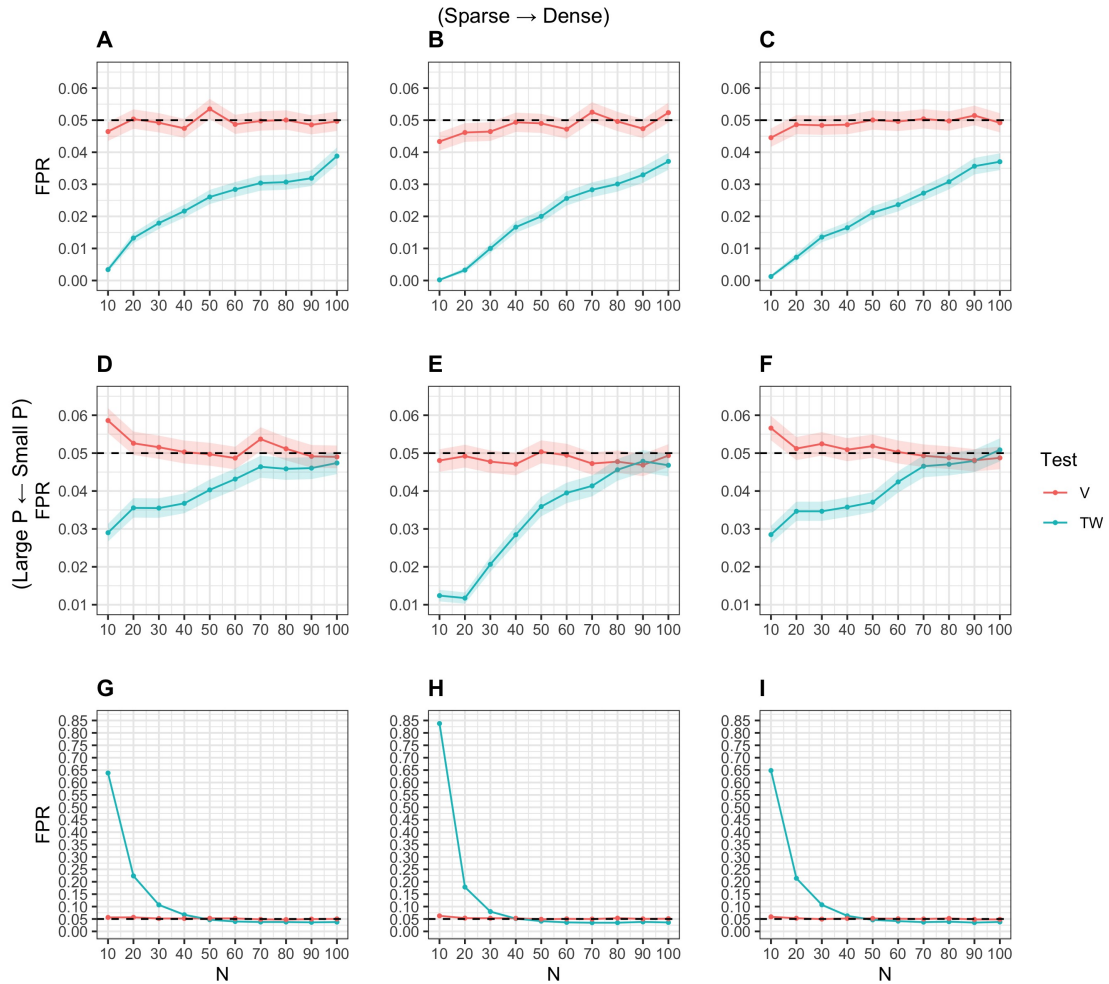


FIGURE S1. FPR of our test versus TW at significance threshold  $\alpha = 0.05$ , plotted across both numbers of features  $P$  (10, 100 or 1000) and marker frequency scenarios. The solid lines connect Monte Carlo estimates of the FPR at each value of  $N$ , with red corresponding to our test and blue corresponding to TW.

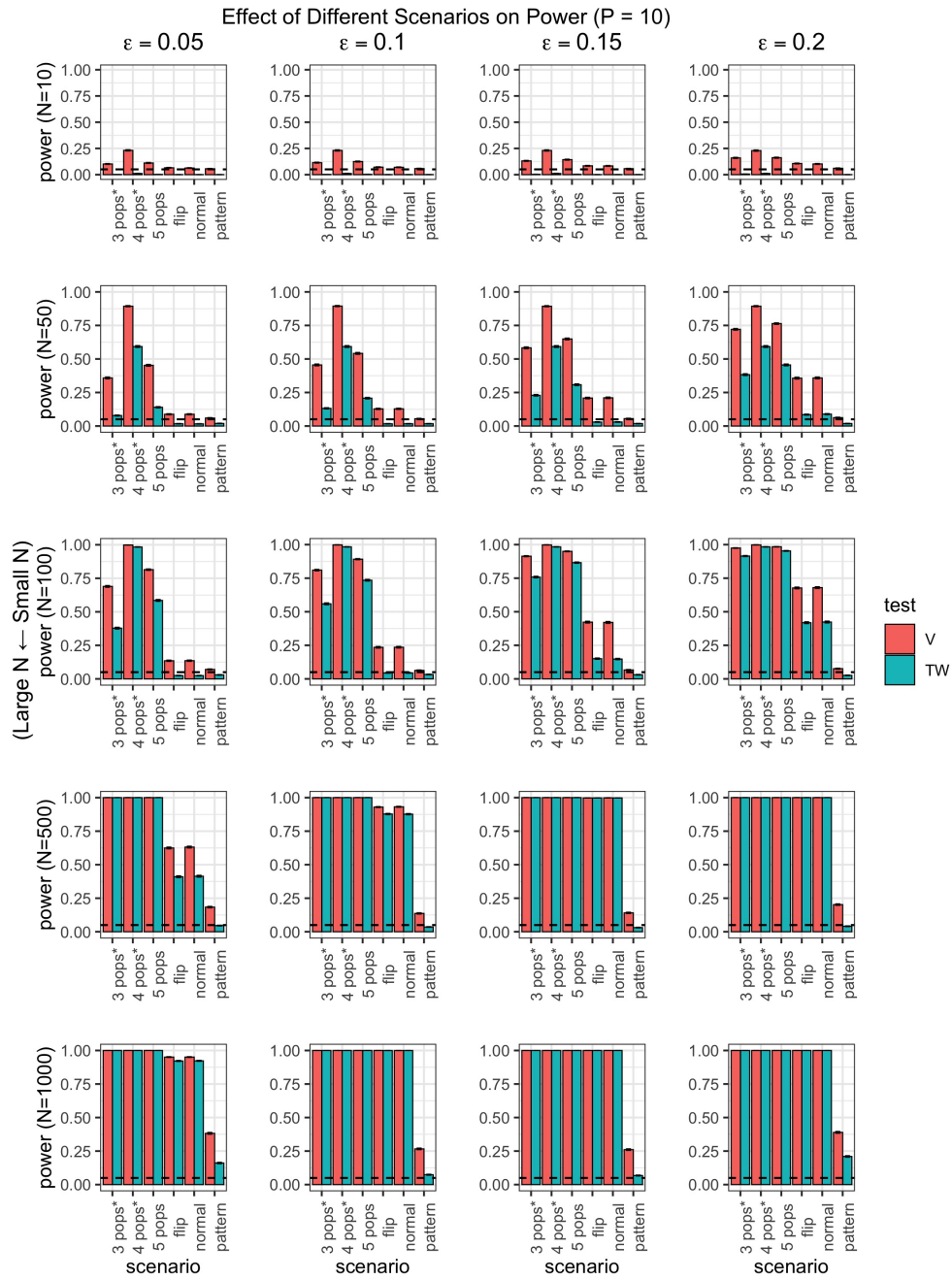


FIGURE S2. The impact of various scenarios on the statistical power of V and TW tests, with  $P = 10$  features considered.

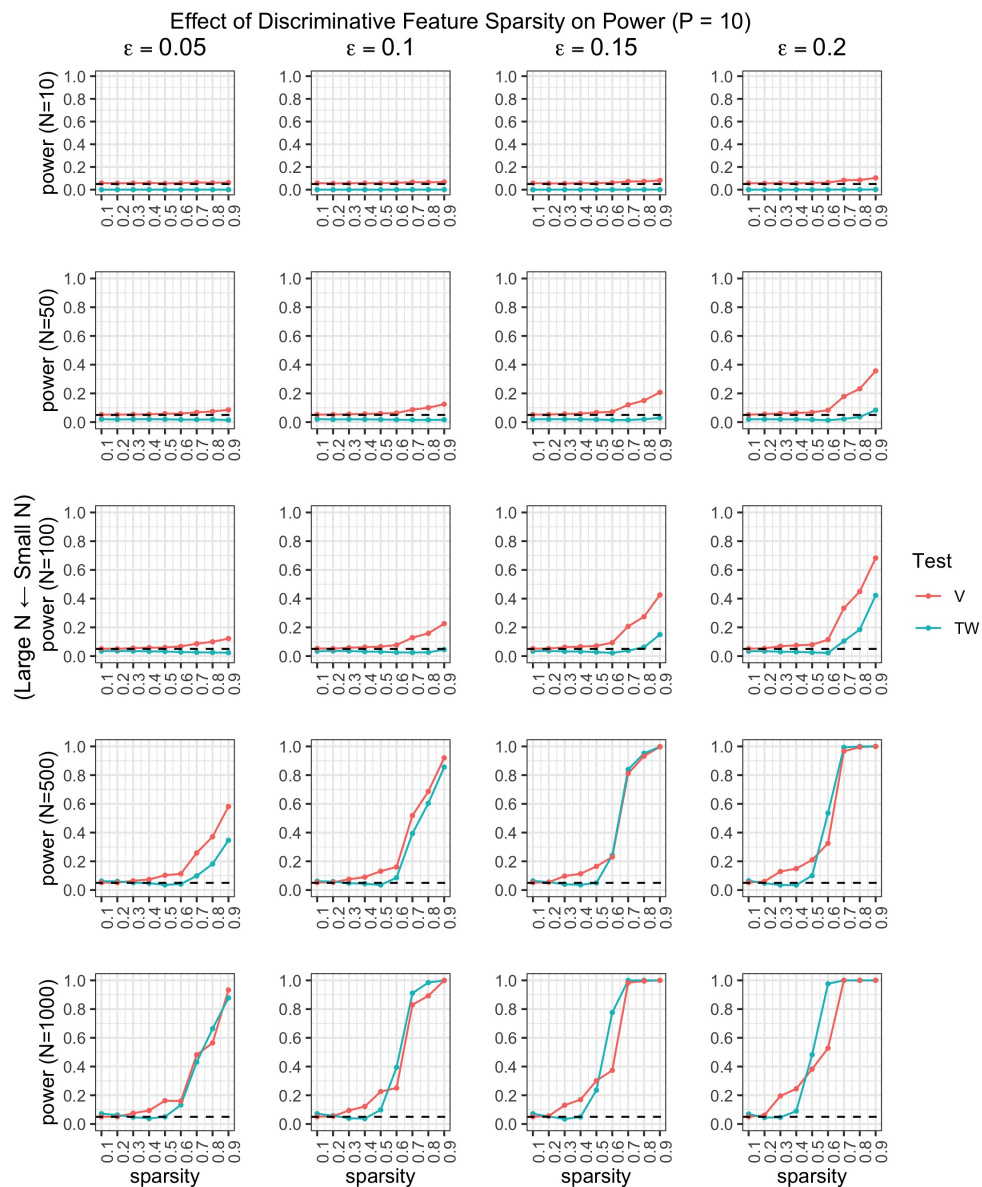


FIGURE S3. The impact of the sparsity of discriminative features on the statistical power of V and TW tests, with  $P = 10$  features considered.

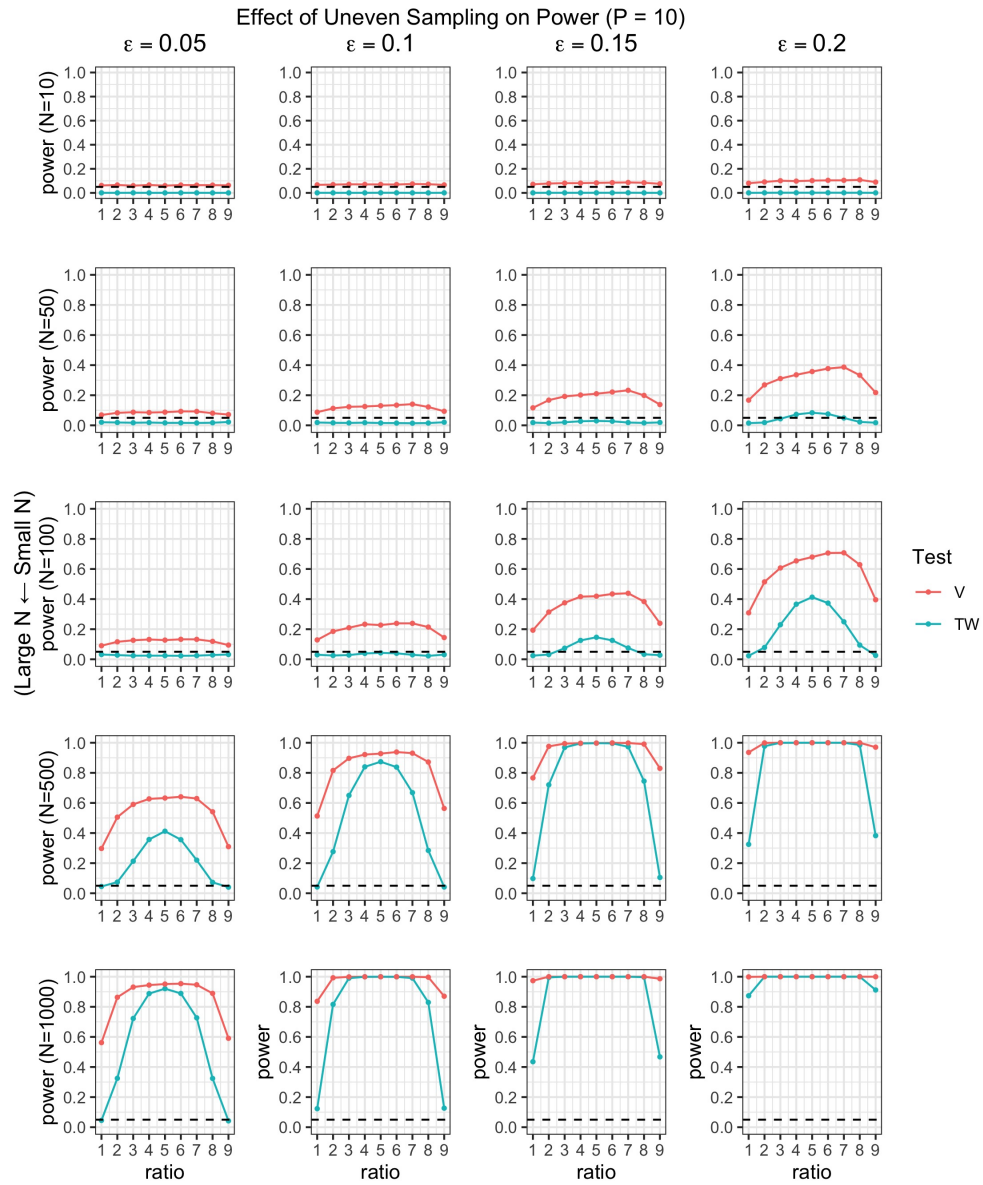


FIGURE S4. The impact of uneven sampling on the statistical power of V and TW tests, with  $P = 10$  features considered.

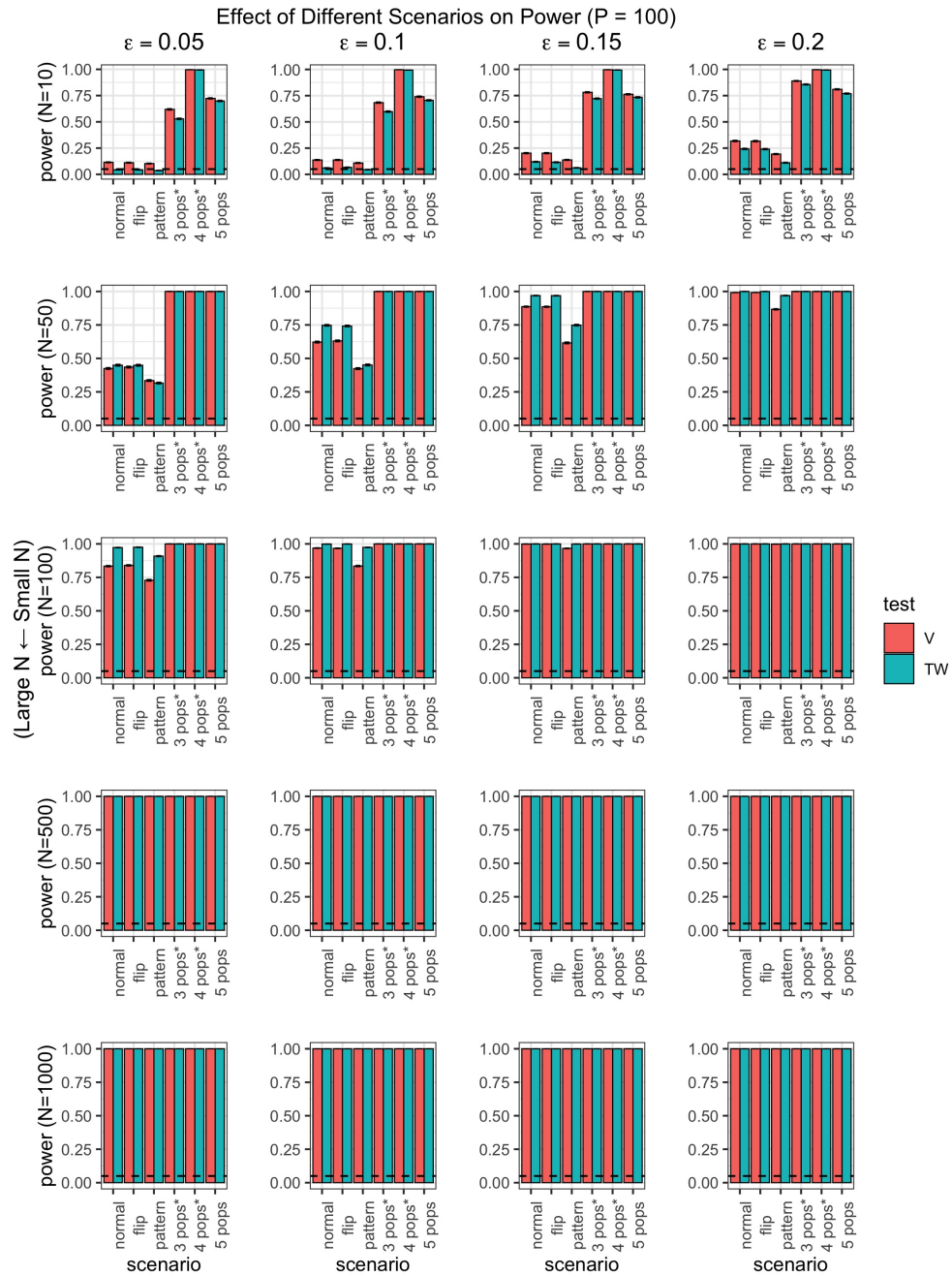


FIGURE S5. The impact of various scenarios on the statistical power of V and TW tests, with  $P = 100$  features considered.

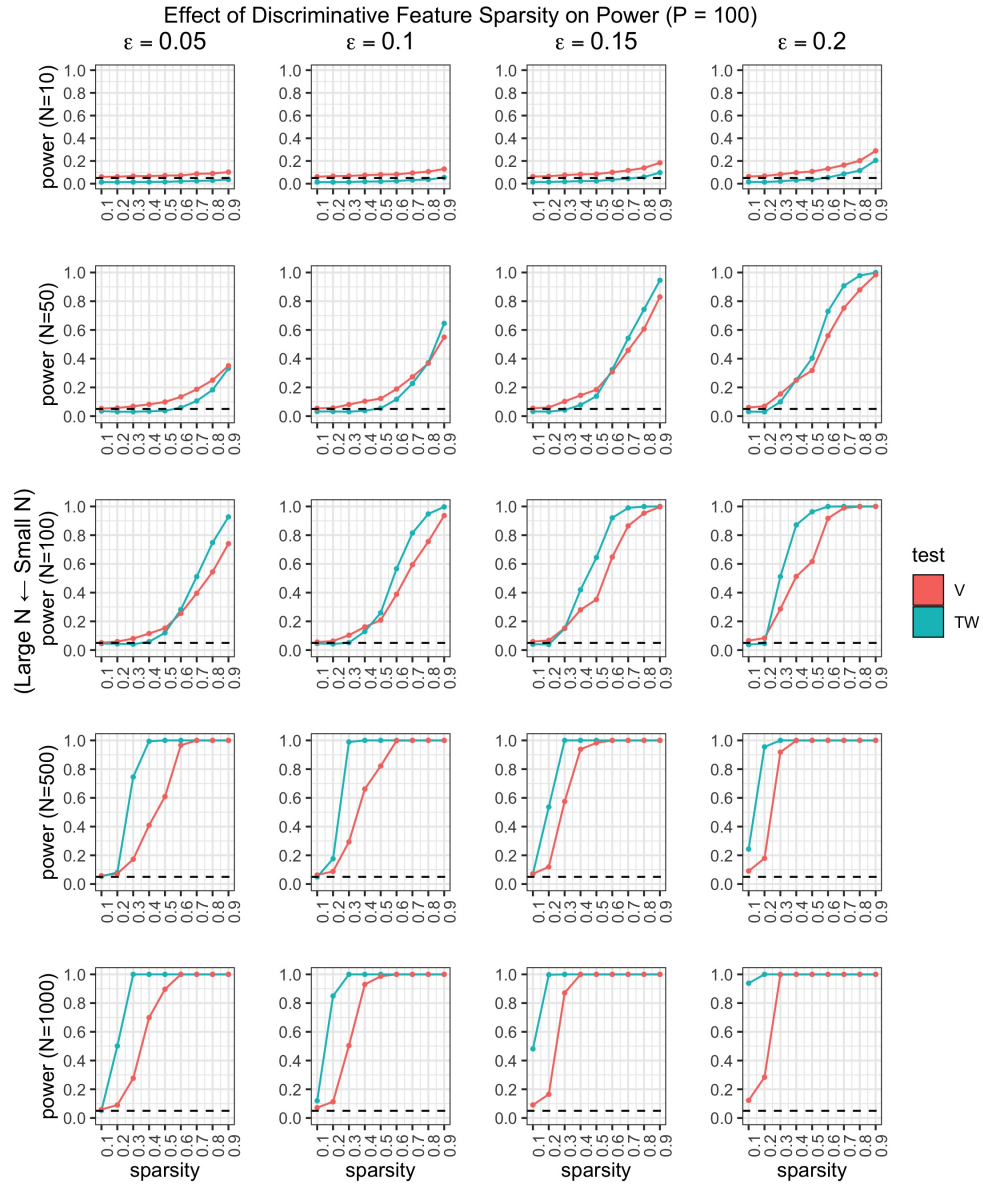


FIGURE S6. The impact of the sparsity of discriminative features on the statistical power of V and TW tests, with  $P = 100$  features considered.

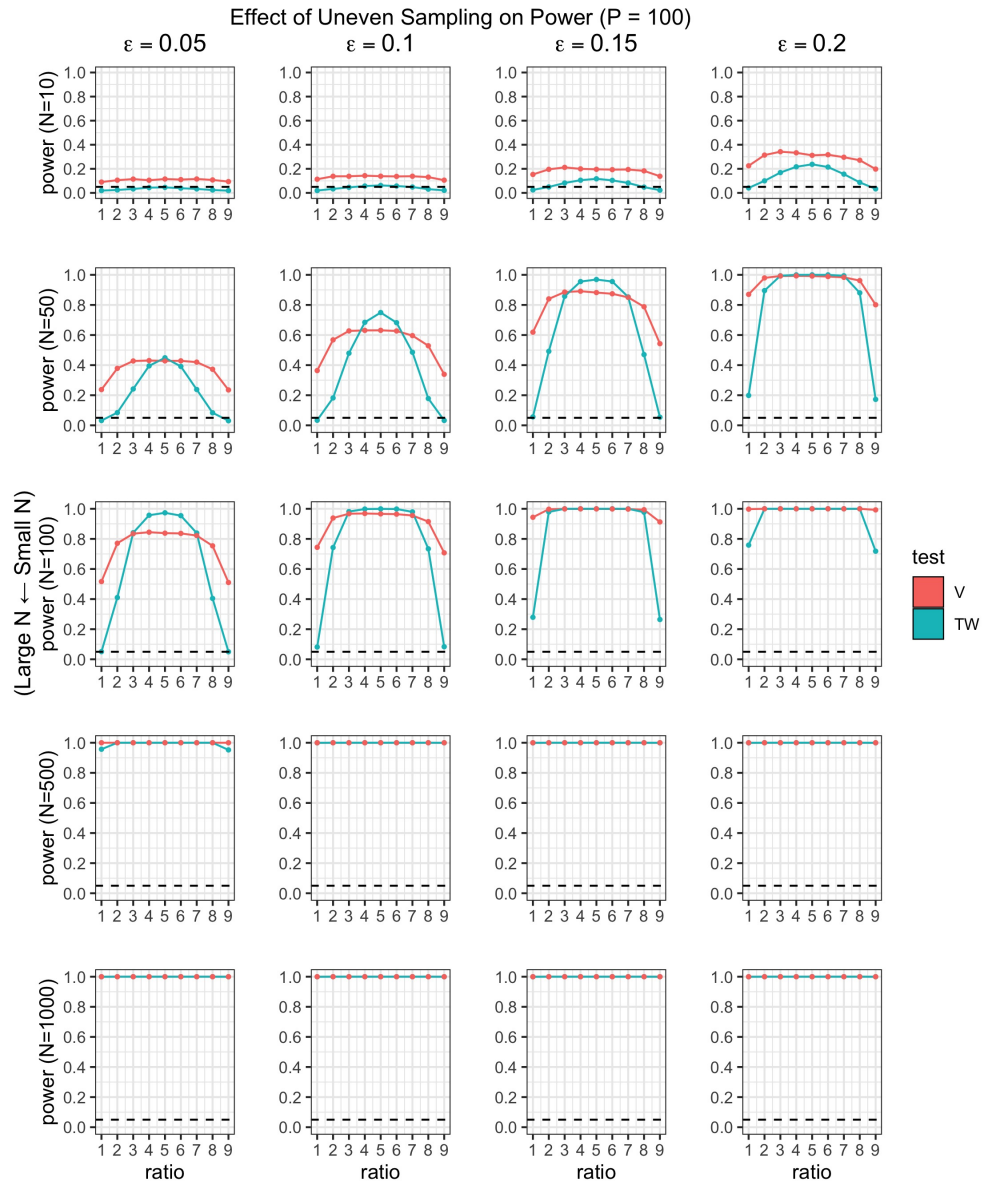


FIGURE S7. The impact of uneven sampling on the statistical power of V and TW tests, with  $P = 100$  features considered.

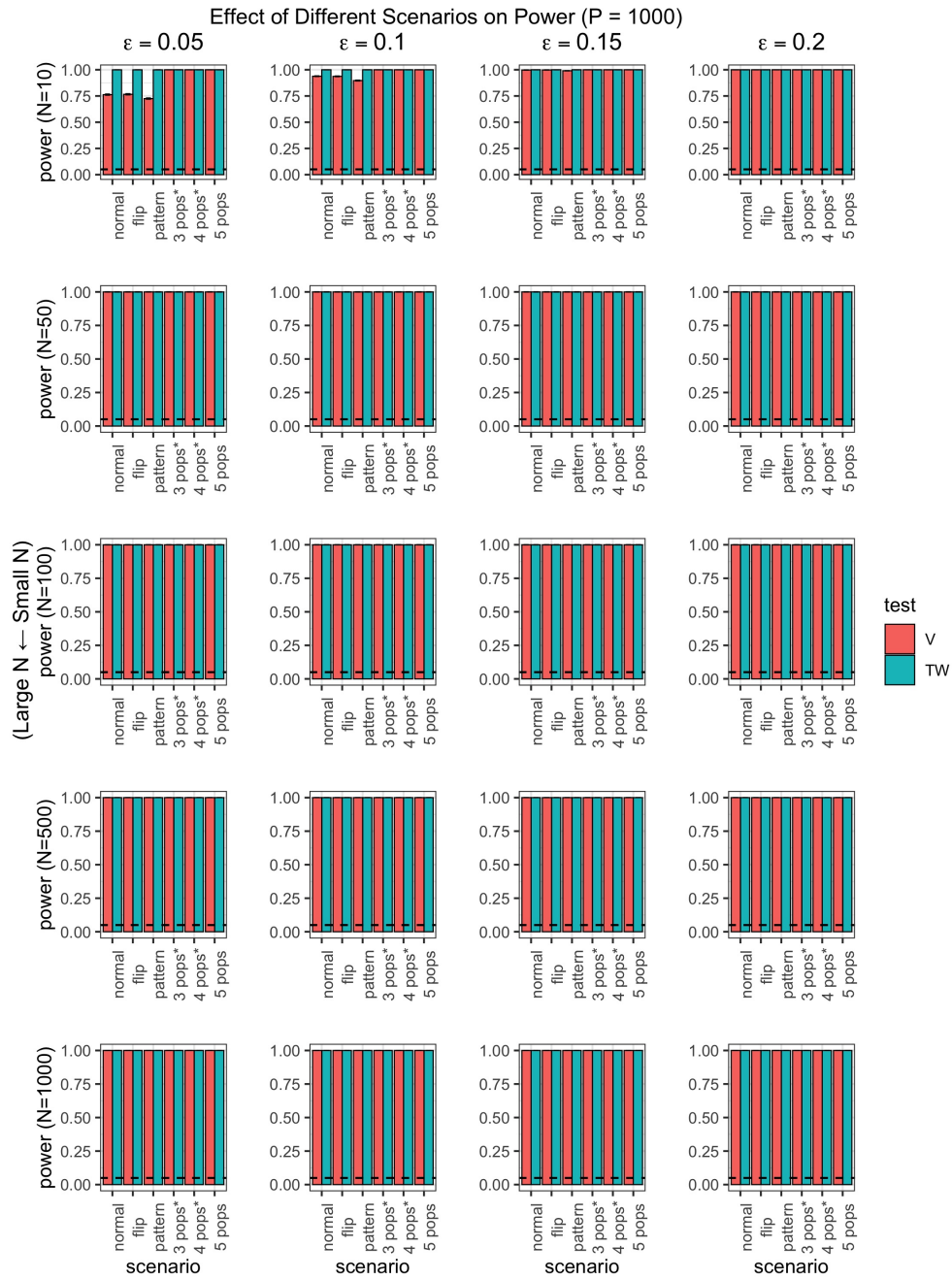


FIGURE S8. The impact of various scenarios on the statistical power of V and TW tests, with  $P = 1000$  features considered.

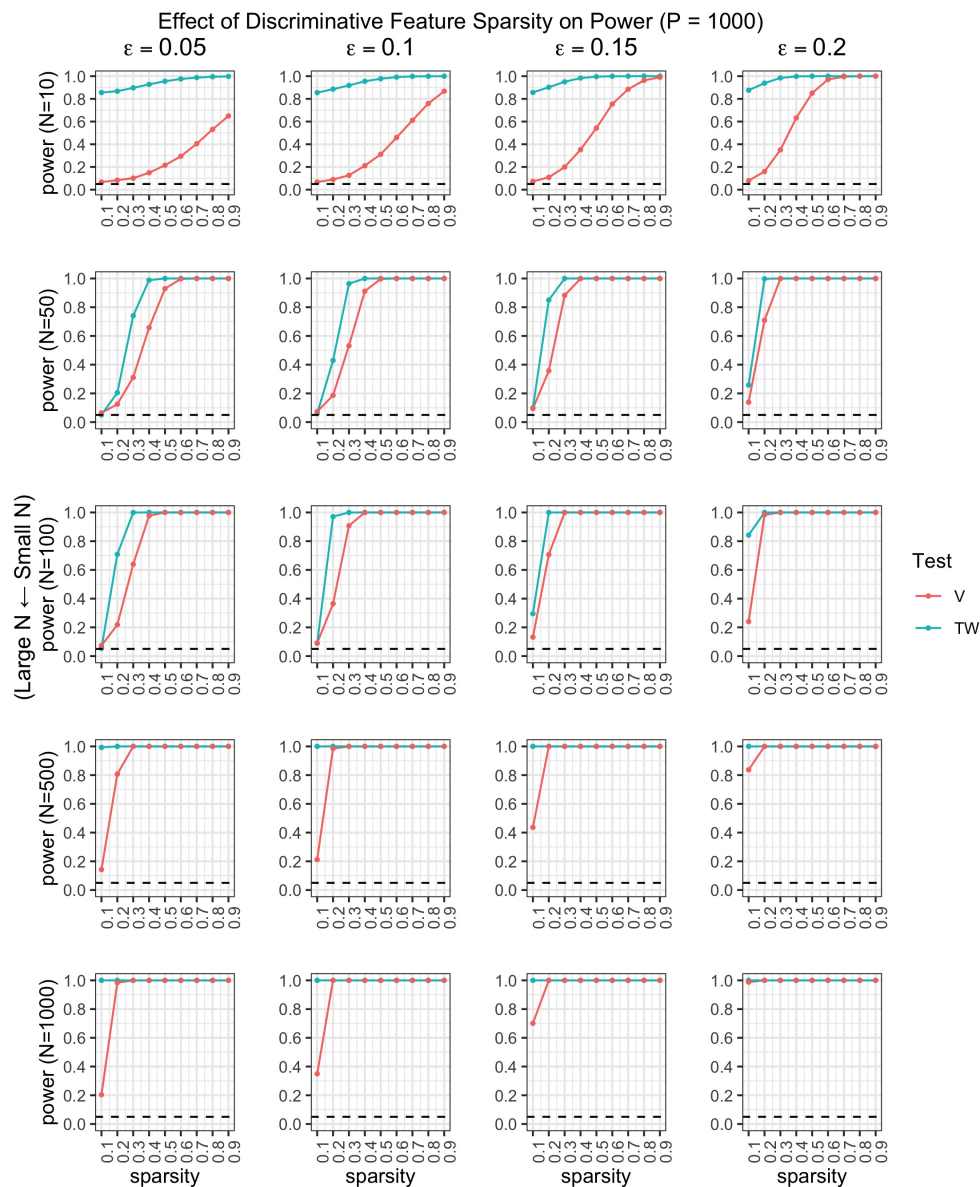


FIGURE S9. The impact of the sparsity of discriminative features on the statistical power of V and TW tests, with  $P = 1000$  features considered.

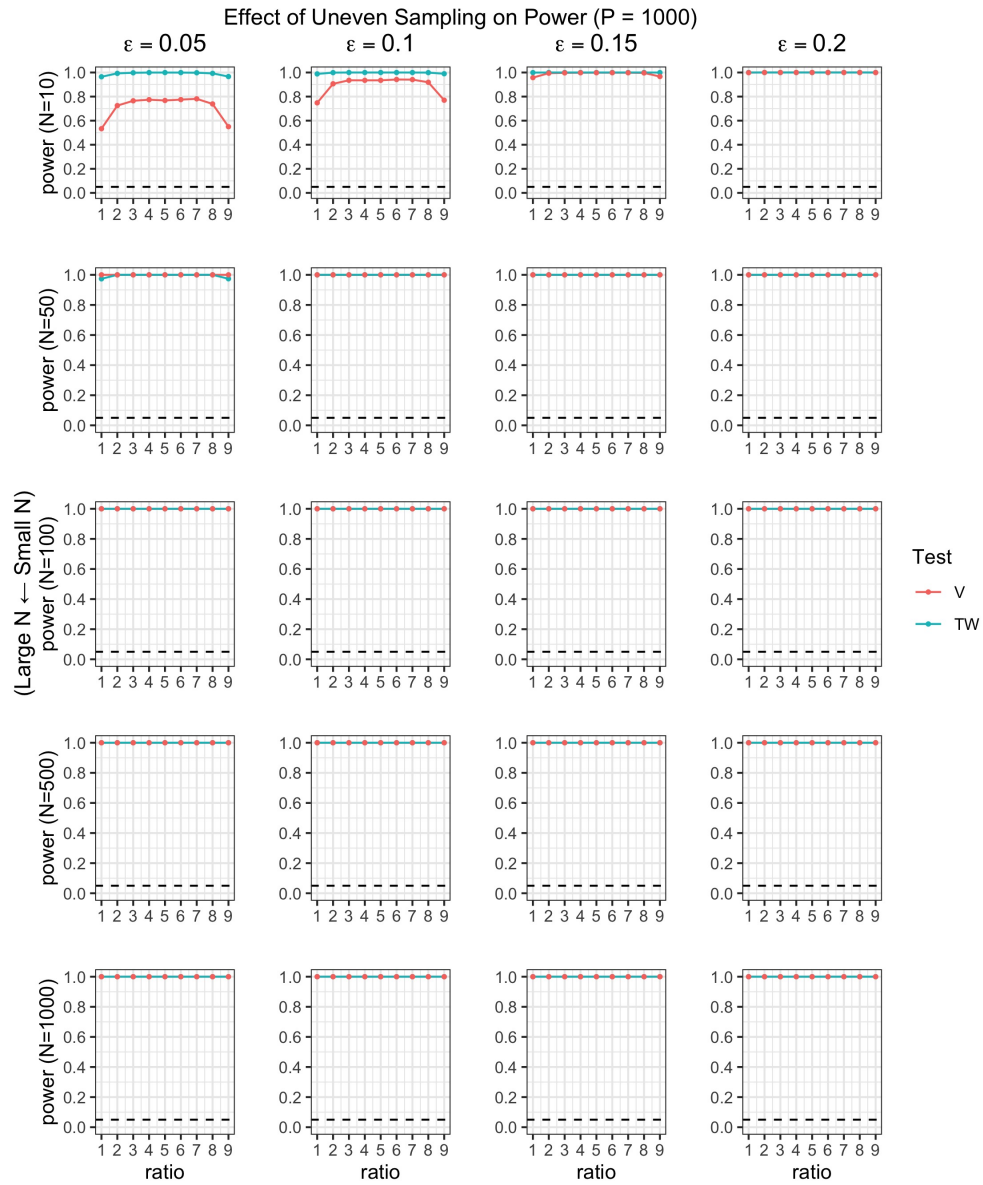


FIGURE S10. The impact of uneven sampling on the statistical power of V and TW tests, with  $P = 1000$  features considered.

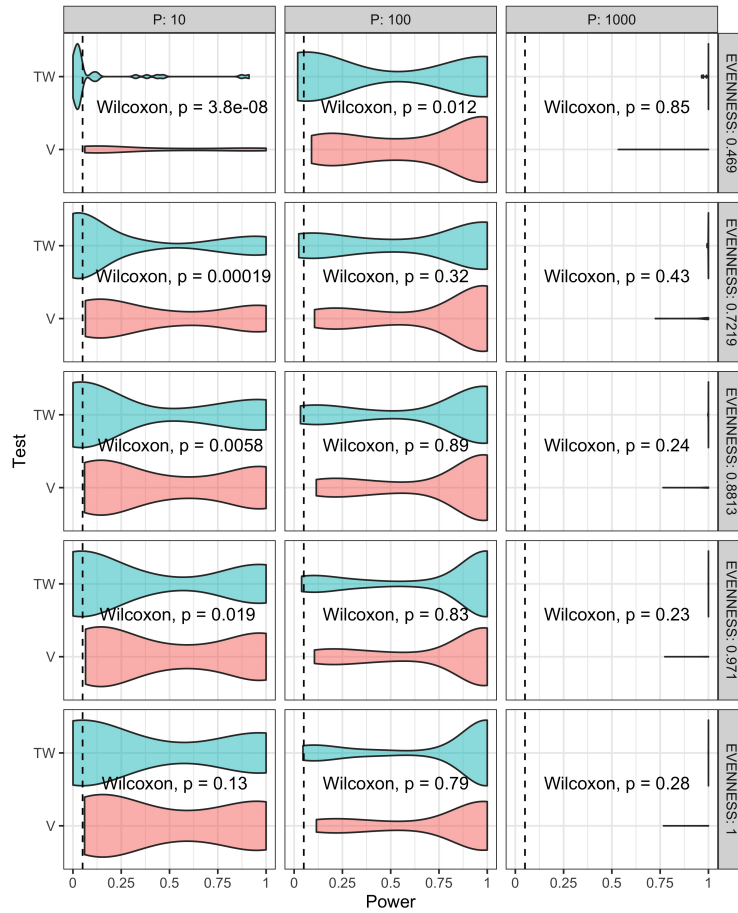


FIGURE S11. Comparison of statistical power between our test and the TW test, across all simulations involving unevenly sampled datasets. Violin plots show kernel density estimates of power. Dashed black line has  $x$ -intercept 0.05, which is the nominal significance level  $\alpha$  at which statistical powers are computed. For each (UNEVENNESS,  $P$ ) setting we report Mann-Whitney-Wilcoxon test  $p$ -values comparing the two distribution of powers.

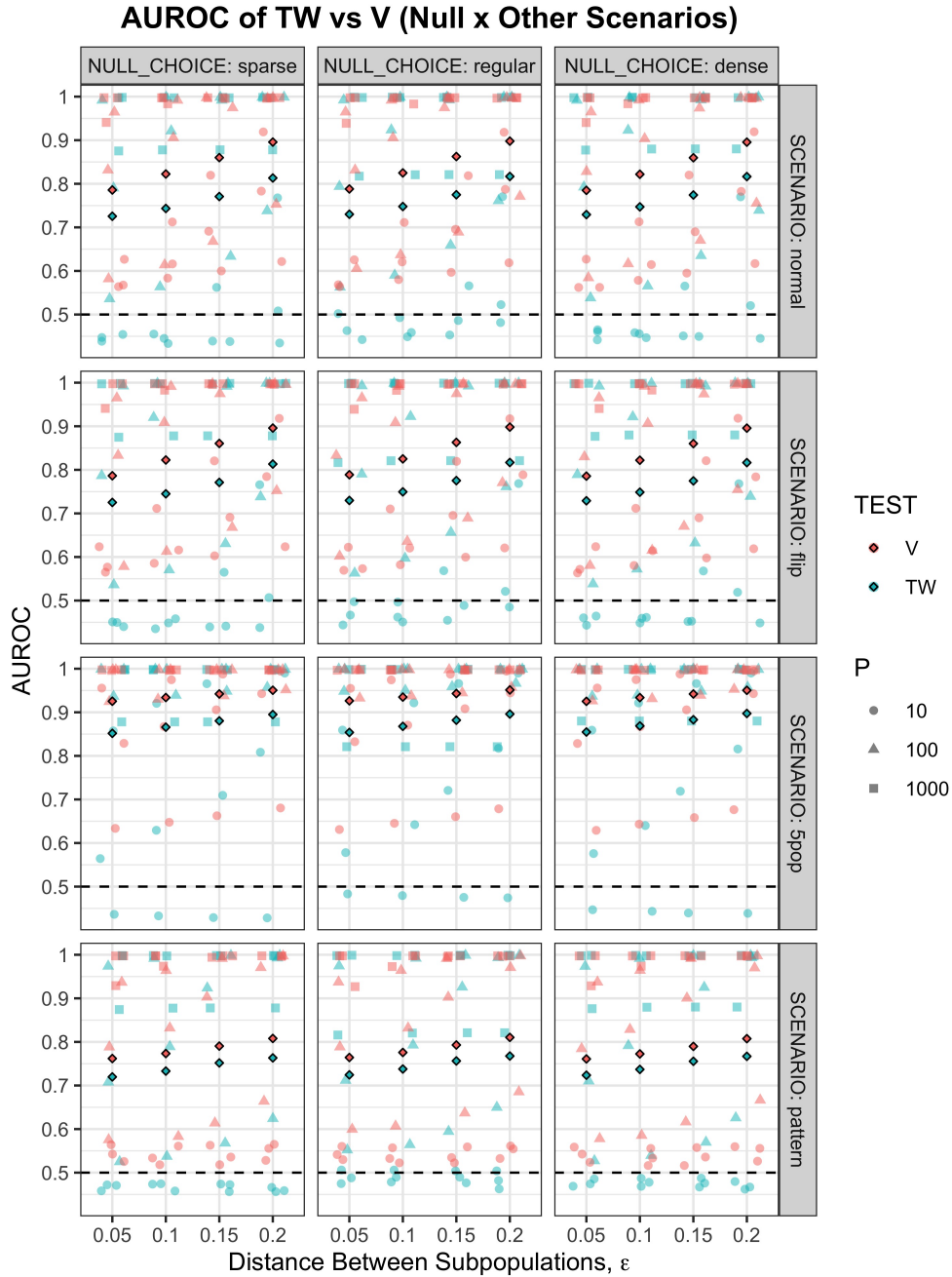


FIGURE S12. AUROC of each classifier based on pairing a null model from our FPR control simulations with a non-null model from our power estimation simulations covering Scenarios (3), (6) and (7) on top of the "normal" scenario. Each AUROC is represented by a point, coloured by the test used, and shaped according to the number of features  $P$  involved. Coloured diamonds show the average AUROC across all pairs  $(N, P)$  considered for the corresponding test in the particular configuration of (SCENARIO,  $\epsilon$ ).

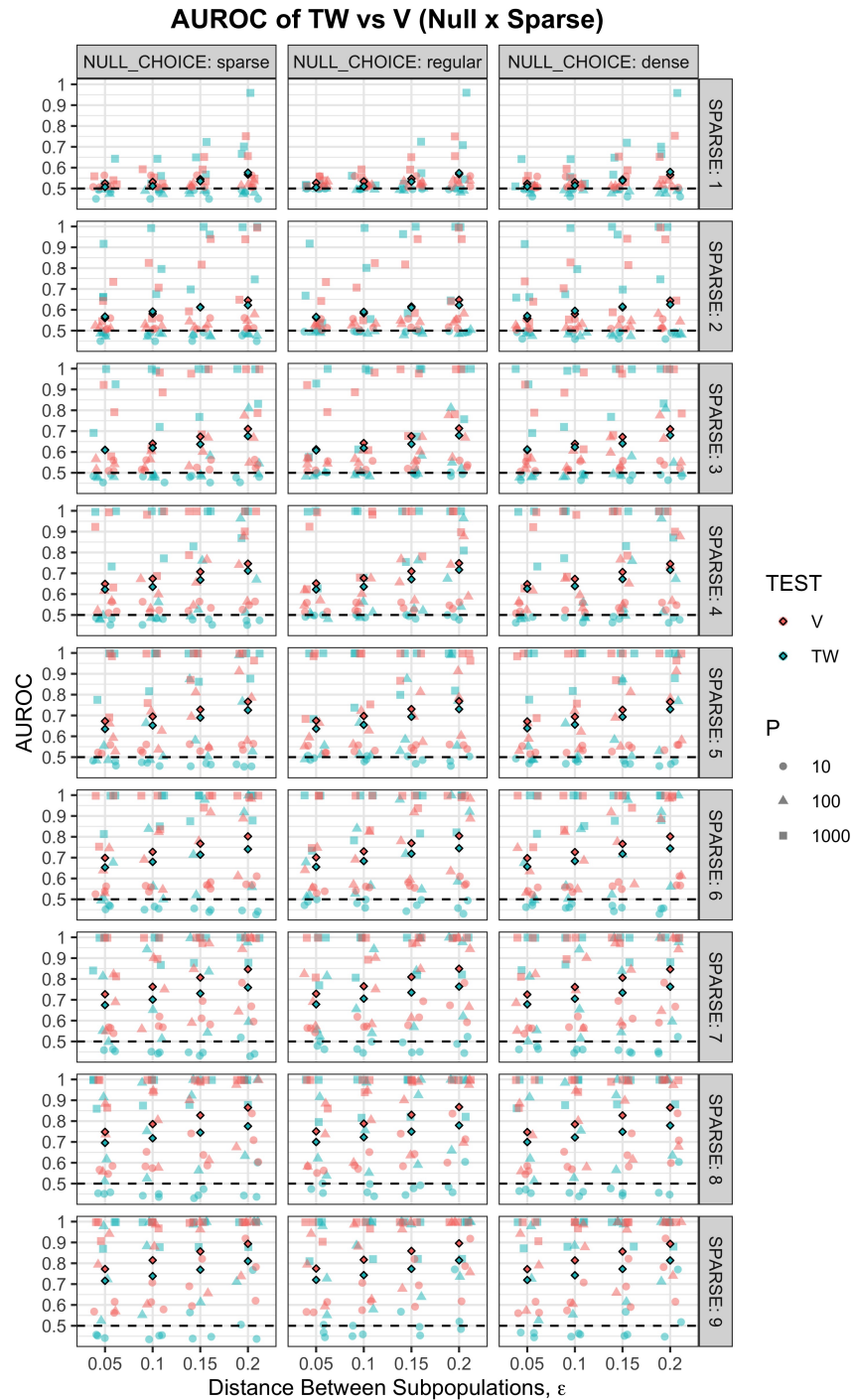


FIGURE S13. AUROC of each classifier based on pairing a null model from our FPR control simulations with a non-null model from our power estimation simulations covering Scenario 4 (sparsity of discriminative features). Each AUROC is represented by a point, coloured by the test used, and shaped according to the number of features  $P$  involved. Coloured diamonds show the average AUROC across all pairs  $(N, P)$  considered for the corresponding test in the particular configuration of  $(\text{SPARSE}, \varepsilon)$ .

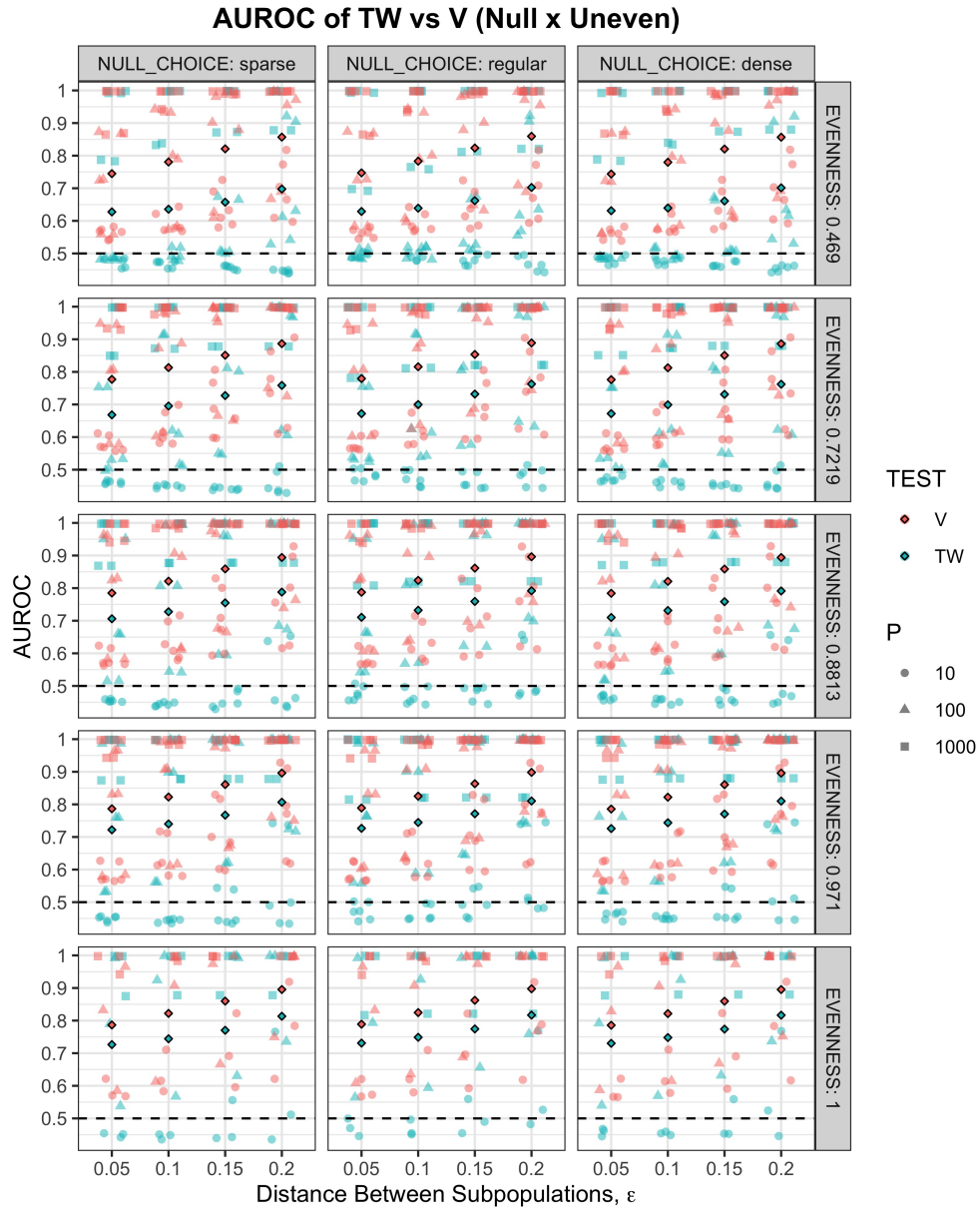


FIGURE S14. AUROC of each classifier based on pairing a null model from our FPR control simulations with a non-null model from our power estimation simulations covering Scenario 5 (uneven sampling). Each AUROC is represented by a point, coloured by the test used, and shaped according to the number of features  $P$  involved. Coloured diamonds show the average AUROC across all pairs  $(N, P)$  considered for the corresponding test in the particular configuration of  $(\text{EVENNESS}, \epsilon)$ .

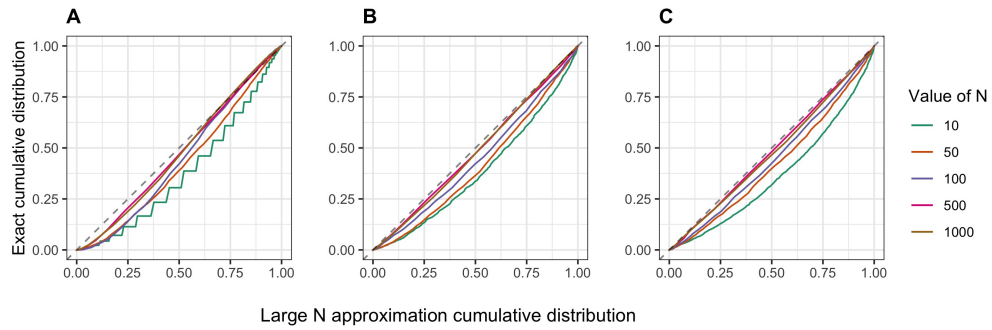


FIGURE S15. Probability-probability plots of the permutation null distribution,  $F_{\text{perm}}$ , against the parametric bootstrap. **A.**  $P = 10$ . **B.**  $P = 100$ . **C.**  $P = 1000$ .

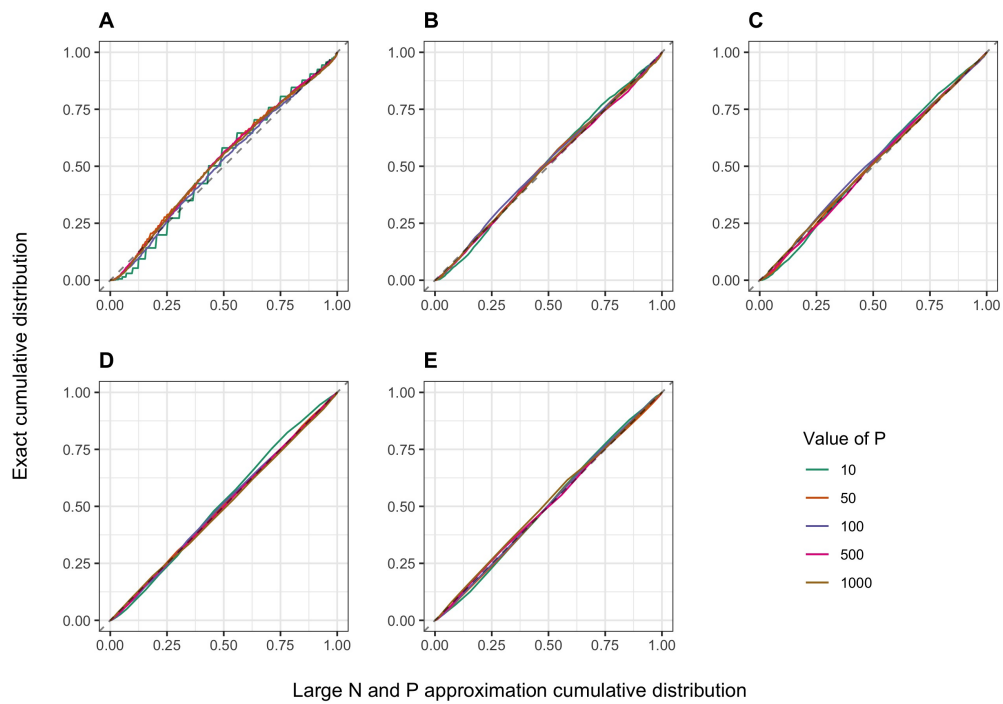


FIGURE S16. Probability-probability plots of the permutation null distribution,  $F_{\text{perm}}$ , against the large  $N$ , large  $P$  approximation. **A.**  $N = 10$ . **B.**  $N = 50$ . **C.**  $N = 100$ . **D.**  $N = 500$ . **E.**  $N = 1000$ .

TABLE S1. Cell composition for each cluster in 10X PBMC data.

Cluster	Cell Composition
0	2511 CD14+ Monocytes (99.2%) 6 CD4 Memory (0.2%) 5 CD4 Naive (0.2%) 2 B cell progenitor (0.1%) 2 CD16+ Monocytes (0.1%) 2 pre-B cell (0.1%) 1 CD8 Naive (0.0%) 1 Double negative T cell (0.0%)
1	691 CD4 Memory (95.7%) 16 CD4 Naive (2.2%) 12 Double negative T cell (1.7%) 2 NK cell (0.3%) 1 CD8 Naive (0.1%)
2	565 CD8 effector (85.3%) 34 CD4 Memory (5.1%) 30 Double negative T cell (4.5%) 18 NK cell (2.7%) 8 CD4 Naive (1.2%) 6 CD8 Naive (0.9%) 1 pre-B cell (0.2%)
3	541 CD4 Naive (92.2%) 30 CD4 Memory (5.1%) 15 CD8 Naive (2.6%) 1 pre-B cell (0.2%)
4	572 CD14+ Monocytes (99.0%) 2 CD4 Naive (0.3%) 1 CD16+ Monocytes (0.2%) 1 CD4 Memory (0.2%) 1 CD8 Naive (0.2%) 1 pre-B cell (0.2%)
5	273 CD8 Naive (68.6%) 117 CD4 Naive (29.4%) 7 CD4 Memory (1.8%) 1 NK cell (0.3%)
6	347 Double negative T cell (97.2%) 7 CD4 Memory (2.0%) 2 CD4 Naive (0.6%) 1 CD8 effector (0.3%)
7	280 NK cell (99.3%) 1 CD4 Naive (0.4%) 1 CD8 effector (0.4%)
8	244 pre-B cell (100%)
9	197 CD16+ Monocytes (84.2%) 35 CD14+ Monocytes (15.0%) 2 Double negative T cell (0.9%)
10	165 B cell progenitor (81.7%) 34 pre-B cell (16.8%) 2 CD4 Naive (1.0%) 1 CD4 Memory (0.5%)
11	87 CD14+ Monocytes (68.0%) 34 Dendritic cell (26.6%) 3 CD4 Memory (2.3%) 2 CD8 effector (1.6%) 1 CD4 Naive (0.8%) 1 NK cell (0.8%)
12	59 NK cell (98.3%) 1 CD8 Naive (1.7%)
13	49 pDC (98.0%) 1 CD8 effector (2.0%)
14	17 CD14+ Monocytes (65.4%) 8 CD4 Memory (30.8%) 1 CD8 Naive (3.8%)

## References

- David J Aldous. Exchangeability and related topics. In *École d'Été de Probabilités de Saint-Flour XIII—1983*, pages 1–198. Springer, 1985.
- Genevera I Allen and Robert Tibshirani. Inference with transposable data: modelling the effects of row and column correlations. *Journal of the Royal Statistical Society: Series B (Statistical Methodology)*, 74(4):721–743, 2012.
- Luis Aparicio, Mykola Bordyuh, Andrew J Blumberg, and Raul Rabadan. A random matrix theory approach to denoise single-cell data. *Patterns*, page 100035, 2020.
- Zhidong Bai and Jack W Silverstein. *Spectral analysis of large dimensional random matrices*, volume 20. Springer, 2010.
- Peter J Bickel and Purnamrita Sarkar. Hypothesis testing for automated community detection in networks. *Journal of the Royal Statistical Society: Series B (Statistical Methodology)*, 78(1):253–273, 2016.
- Louis J Billera, Susan P Holmes, and Karen Vogtmann. Geometry of the space of phylogenetic trees. *Advances in Applied Mathematics*, 27(4):733–767, 2001.
- Scott Deerwester, Susan T Dumais, George W Furnas, Thomas K Landauer, and Richard Harshman. Indexing by latent semantic analysis. *Journal of the American society for Information Science*, 41(6):391–407, 1990.
- Persi Diaconis and Bernd Sturmfels. Algebraic algorithms for sampling from conditional distributions. *The Annals of Statistics*, 26(1):363–397, 1998.
- Edgar Dobriban et al. Permutation methods for factor analysis and PCA. *Annals of Statistics*, 48(5):2824–2847, 2020.
- David Draper, James S Hodges, Colin L Mallows, and Daryl Pregibon. Exchangeability and data analysis. *Journal of the Royal Statistical Society: Series A (Statistics in Society)*, 156(1):9–28, 1993.
- Bradley Efron. Are a set of microarrays independent of each other? *The Annals of Applied Statistics*, 3(3):922, 2009.
- Chao Gao and John Lafferty. Testing network structure using relations between small subgraph probabilities. *arXiv preprint arXiv:1704.06742*, 2017.
- Lucy L Gao, Jacob Bien, and Daniela Witten. Selective inference for hierarchical clustering. *arXiv preprint arXiv:2012.02936*, 2021.
- Eunjung Han, Peter Carbonetto, Ross E Curtis, Yong Wang, Julie M Granka, Jake Byrnes, Keith Noto, Amir R Kermany, Natalie M Myres, Mathew J Barber, et al. Clustering of 770,000 genomes reveals post-colonial population structure of North America. *Nature Communications*, 8(1):1–12, 2017.
- Miguel A Hernán and James M Robins. Causal inference: What if, 2020.
- Miriam Huntley. *Quantitative Methods for Analyzing Structure in Genomes, Self-Assembly, and Random Matrices*. PhD thesis, Harvard University, 2016.
- R. Inglehart, C. Haerpfel, A. Moreno, C. Welzel, K. Kizilova, J. Diez-Medrano, M. Lagos, P. Norris, E. Ponarin, B. Puranen, et al. (eds.), 2014.
- Jiashun Jin, Zheng Tracy Ke, and Shengming Luo. Optimal adaptivity of signed-polygon statistics for network testing. *arXiv preprint arXiv:1904.09532*, 2019.
- Jack Kamm, Jonathan Terhorst, Richard Durbin, and Yun S Song. Efficiently inferring the demographic history of many populations with allele count data. *Journal of the American Statistical Association*, 115(531):1472–1487, 2020.
- Jerome Kelleher, Alison M Etheridge, and Gilean McVean. Efficient coalescent simulation and genealogical analysis for large sample sizes. *PLoS Comput Biol*, 12(5):1–22, 05 2016. doi: 10.1371/journal.pcbi.1004842. URL <http://dx.doi.org/10.1371/journal.pcbi.1004842>.
- Nikolaus Kriegeskorte, W Kyle Simmons, Patrick SF Bellgowan, and Chris I Baker. Circular analysis in systems neuroscience: the dangers of double dipping. *Nature neuroscience*, 12(5):535, 2009.
- David Lähnemann, Johannes Köster, Ewa Szczurek, Davis J McCarthy, Stephanie C Hicks, Mark D Robinson, Catalina A Vallejos, Kieran R Campbell, Niko Beerenwinkel, Ahmed Mahfouz, et al. Eleven grand challenges in single-cell data science. *Genome biology*, 21(1):1–35, 2020.
- Dennis V Lindley and Melvin R Novick. The role of exchangeability in inference. *The Annals of Statistics*, pages 45–58, 1981.

- Leland McInnes, John Healy, and James Melville. UMAP: Uniform manifold approximation and projection for dimension reduction. *arXiv preprint arXiv:1802.03426*, 2018.
- Michael Muthukrishna, Adrian V Bell, Joseph Henrich, Cameron M Curtin, Alexander Gedranovich, Jason McInerney, and Braden Thue. Beyond western, educated, industrial, rich, and democratic (weird) psychology: measuring and mapping scales of cultural and psychological distance. *Psychological Science*, page 0956797620916782, 2020.
- Masatoshi Nei and Wen-Hsiung Li. Mathematical model for studying genetic variation in terms of restriction endonucleases. *Proceedings of the National Academy of Sciences*, 76(10):5269–5273, 1979.
- Nick Patterson, Alkes L Price, and David Reich. Population structure and eigenanalysis. *PLoS Genetics*, 2(12):e190, 2006.
- Aluísio Pinheiro, Hildete Prisco Pinheiro, and Pranab Kumar Sen. The use of Hamming distance in Bioinformatics. In *Handbook of Statistics*, volume 28, pages 129–162. Elsevier, 2012.
- Antoni Prevosti, Jy Ocana, and G Alonso. Distances between populations of *Drosophila subobscura*, based on chromosome arrangement frequencies. *Theoretical and Applied Genetics*, 45(6):231–241, 1975.
- Chongli Qin and Lucy J Colwell. Power law tails in phylogenetic systems. *Proceedings of the National Academy of Sciences*, 115(4):690–695, 2018.
- Martin Raič. A multivariate Berry–Essén theorem with explicit constants. *Bernoulli*, 25(4A):2824–2853, 2019.
- Olli Saarela, David A Stephens, and Erica EM Moodie. The role of exchangeability in causal inference. *arXiv preprint arXiv:2006.01799*, 2020.
- Alexander Soshnikov. A note on universality of the distribution of the largest eigenvalues in certain sample covariance matrices. *Journal of Statistical Physics*, 108(5-6):1033–1056, 2002.
- Tim Stuart, Andrew Butler, Paul Hoffman, Christoph Hafemeister, Efthymia Papalexi, William M Mauck III, Yuhao Hao, Marlon Stoeckius, Peter Smibert, and Rahul Satija. Comprehensive integration of single-cell data. *Cell*, 177(7):1888–1902, 2019.
- Tim Stuart, Avi Srivastava, Caleb Lareau, and Rahul Satija. Multimodal single-cell chromatin analysis with signac. *bioRxiv*, 2020. doi: 10.1101/2020.11.09.373613. URL <https://doi.org/10.1101/2020.11.09.373613>.
- Craig A Tracy and Harold Widom. Distribution functions for largest eigenvalues and their applications. *Proceedings of the International Congress of Mathematicians*, Vol. I:587–596, August 2002.
- Abraham Wald and Jacob Wolfowitz. An exact test for randomness in the non-parametric case based on serial correlation. *The Annals of Mathematical Statistics*, 14(4):378–388, 1943.
- Jesse M Zhang, Govinda M Kamath, and David N Tse. Valid post-clustering differential analysis for single-cell RNA-seq. *Cell Systems*, 9(4):383–392, 2019.
- Yunpeng Zhao, Elizaveta Levina, and Ji Zhu. Community extraction for social networks. *Proceedings of the National Academy of Sciences*, 108(18):7321–7326, 2011.
- Yi-Hui Zhou. A note on cyclic shift permutation testing for large eigenvalues. *Stat*, 8(1):e257, 2019.
- Yi-Hui Zhou, JS Marron, and Fred A Wright. Eigenvalue significance testing for genetic association. *Biometrics*, 74(2):439–447, 2018.